

Cleared: December 19th, 1983

Clearing Authority: Air Force Wright Aeronautical Laboratories

NOTICES

When Government drawings, specifications, or other data are used for any purpose other than in connection with a definitely related Government procurement operation, the United States Government thereby incurs no responsibility nor any obligation whatsoever; and the fact that the Government may have formulated, furnished, or in any way supplied the said drawings, specifications, or other data, is not to be regarded by implication or otherwise as in any manner licensing the holder or any other person or corporation, or conveying any rights or permission to manufacture, use, or sell any patented invention that may in any way be related thereto.

The nature of this research program requires the evaluation of a certain number of products under conditions peculiar to the research equipment and environments investigated. Many of the materials subjected to experiments were not developed or intended by the manufacturer for the conditions to which they have been subjected. Any failure or poor performance of a material is, therefore, not necessarily indicative of the utility of this material under less stringent conditions or for other applications.

Defense Documentation Center release to Office of Technical Services is not authorized.

Copies of this report should not be returned to the Research and Technology Division, Wright-Patterson Air Force Base, Ohio, unless return is required by security considerations, contractual obligations, or notice on a specific document.

Cleared: December 19th, 1983

Clearing Authority: Air Force Wright Aeronautical Laboratories

FOREWORD

This report was prepared by Mechanical Technology, Incorporated, Latham, New York, under AF Contract No. AF 33(657)-10694. The work was initiated under Project 3044, "Aerospace Lubrication," Task 304402, "Advanced Propulsion Lubrication Engineering." The program was administered by AF Aero Propulsion Laboratory, Technical Support Division, Wright-Patterson Air Force Base, Ohio with M. A. Sheets acting as Project Engineer.

The first part of APL TDR 64-56 dated March 1964 bore the same title as this report, but was not marked Part I. The research was conducted from March 1964 to March 1965 by P. Lewis and M. Eusepi, the authors, and the manuscript was released by them 1 March 1965 for publication as an RTD Technical Documentary Report.

DDC release to OTS is not authorized in order to prevent foreign announcement and distribution of this report. The distribution of this report is limited because it contains technology identifiable with items on the strategic embargo lists excluded from export or re-export under U.S. Export Control Act of 1949 (63 STAT 7), as amended (50 U.S.O. App. 2020, 2031), as implemented by AFR 400-10.


Cleared: December 19th, 1983

Clearing Authority: Air Force Wright Aeronautical Laboratories

ABSTRACT

This report describes the second year's effort on a program that has as its objective the development of nitrogen gas lubricated journal and thrust bearings that have the best potential for stable operation at temperatures to 1900 F and speeds to 60,000 RPM with low flow rates. The program concentrated on attaining quantitative performance data on dynamic rotor bearing behavior. The report summarizes equipment, instrumentation, and experimental work. Quantitative performance data and a dimensionless map which summarizes the stable speed capability of the 360 degree hybrid bearing are provided.

This technical documentary report has been reviewed and is approved.



BLACKWELL C. DUNNAM, Chief
Fuels and Lubricants Branch
Technical Support Division
Air Force Aero Propulsion
Laboratory

TABLE OF CONTENTS

	<u>Page</u>
INTRODUCTION.....	1
BACKGROUND DISCUSSION.....	2
360 DEGREE HYBRID BEARING.....	3
Load Capacity and Flow Rate.....	3
Rotor-Bearing Stability.....	7
Experimental Program - Low Temperature Evaluations.....	9
Inherently Compensated 360 Degree Hybrid Bearing.....	10
360 Degree Hybrid Bearing, Orifice Compensated.....	27
Test Results for .040 Inch Recess.....	28
Test Results for .080 Inch Recess.....	29
Experimental Program - Elevated Temperature Evaluations.....	40
Modified 360 Degree Hybrid Bearing Design.....	55
FLEXURE MOUNTED HYBRID PAD BEARING.....	57
TEST FACILITY.....	67
Test Rig.....	67
Oven and Enclosure.....	67
Preheater.....	69
Controls.....	69
REFERENCES.....	78
DOCUMENT CONTROL DATA (DD FORM 1473)	

Cleared: December 19th, 1983
Clearing Authority: Air Force Wright Aeronautical Laboratories

LIST OF ILLUSTRATIONS

<u>Figure</u>	<u>Page</u>
1. Load Capacity - Double Row Hydrostatic Bearing	5
2. Flow - Double Row Hydrostatic Bearing	6
3. Speed Ratio versus Feeding Parameter Ratio for 360 Degree Hybrid Bearings	10
4. 360 Degree Test Bearing	11
5. Radial Stiffness as a Function of Supply Pressure $2a = .0136$	15
6. Radial Stiffness as a Function of Supply Pressure $2a = .026$	16
7. Radial Stiffness as a Function of Supply Pressure $2a = .040$	17
8. Bearing Gas Flow as a Function of Supply Pressure $2a = .0136$	18
9. Bearing Gas Flow as a Function of Supply Pressure $2a = .026$	19
10. Bearing Gas Flow as a Function of Supply Pressure $2a = .040$	20
11. Whirl Threshold Speed as a Function of Supply Pressure $2a = .0136$	21
12. Whirl Threshold Speed as a Function of Supply Pressure $2a = .026$	22
13. Whirl Threshold Speed as a Function of Supply Pressure $2a = .040$	23
14. Speed Ratio versus Feeding Parameter Ratio - Inherently Compensated 360 Degree Hybrid Bearings	24
15. Whirl Threshold Speed as a Function Supply Pressure for Two Rotor Masses	25
16. Speed Ratio versus Feeding Parameter Ratio - Comparison of Two Rotor Masses	26
17. Bearing Gas Flow as a Function of Supply Pressure $d = .040$ in	30
18. Bearing Gas Flow as a Function of Supply Pressure $d = .080$ in	31
19. Radial Stiffness as a Function of Supply Pressure $d = .040$ in	32
20. Radial Stiffness as a Function of Supply Pressure $d = .080$ in	33
21. Whirl Threshold Speed as a Function of Supply Pressure $d = .040$ in	34
22. Critical Speeds and Instabilities as a Function of Supply Pressure $\delta = .465$	35
23. Critical Speeds and Instabilities as a Function of Supply Pressure $\delta = .371$	36
24. Critical Speeds and Instabilities as a Function of Supply Pressure $\delta = .285$	37

Contracts

Cleared: December 19th, 1983

Clearing Authority: Air Force ~~Wright Aeronautical Laboratories~~ ~~ILSW ON AUSTRIAN LABORATORIES~~

<u>Figure</u>	<u>Page</u>
25. Speed Ratio versus Feeding Parameter - Orifice Compensated 360 Degree Hybrid Bearing	38
26. Some Operational Photographs of Orifice Compensated 360 Degree Hybrid Bearing	39
27. Speed Ratio versus Feeding Parameter - Elevated Temperature Operation - With Comparison to Previous Data	41
28. Journal Bearing Load Deflection Characteristics C = .00121 T = 70 ^o F	42
29. Journal Bearing Load Deflection Characteristics C = .00121 T = 300 ^o F	43
30. Journal Bearing Load Deflection Characteristics C = .00121 T = 500 ^o F	44
31. Journal Bearing Load Deflection Characteristics C = .00165 T = 70 ^o F	45
32. Journal Bearing Load Deflection Characteristics C = .00165 T = 300 ^o F	46
33. Journal Bearing Load Deflection Characteristics C = .00165 T = 500 ^o F	47
34. Temperature Effects on Journal Bearing Stiffness C = .00121	48
35. Temperature Effects on Journal Bearing Stiffness C = .00165	49
36. Thrust Bearing Stiffness versus Feeding Parameter	50
37. Thrust Bearing Load Deflection Characteristics T = 70 ^o F	51
38. Thrust Bearing Load Deflection Characteristics T = 300 ^o F	52
39. Thrust Bearing Load Deflection Characteristics T = 500 ^o F	53
40. Temperature Effects on Thrust Bearing Stiffness	54
41. Tangential Spoke 360 Degree Hybrid Bearing	56
42. Assembly of Flexure-Mounted Hybrid Pad Bearings	59
43. Detail of Flexure Assembly	60
44. Hybrid Pad Design	61
45. Lapping Fixture for Flex Bearing	62
46. Radial Stiffness as a Function of Supply Pressure: Load Vector on Pad	63
47. Bearing Gas Flow as a Function of Supply Pressure: Load Vector on Pad	64
48. Flex-Pad Measurement Fixture	66
49. Assembly Drawing of Test Rig	68
50. Pressure Vessel	70
51. Early Stages of Assembly of Rig to Pressure Vessel Flange	71
52. Pressure Hull, Insulation and Radiation Shield for High Temperature Testing	72

Contrails

Cleared: December 19th, 1983

Clearing Authority: Air Force Wright Aeronautical Laboratories

LIST OF ILLUSTRATIONS (Cont'd)

<u>Figure</u>	<u>Page</u>
53. Fail Safe Schematic Diagram	73
54. Fail Safe Wiring Diagram	74
55. Fail Safe Tubing Diagram	75
56. Relay Panel of Fail Safe	76
57. Pneumatic Controls of Fail Safe	77

Cleared: December 19th, 1983
Clearing Authority: Air Force Wright Aeronautical Laboratories

INTRODUCTION

Requirements for equipment which must operate at high temperatures and high speeds, have prompted investigations on gas-lubricated bearings to establish the potential usefulness of this technique. The gas bearing has many characteristics which recommend it for such applications. Some of these are:

1. No deterioration at high temperatures.
2. Phase stability
3. Beneficial physical property for load capacity (viscosity increases with temperature).
4. Low friction

The investigations carried on to date have given qualitative evidence that gas bearings can be applied to high-temperature, high-speed applications. However, in order to apply gas bearings to specific designs, quantitative information must be obtained on their performance characteristics.

The research work called for in AF 33(657)-10694 has as its objective the development of nitrogen gas-lubricated journal and thrust bearings that have the best potential for stable operation over the following ranges of operating conditions:

Ambient Temperature: 80 to 1900 F

Speed: 0 to 60,000 RPM

Supply Pressure: to 300 psig

The bearings must support static, unidirectional loads (not rotor mass of up to 100 pounds radial and thrust). Gas flow should not exceed 40 pounds per hour under any operating condition. One additional requirement is to consider situations where the factor controlling performance is dynamic, multidirectional loading, in place of static unidirectional loading. Unless proven impractical for the requirements, the bearing sizes should be no larger than:

1-1/2" diameter x 1-1/2" long radial bearing

1-1/2" diameter thrust bearing

A further requirement has been added: that the design characteristics consider the support of rotor masses from 3 to 30 pounds. This latter is particularly important with respect to dynamic rotor behavior.

This report summarizes the efforts on the subject contract during the second year covering the period March 31, 1964, to March 31, 1965. It includes design considerations, test equipment, instrumentation, and experimental work. Major emphasis was placed on obtaining performance data with regard to establishing the stable operating range of the 360 degree hybrid bearing.

Cleared: December 19th, 1983
Clearing Authority: Air Force Wright Aeronautical Laboratories

BACKGROUND DISCUSSION

In the first annual report (Reference 1), five major problem areas were defined as follows:

1. Obtaining the required load carrying capacity at the minimum flow rate,
2. Achieving stable rotor bearing behavior over the required operating range,
3. Selecting materials with suitable properties,
4. Compensating for geometry changes due to thermal gradients, growth and distortion,
5. The possible deterioration of restrictor and flow passages due to high gas velocity and impingement.

Each of the above represents a major study in its own right. However, each had to be considered, the degree determined by the basic intent of the program. Since the objective was to define gas bearing performance by examining the effects of controlled and dependent variables over an operating range from 80 F to a temperature approaching 1900 F. Items 1; 2 and 4 were given major emphasis. The review and decisions with regard to items 3 and 5, materials selection and deterioration of restrictors and flow passages is summarized in Reference 1.

The remaining items were selected for major attention with regard to the evaluation program. The approach was to generate the bulk of the design information on a geometry which has received sufficient previous attention, and which would serve as a performance datum. At the same time, a more advanced concept was to be explored. To this end, two bearing concepts were selected as the basis for the experimental program:

1. Evaluations on the 360 degree hybrid bearing. These were used to gather design data on the capabilities and limitations of this bearing type as well as to serve as a basis for comparison of other bearing types.
2. The flex pad hybrid bearing. This bearing type, shown in Fig. 42, sought to embody a design which has some of the characteristics of a pivoted shoe type of bearing such as the ability to adjust to certain types of distortion and to have a high stable range of operation. It should be noted that this is an intermediate step in the compensation for geometry changes since this design would not compensate for radial growth.

The detailed discussion of the work on these two bearing types is given in the following sections.

Cleared: December 19th, 1983
Clearing Authority: Air Force Wright Aeronautical Laboratories

360 DEGREE HYBRID BEARING

This bearing type had received by far the greatest attention, analytical as well as experimental, of the externally pressurized bearings. There have been several analytical (References 2 through 5) and experimental (References 6 and 7) treatments. Although these data were not always in readily usable design form, they did form the basis for a logical program formulation.

Load Capacity and Flow Rate

One of the initial steps was to provide the steady state performance data for the 360 degree hybrid bearing in a readily usable form.

For design purposes, the type of information required to define static behavior is as follows:

- a. Load Capacity as a function of bearing geometry and gas properties.
- b. Flow as a function of bearing geometry and gas properties.
- c. Stiffness as a function of bearing geometry and gas properties.

The above information was obtained from an approximate analysis which considered the feeding system as a line feed with an area equivalent to the line of orifices. The data was presented in terms of the dimensionless load \bar{W} , dimensionless flow \bar{q} , and the feeding parameter Λ_s .

These parameters are defined as follows:

$$\Lambda_s = \frac{6\mu N a^2 \sqrt{RT}}{P_s C^3}$$

$$\bar{W} = \frac{W}{DL(P_s - P_a)\epsilon}$$

$$\bar{q} = \frac{6\mu RT \cdot Q}{\pi P_a^2 C^3}$$

Contrails

Cleared: December 19th, 1983

Clearing Authority: Air Force Wright Aeronautical Laboratories

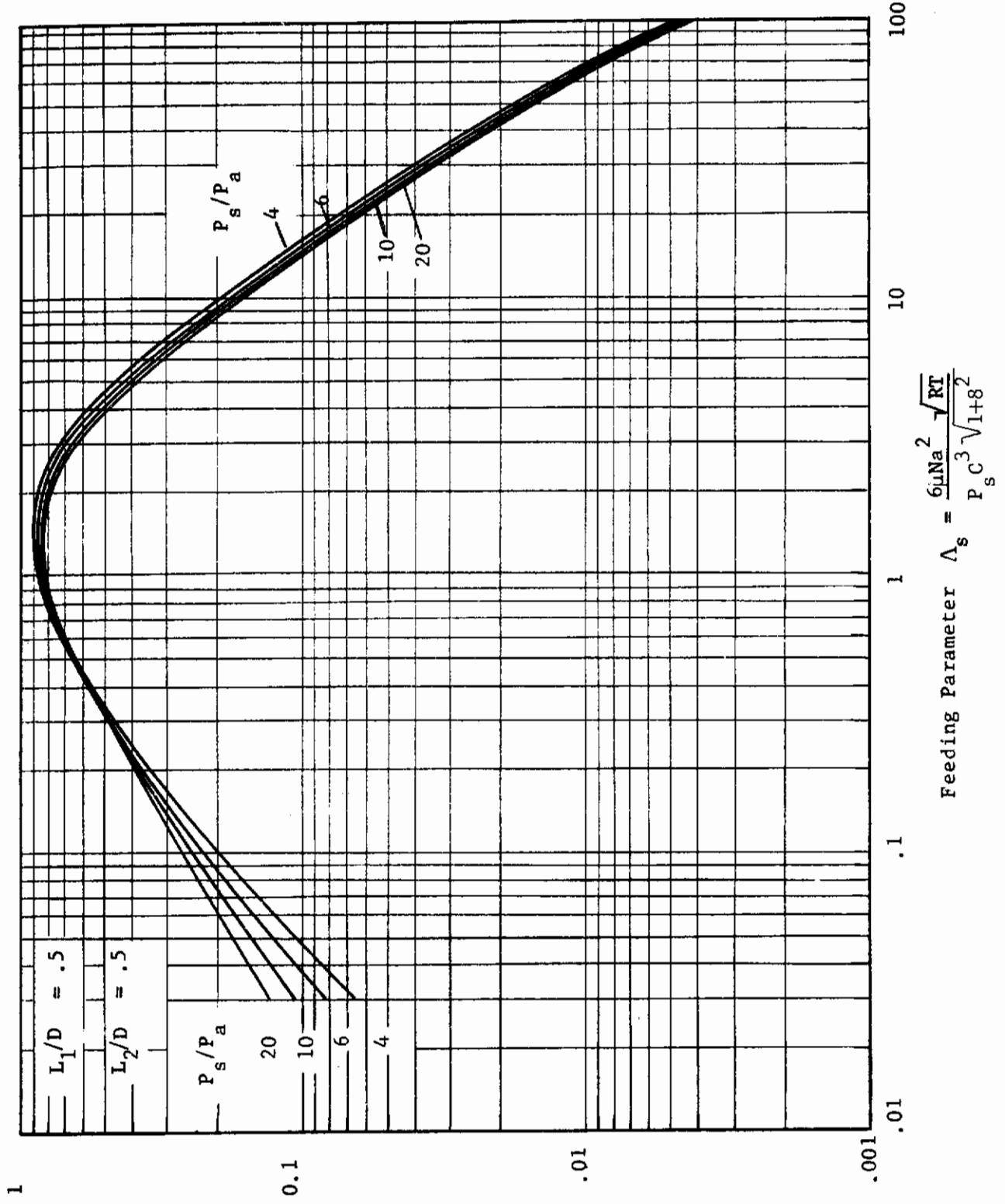
where μ = Viscosity # sec/in²
N = Number of orifices in bearing
a = Orifice radius in
P_s = Supply pressure psia
P_a = Ambient pressure psia
C = Radial clearance in
R = Gas Constant in²/sec² °R
T = Gas Temperature °R
W = Load on bearing #
Q = Gas flow # sec/in

Since $W/\epsilon C$ is bearing stiffness, the dimensionless load may be rewritten as

$$\bar{W} = \frac{KC}{DL(P_s - P_a)} \quad \text{and} \quad K = \frac{\bar{W} DL (P_s - P_a)}{C}$$

where $K = W/\epsilon C =$ bearing stiffness #/in

Figures 1 and 2 which were based on the analysis from Reference 2 present \bar{W} , and q as a function of the feeding parameter Λ_s . These permit determination of load carrying ability, stiffness and flow.



$$W = \frac{DL(P_s - P_a)\epsilon}{W} \left(\frac{1 + 8/2}{1 + 2/3/8} \right)$$

$$\text{Feeding Parameter } \Lambda_s = \frac{6\mu Na^2 \sqrt{RT}}{P_s C^3 \sqrt{1+8^2}}$$

Fig. 1 Load Capacity - Double Row Hydrostatic Bearing

Cleared: December 19th, 1983
 Clearing Authority: Air Force Wright Aeronautical Laboratories

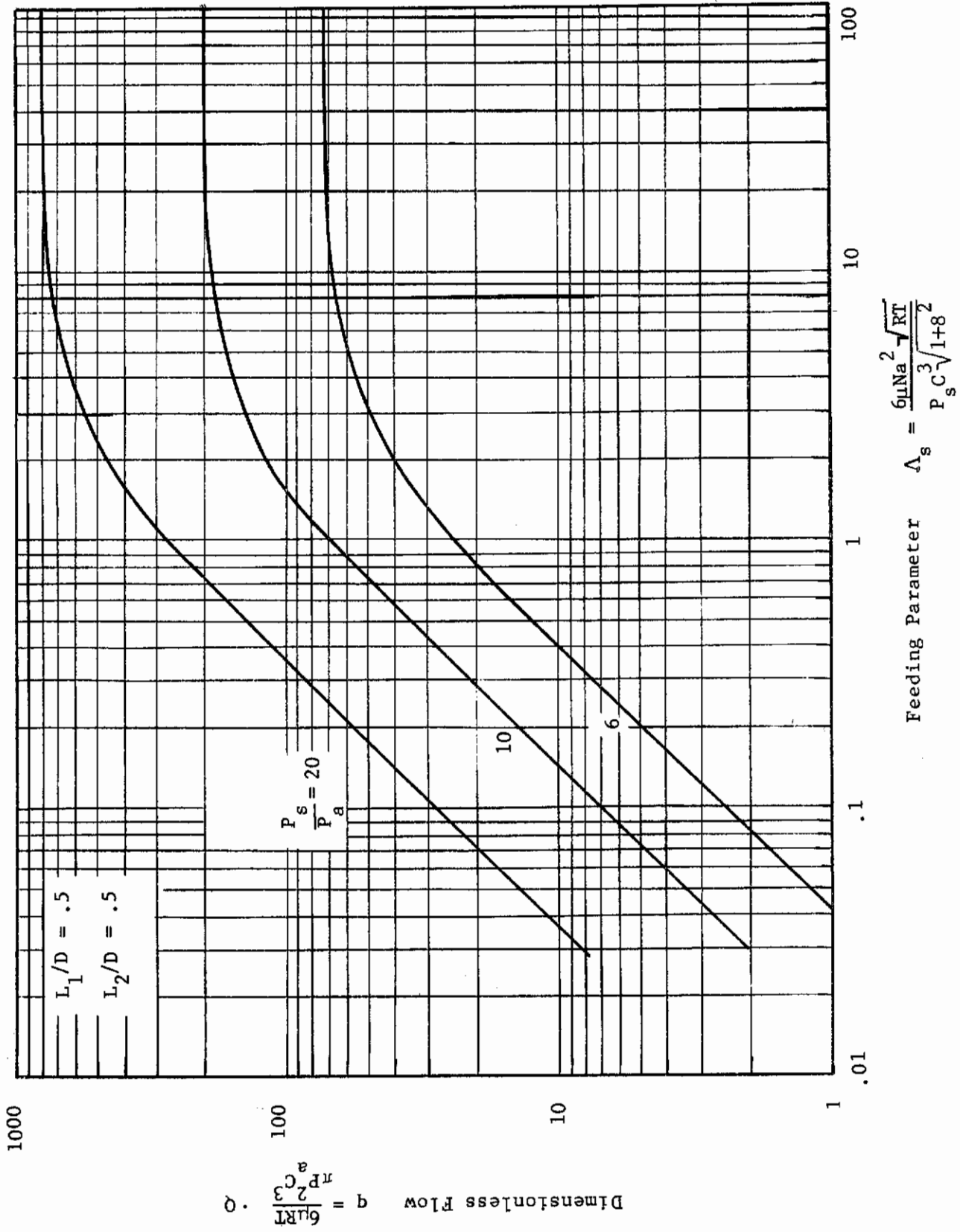


Fig. 2 Flow - Double Row Hydrostatic Bearing

Cleared: December 19th, 1983
 Clearing Authority: Air Force Wright Aeronautical Laboratories
Rotor-Bearing Stability

In considering the approach to the stability problem, two types of information were considered: An analytical prediction of the behavior and previous experimental work. On the basis of previous experimental work, there appeared to be an influence governed both by the feeding system and the relation to the theoretical optimum design point. The analysis of Reference 8 suggests that the whirl threshold speed should be twice the system rigid body critical. Referring to Figure 1, the ordinate is $W/DL(P_s - P_a) \epsilon \left(\frac{1 + \delta^2}{1 + \frac{2}{3} \delta^2} \right)$. This can be used to define stiffness.

$$K = \frac{\bar{W} DL (P_s - P_a)}{c} \left(\frac{1 + \frac{2}{3} \delta^2}{1 + \delta} \right) \quad [1]$$

The translatory rigid body critical is related to the bearing stiffness K and rotor mass M as follows:

$$N_{crit} = \sqrt{\frac{2K}{M}} = \sqrt{\frac{2 W DL (P_s - P_a)}{c M} \left(\frac{1 + \frac{2}{3} \delta^2}{1 + \delta^2} \right)} \quad [2]$$

If the stiffness at the whirl threshold is designated by \bar{W}_t , the

$$N_{FFW} = \sqrt{\frac{2 \bar{W}_t DL (P_s - P_a)}{c M} \left(\frac{1 + \frac{2}{3} \delta^2}{1 + \delta^2} \right)} \quad [3]$$

The ratio of whirl threshold speed to the rigid body critical speed is given by the ratio of Equation 3 to Equation 2 or

$$\frac{N_{FFW}}{N_{crit}} = \frac{\sqrt{\frac{2 \bar{W}_t DL (P_s - P_a)}{c M} \left(\frac{1 + \frac{2}{3} \delta^2}{1 + \delta^2} \right)}}{\sqrt{\frac{2 \bar{W} DL (P_s - P_a)}{c M} \left(\frac{1 + \frac{2}{3} \delta^2}{1 + \delta^2} \right)}} = \sqrt{\frac{\bar{W}_t}{\bar{W}}} \quad [4]$$

If this ratio takes on the value of 2 at the maximum stiffness (optimum value of \bar{W} from Figure 1), Equation 4 can be rewritten

$$\frac{N_{FFW}}{N_{crit}} = \frac{2 \sqrt{\bar{W}_t}}{\sqrt{\bar{W}_{opt}}} \quad [5]$$

As will be described in the experimental portion of the report, this criterion is used as a basis for comparison. The optimum design point is defined by the value of the feeding parameter which yields the maximum load capacity and stiffness parameter as shown in Figure 1.

Contrails

Cleared: December 19th, 1983

Clearing Authority: Air Force Wright Aeronautical Laboratories

A similar procedure is used when the lowest rigid body critical is conical. However, it is often more convenient to base all calculations on the translatory and convert to the conical case. In order to determine which is the lower critical, the whirl ratio is determined.

The whirl ratio, threshold of translatory to conical whirl speeds is given by

$$\frac{\omega_T}{\omega_c} = \sqrt{\frac{12 (I_T - I_P)}{m (3\ell^2 + L^2)} \frac{K_2}{K_c}} \quad (2 \text{ bearing system}) \quad [6]$$

where ω_T = Rotational speed, translatory threshold

ω_c = Rotational speed, conical threshold

I_T = Transverse moment of inertia, about c.g.

I_P = Polar moment of inertia

ℓ = Bearing span, $\underline{\ell}$ to $\underline{\ell}$

L = Bearing length

K_2 = Radial bearing stiffness

K_c = Radial translatory stiffness @ ω_c

For a hydrostatic bearing, K_2 is found experimentally from a load-deflection determination or calculated from Λ versus dimensionless load curves. Another stiffness K_3 is defined as the radial component of tilt, or misaligned, stiffness of the bearing. The relation between K_3 and K_c is given as

$$K_3 = K_c L^2/12 \quad [7]$$

for the externally pressurized bearing $K_c = K_2$ (neglecting hybrid effects) and Equation 6 becomes

$$\frac{\omega_T}{\omega_c} = \sqrt{\frac{12 (I_T - I_P)}{m (3\ell^2 + L^2)}} \quad [8]$$

where m = rotor mass

Cleared: December 19th, 1983
Clearing Authority: Air Force Wright Aeronautical Laboratories

Experimental Program - Low Temperature Evaluations

As was shown in the previous section, the analytical treatment suggested a relation between the system rigid body critical and the threshold of fractional frequency whirl. Also, this relation was predicted to vary with the design point as defined by the feeding parameter Λ_s . It was desirable to establish some reference datum which would be fixed for any specific geometry. The value of feeding parameter and load parameter at the optimum point was selected. The optimum feeding parameter is defined as the feeding parameter which yields the highest value of theoretical load and stiffness. (See Figure 1). The operating feeding parameter based on any given design can then be related to the optimum. Consequently, a ratio of the operating feeding parameter to the optimum feeding parameter is used to designate the operating point. In addition, the threshold speed is related to the rigid body critical based upon the optimum stiffness.

The use of the above permits the use of Figure 1 to define the rigid body critical speed which could be adjusted by a modifying factor to indicate the threshold of fractional frequency whirl.

To achieve the above, the ratio of whirl threshold to rigid body critical was usually plotted as a function of the feeding parameter ratio. Prior experimental data evaluated in this manner yielded the behavior shown in Figure 3. Although this data was not sufficiently complete to permit exact interpretation, there was an indication that a predictable pattern with optimum values existed. In many cases, certain discrepancies appeared to be governed by the degree of compensation. It was therefore decided that the experimental work in this program should be designed to either complete and define the pattern suggested by Figure 3 or to refute the pattern. Therefore, both orifice and inherently compensated bearings were considered.

The first step in the program was to consider the inherently compensated bearing. (Orifices are drilled directly into the bearing bore, and the major restriction is in the bearing film.) The degree of compensation for the inherently compensated bearing is defined by $\delta = a/2c$, where a is orifice radius and c is bearing radial clearance. The second step in the experimental evaluation was to test the orifice compensated bearing. Compensation of this type is obtained by providing small recess at each orifice location at the point where the pressurized gas enters the bearing clearance and immediately downstream of a small diameter orifice. Under these conditions, the annular area described by the recess diameter and the bearing clearance will be significantly larger than the area of the orifice, making the orifice the major restriction.

For the inherently compensated bearing, the degree of compensation was varied by changing clearance and orifice size. Once the largest orifice was evaluated, .040 diameter, orifice inserts were added to obtain purely orifice compensation. This is assured by virtue of the pocket in series with the orifice insert. Figure 4 shows the test bearing. The tests consisted of the following:

Cleared: December 19th, 1983
 Clearing Authority: Air Force Wright Aeronautical Laboratories

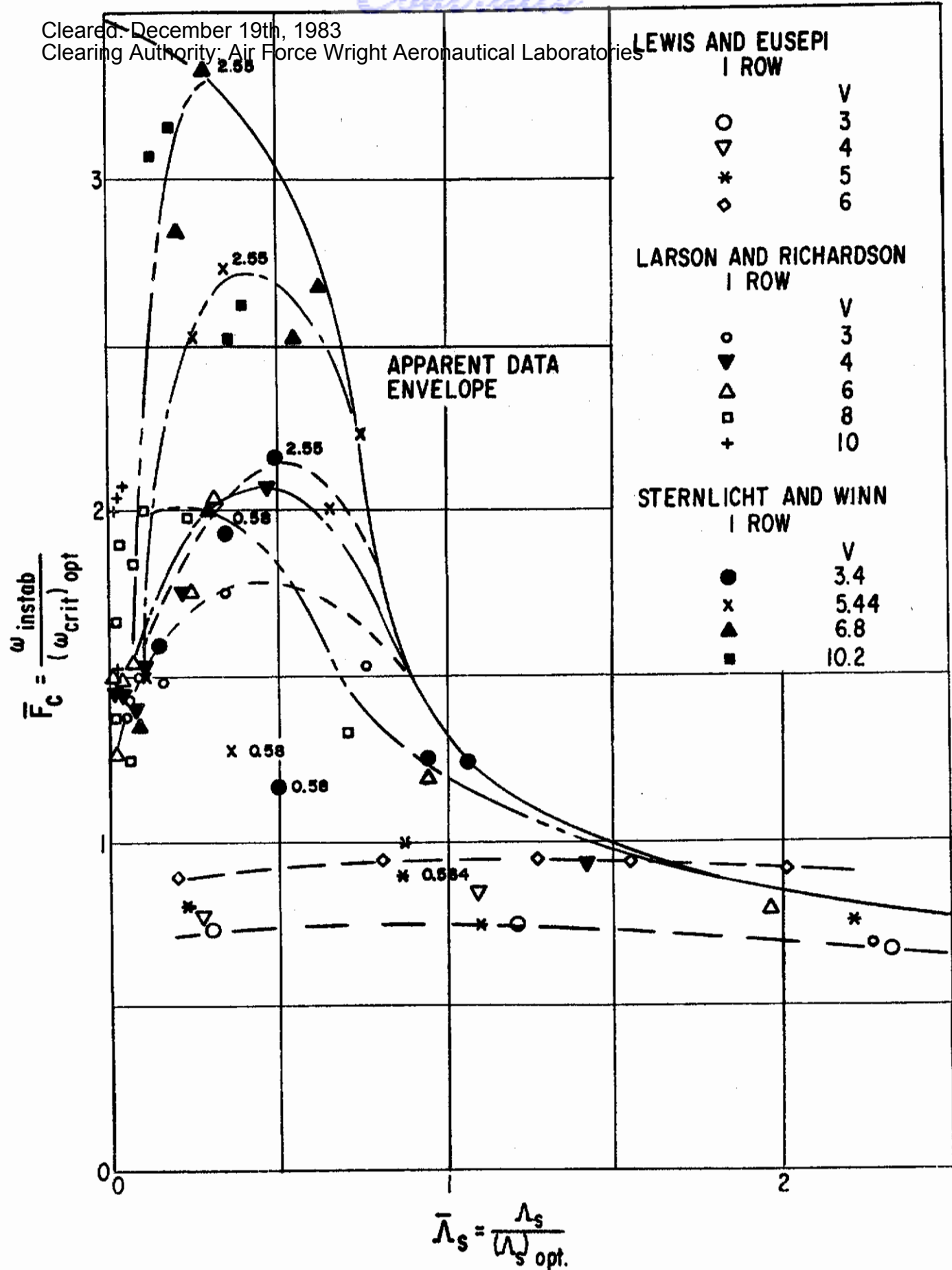


Fig. 3 Speed Ratio versus Feeding Parameter Ratio for 360 Degree Hybrid Bearings

Cleared: December 19th, 1983
 Clearing Authority: Air Force Wright Aeronautical Laboratories

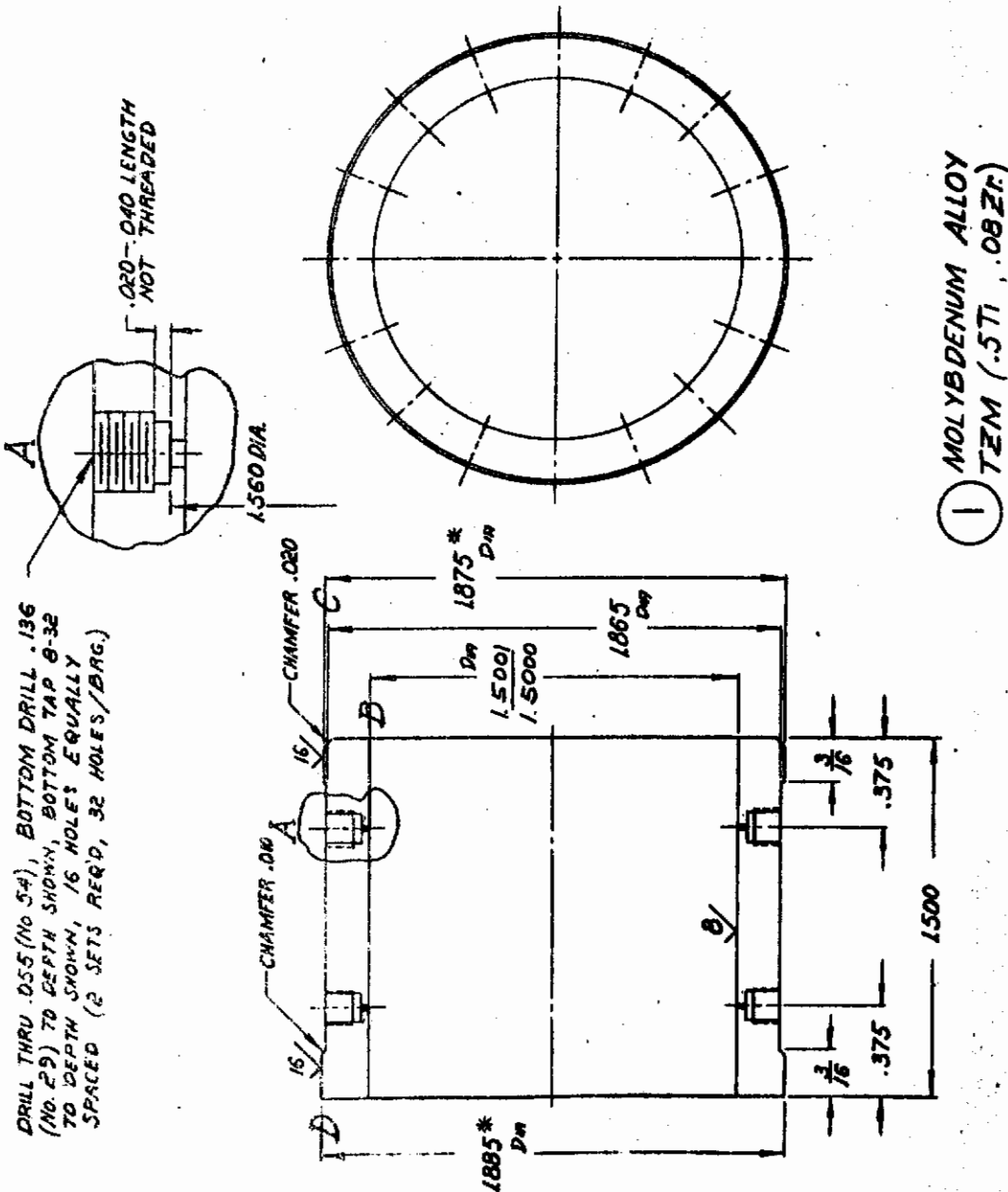


Fig. 4 360 Degree Test Bearing

Contracts

Cleared: December 19th, 1983

Clearing Authority: Air Force Wright Aeronautical Laboratories

1. Inherently compensated configurations (orifices drilled directly into bearing clearance)
 - 1.1 With each of three different orifice diameters, namely 0.0135, 0.026, 0.040 inches
 - 1.1.1 With each of three different radial clearances, namely .0013, .00165, .00215 inches
 - 1.1.1.1 At each of 12 pressure ratios where applicable from 1.5 to 20, tests are made to determine the following:
 - 1.1.1.1.1 Static stiffness and flow
 - 1.1.1.1.2 Whirl threshold and whirl ratio for selected tests
 - 1.1.1.1.3 Critical speed and phase angle (for selected combinations of the above factors)
 - 1.1.1.1.4 Variation of whirl threshold with eccentricity, (for selected combinations of the above factors)
2. Orifice compensated configurations
 - 2.1 With a pocket diameter of 0.040 inches
 - 2.1.1 With an orifice diameter of 0.0135 and a clearance of 0.0012 inches
 - 2.1.1.1 At pressure ratios from 1.5 to 20, tests to determine the following:
 - 2.1.1.1.1 Static stiffness and flow
 - 2.1.1.1.2 Whirl threshold and whirl ratio
 - 2.1.1.1.3 Critical Speed
 - 2.2 With a pocket diameter of 0.080, orifice diameter of 0.0135, clearance of 0.0012, same tests as under 2.1 above.

Generally the test procedure consisted of assembling the unit with a given shaft-bearing combination; establishing the static stiffness as a function of pressure ratio; using the loading bearing to balance the shaft weight to bring the eccentricity to zero; and determining the whirl threshold speed as a function of pressure ratio. The feeding parameter Λ_s is a function of geometry, type of gas, temperature and supply pressure. Consequently, the variation of supply pressure results in varying the value of Λ_s . As was previously mentioned, the dimensionless treatment of the data consisted of relating the operating Λ_s to the value at the optimum and the ratio of the observed whirl threshold Λ_s to the rigid body critical based on the optimum stiffness. There are, of course, many different ways in which this data can be presented. Among these referring the critical to the inherently compensated stiffness or basing the critical upon the measured stiffness. For design purposes, the optimum value as deduced from a chart like Figure 1 is most convenient since it is invariant and can be defined without test.

Cleared: December 19th, 1983

Clearing Authority: Air Force Wright Aeronautical Laboratories

For the inherently compensated bearings tested during this portion of the program, the static stiffness data is summarized in Figures 5, 6, and 7. Figure 5 shows the static stiffness for an orifice or nozzle diameter of 0.0136 inches and three shaft clearances. The theoretical stiffness is also plotted for comparison. There is reasonable agreement between theory and experiment in the low range of pressure ratios. At higher pressure ratios, the experimental stiffness falls considerably below that predicted theoretically. Figure 6 shows the stiffness data for a nozzle diameter of 0.026 and three shaft clearances. A similar trend is exhibited with the measured stiffness lower than the theoretical at higher pressure ratios. Only the data for a radial clearance of .00215 inches ($\delta = 3.02$) agreed closely over the range of pressure ratios tested. In fact, the measured stiffness exceeded the theoretical for a portion of the range. Figure 7 shows the stiffness data for a nozzle diameter of 0.040 inches and three shaft clearances. These data show the greatest deviation between predicted and measured stiffness. The predicted is the theoretical value as found from Figure 1.

For purposes of this program, inherent compensation is defined as the geometry which has δ factors equal to or greater than 1-1/2. The orifice compensated bearings are defined as those with a δ factor of less than 1. However, strictly speaking, the orifice compensation should exist when the δ factor is 1/2 or less. The region of δ around 1 is probably a combination of the two.

The comparison between measured and predicted flow is presented in Figures 8, 9, and 10. Figure 8 shows the flow data for a nozzle diameter of 0.0136 inches and three shaft clearances. Generally the flows are higher than predicted for this nozzle size. Figures 9 and 10 show the flows for nozzle diameters of 0.026 and 0.040 inches respectively. The agreement between measured and predicted flow is excellent.

Figures 11, 12 and 13 show the whirl threshold speed as a function of pressure ratio for these same bearings. Figure 11 shows the threshold speed for a nozzle diameter of 0.0136 inches. There is a qualitative agreement with stiffness data previously presented. Of particular interest is the data for $\delta = 2.06$ which shows a decrease in whirl threshold speed at high pressure ratios, greater than 10 (Figure 5 shows the corresponding stiffness plot). Figure 12 shows similar data for a nozzle diameter of 0.026 inches. Again, there is qualitative agreement between the stiffness and whirl speed. It will be noted that the data for a δ of five only goes to a pressure ratio of seven. The limit was

Cleared: December 19th, 1983

Clearing Authority: Air Force Wright Aeronautical Laboratories

set by the turbine. Significantly, however, achievement of the desired 60,000 RPM was not a problem with the 3.70 pound rotor used in the evaluations. Figure 13 shows the whirl threshold speed data for a nozzle diameter of 0.040 inches. There are "dips" in the data for δ values of 6.06 and 4.65. These would not have been predicted from the stiffness data of Figure 7.

The preceding data was presented in dimensional form first so as to avoid some of the confusion which can result from the treatment in dimensionless form. As was previously mentioned, the test program was designed to consider the data as indicated in Figure 3. The analysis of Reference 8 suggests that the whirl threshold speed should be twice the system rigid body critical.

Equation 5 can be plotted as a function of the ratio of operating feeding parameter to the optimum feeding parameter. This provides a predicted envelope of the whirl speed ratio to the geometry as defined by the feeding parameter. The nondimensional data treated in this manner is shown in Figure 14.

Figure 14 shows a similar trend to the data previously reviewed and plotted on Figure 3. Although the maximum achievable ratio of whirl threshold to optimum rigid body critical appears to be two as predicted by the analysis, this does not correspond to the theoretical envelope predicted by the analysis. This indicated that the achievable ratio of whirl threshold to rigid body critical for the inherently compensated bearing was strongly influenced by the degree of compensation. The plot of Figure 14 offers a reasonable means for estimating the stable speed range. At this time, compensation in the order of $\delta = 2$ is indicated.

In order to determine the effect of mass, two rotors with masses greater than the steel rotors yet duplicating all other dimensions were tested in a set of inherently compensated bearing tests. The bearing clearances provided by the two heavy shafts (TZM alloy rotors each weighing 4.79 pounds) were identical to clearances obtained with two lighter shafts (steel rotors each weighing 3.7 pounds). In a dimensional presentation such as in Figure 15, the heavier rotor gives lower threshold speeds. This can be explained in the following manner. For a given set of operating conditions, the whirl threshold speed is some multiple of the lowest shaft critical speed, which is in turn inversely proportional to the square root of rotor mass (\sqrt{M}).

A verification of the dimensionless presentation however can only be obtained if the ratio of threshold speeds is identical to the square root of the mass ratio in the same order. Figure 16 confirms the dimensionless presentation. Except for some deviation at high Λ_s (corresponding to low supply pressures where experimental error is more pronounced) the agreement between the TZM and steel rotor data is excellent.

Cleared: December 19th, 1983
 Clearing Authority: Air Force Wright Aeronautical Laboratories

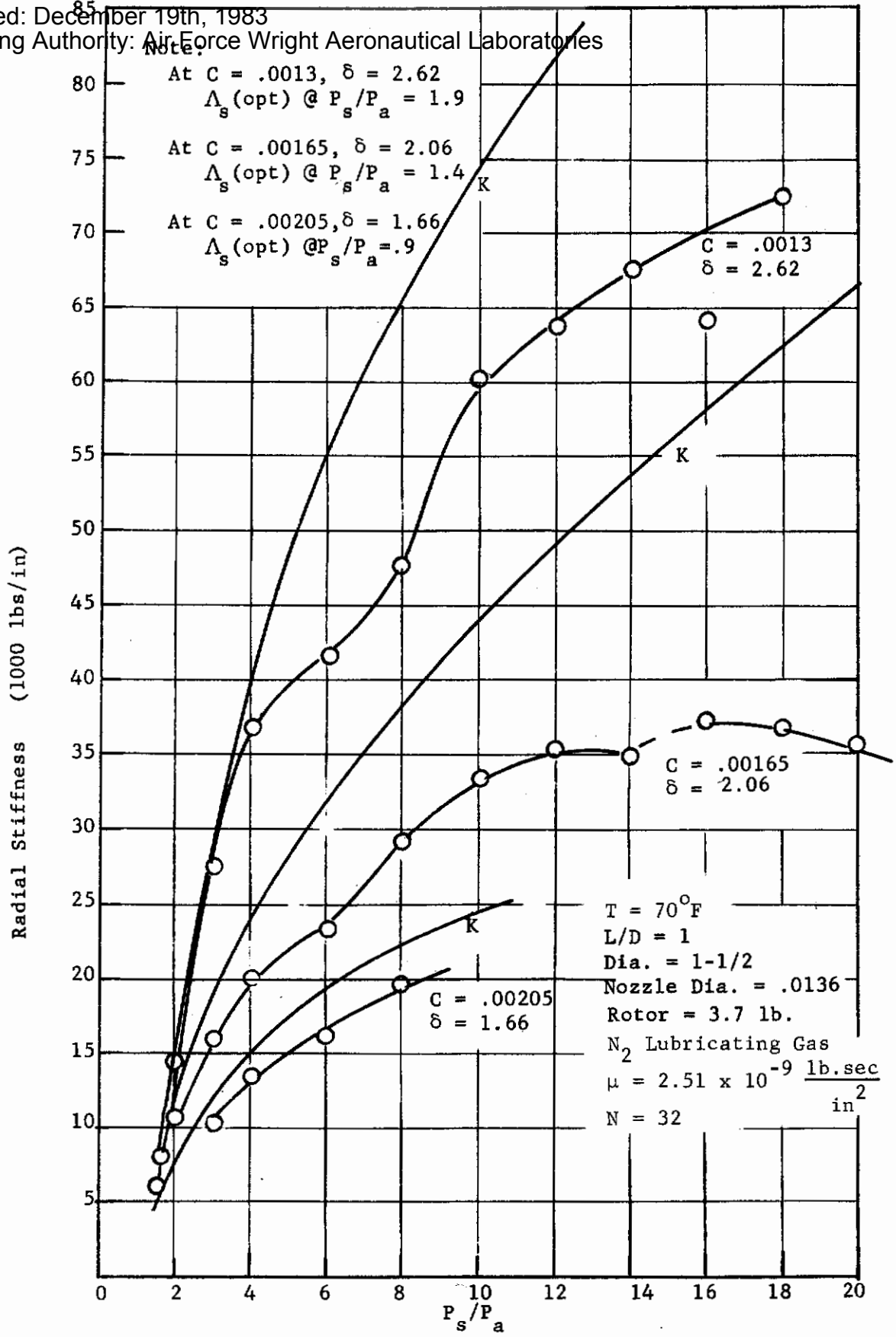


Fig. 5 Radial Stiffness as a Function of Supply Pressure $2a = .0136$

Cleared: December 19th, 1983

Clearing Authority: Air Force Wright Aeronautical Laboratories

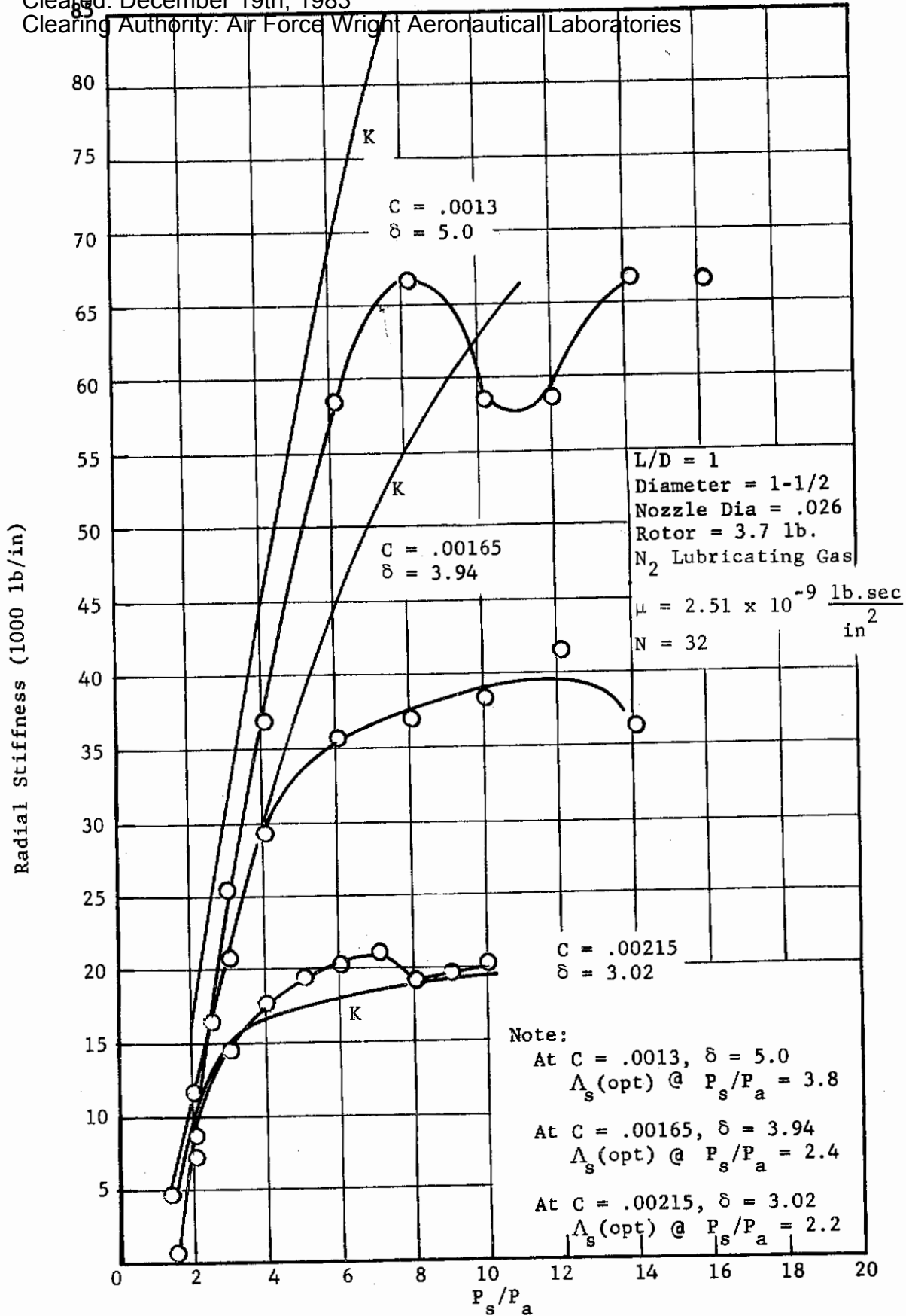


Fig. 6 Radial Stiffness as a Function of Supply Pressure $2a = .026$

Cleared: December 19th, 1983
Clearing Authority: Air Force Wright Aeronautical Laboratories

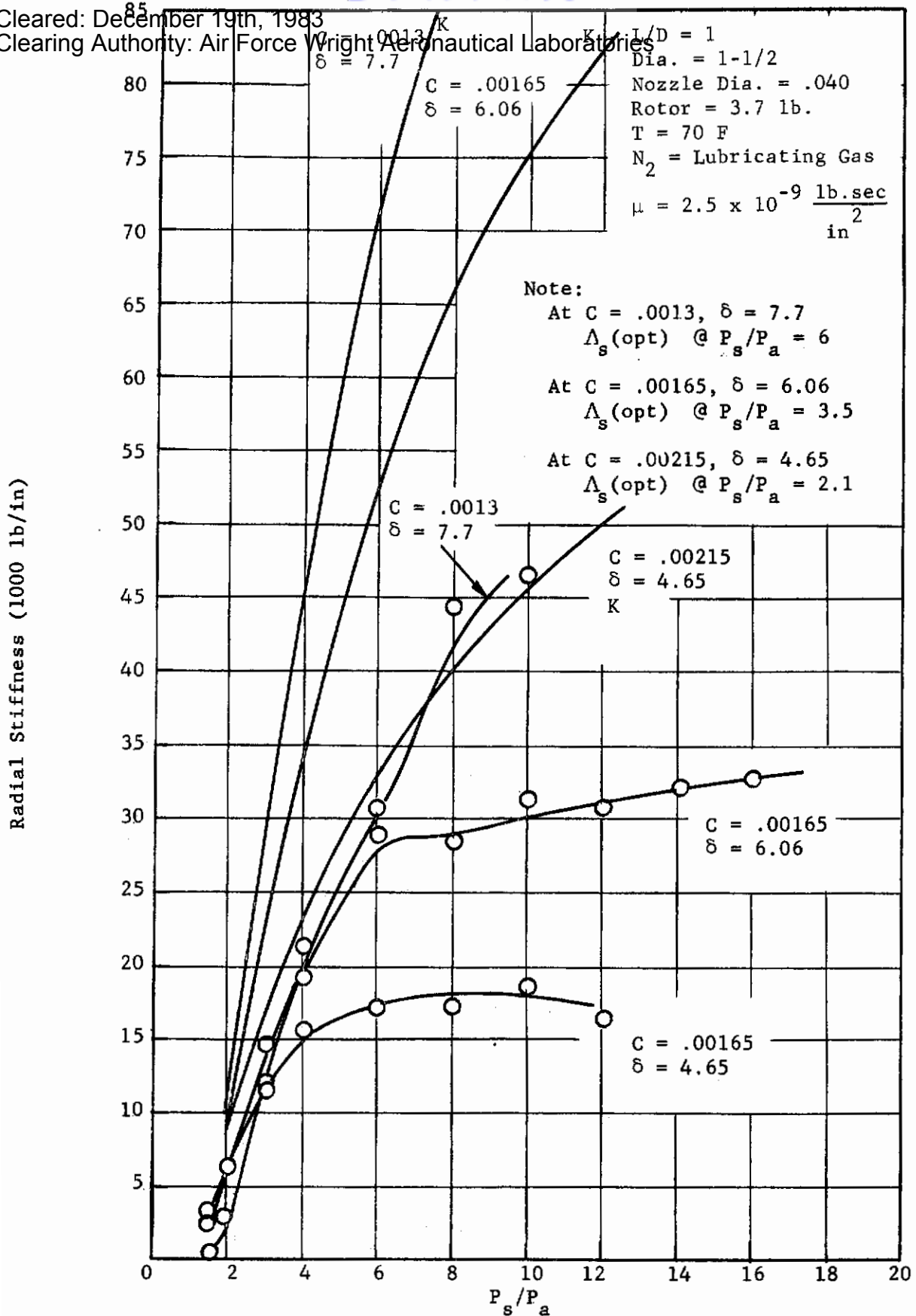


Fig. 7 Radial Stiffness as a Function of Supply Pressure $2a = .040$

Cleared: December 19th, 1983

Clearing Authority: Air Force Wright Aeronautical Laboratories

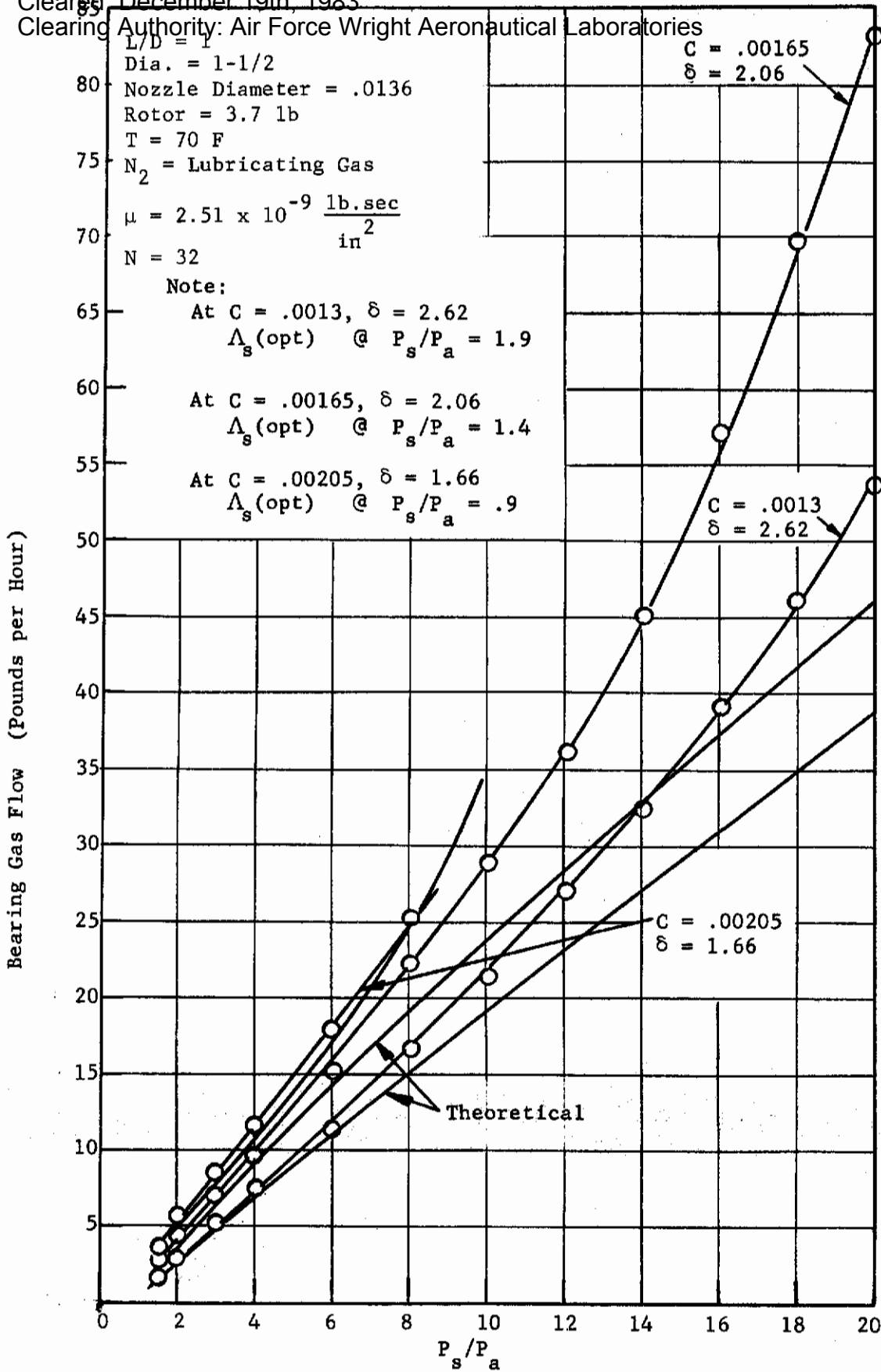


Fig. 8 Bearing Gas Flow as a Function of Supply Pressure $2a = .0136$

85
 Cleared: December 19th, 1983
 Clearing Authority: Air Force Wright Aeronautical Laboratories

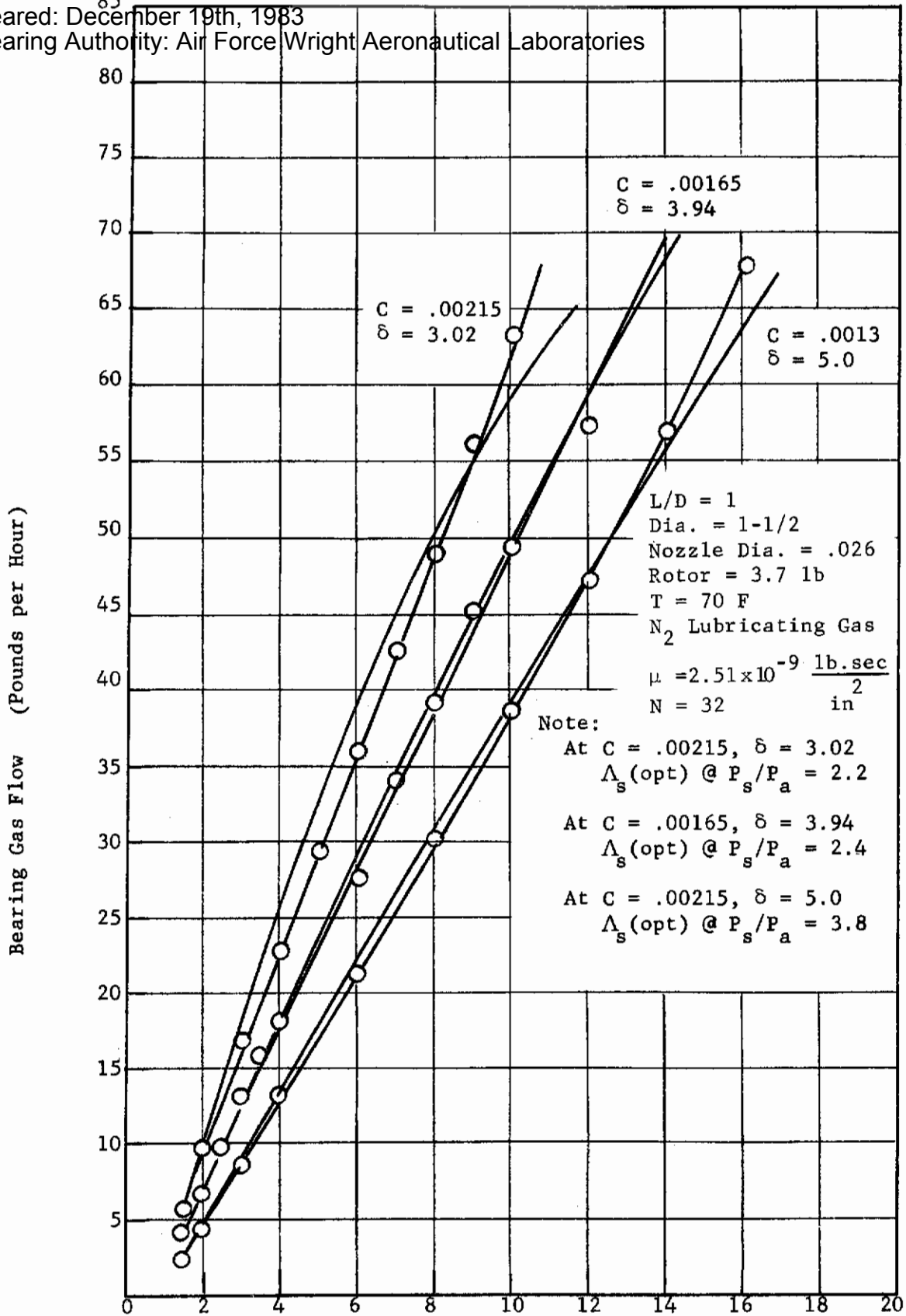


Fig. 9 Bearing Gas Flow as a Function of Supply Pressure $2a = .026$

Classified: December 19th, 1983

Clearing Authority: Air Force Wright Aeronautical Laboratories

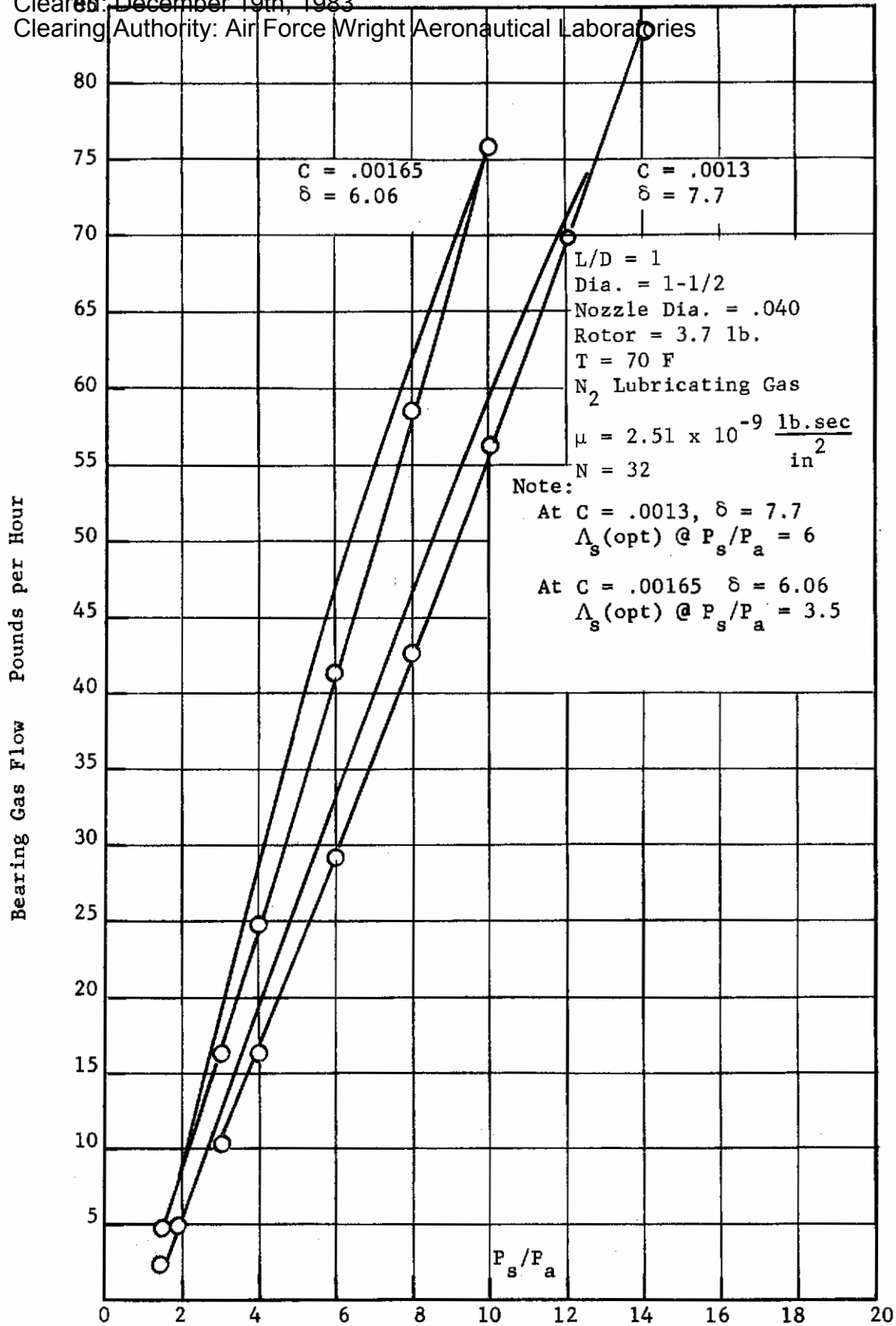


Fig. 10 Bearing Gas Flow as a Function of Supply Pressure $2a = .040$

Cleared: December 19th, 1983
 Clearing Authority: Air Force Wright Aeronautical Laboratories

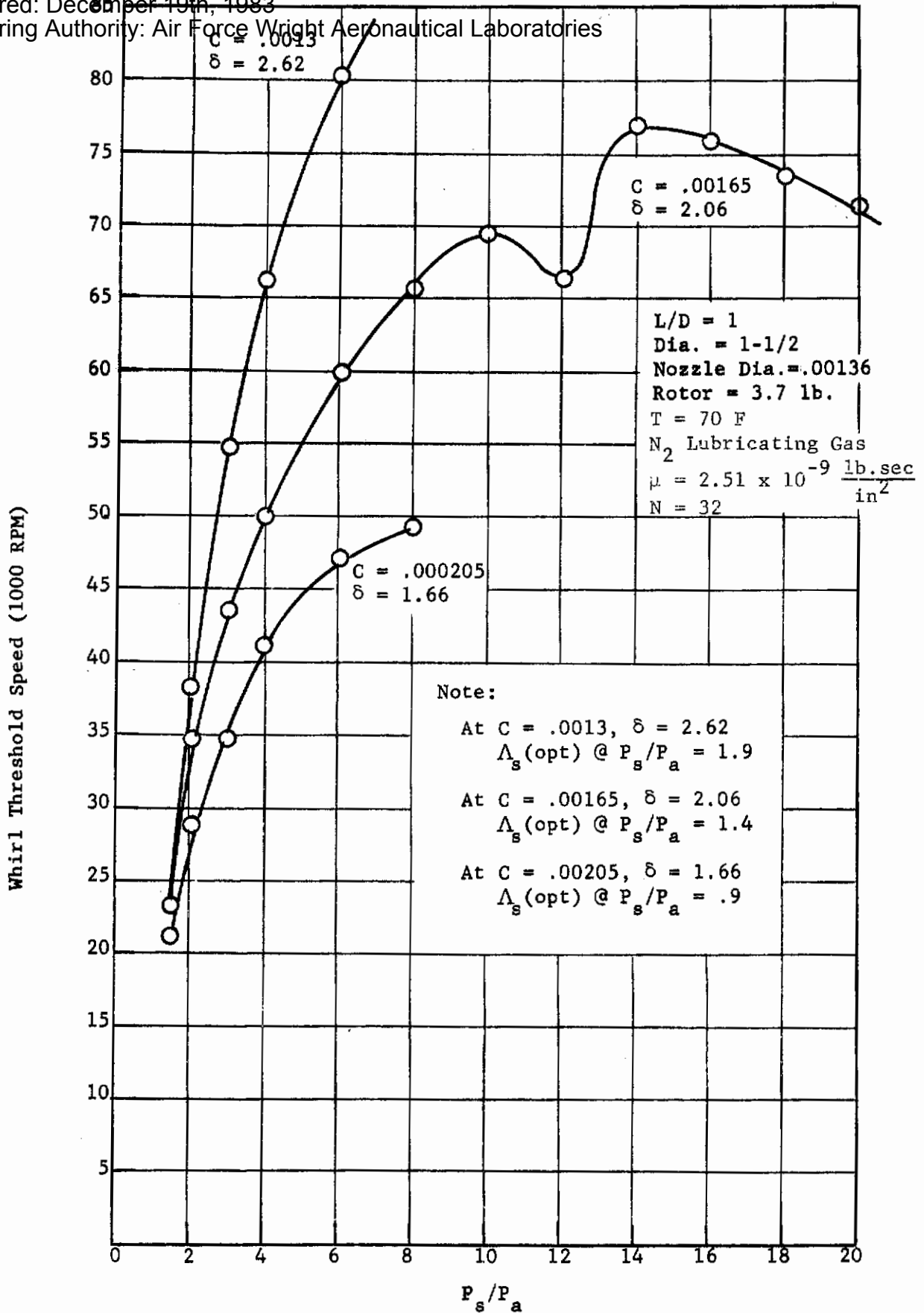


Fig. 11 Whirl Threshold Speed as a Function of Supply Pressure $2a = .0136$

Cleared 05 December 19th 1983
 Clearing Authority: Air Force Wright Aeronautical Laboratories

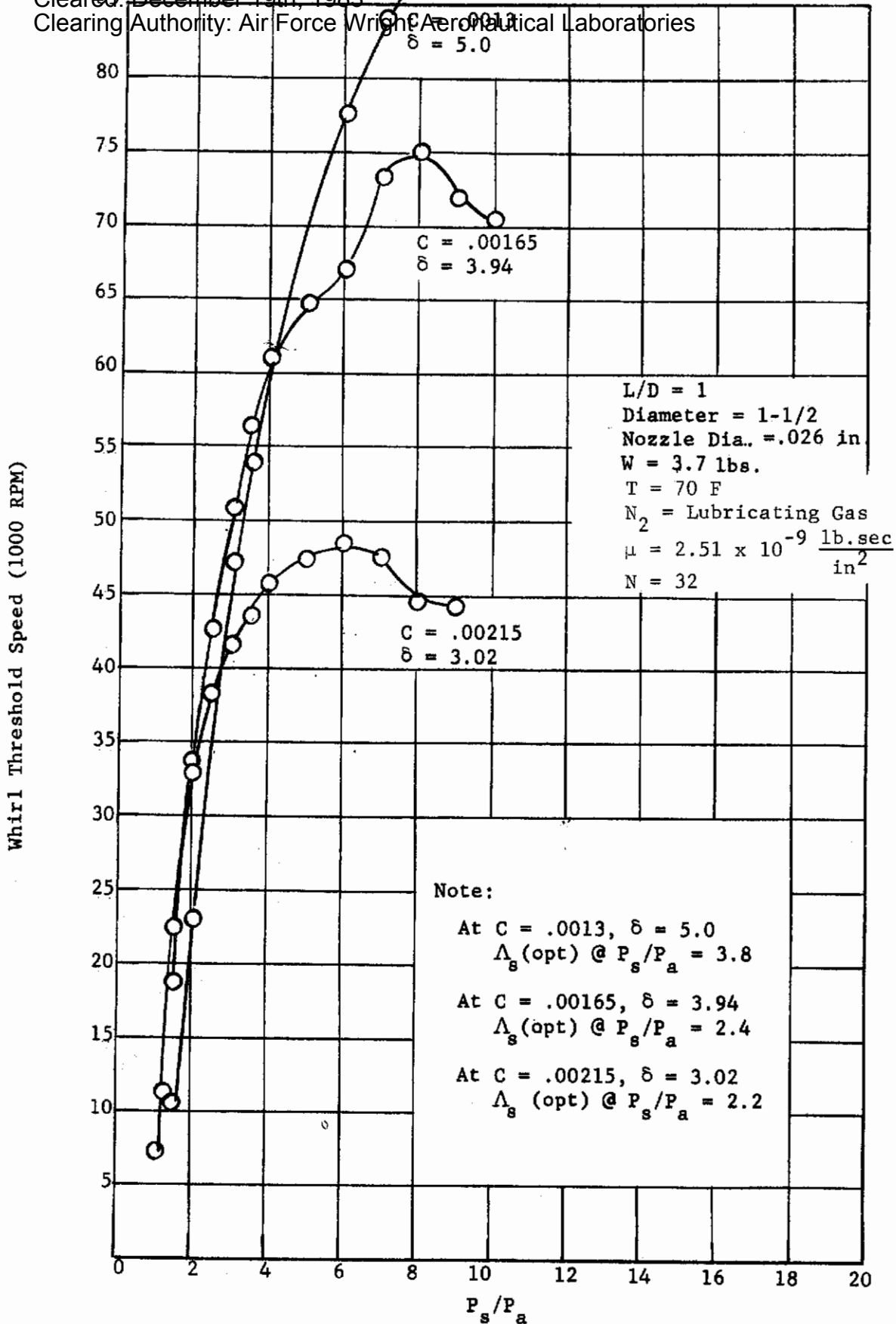


Fig. 12 Whirl Threshold Speed as a Function of Supply Pressure $2a = .026$

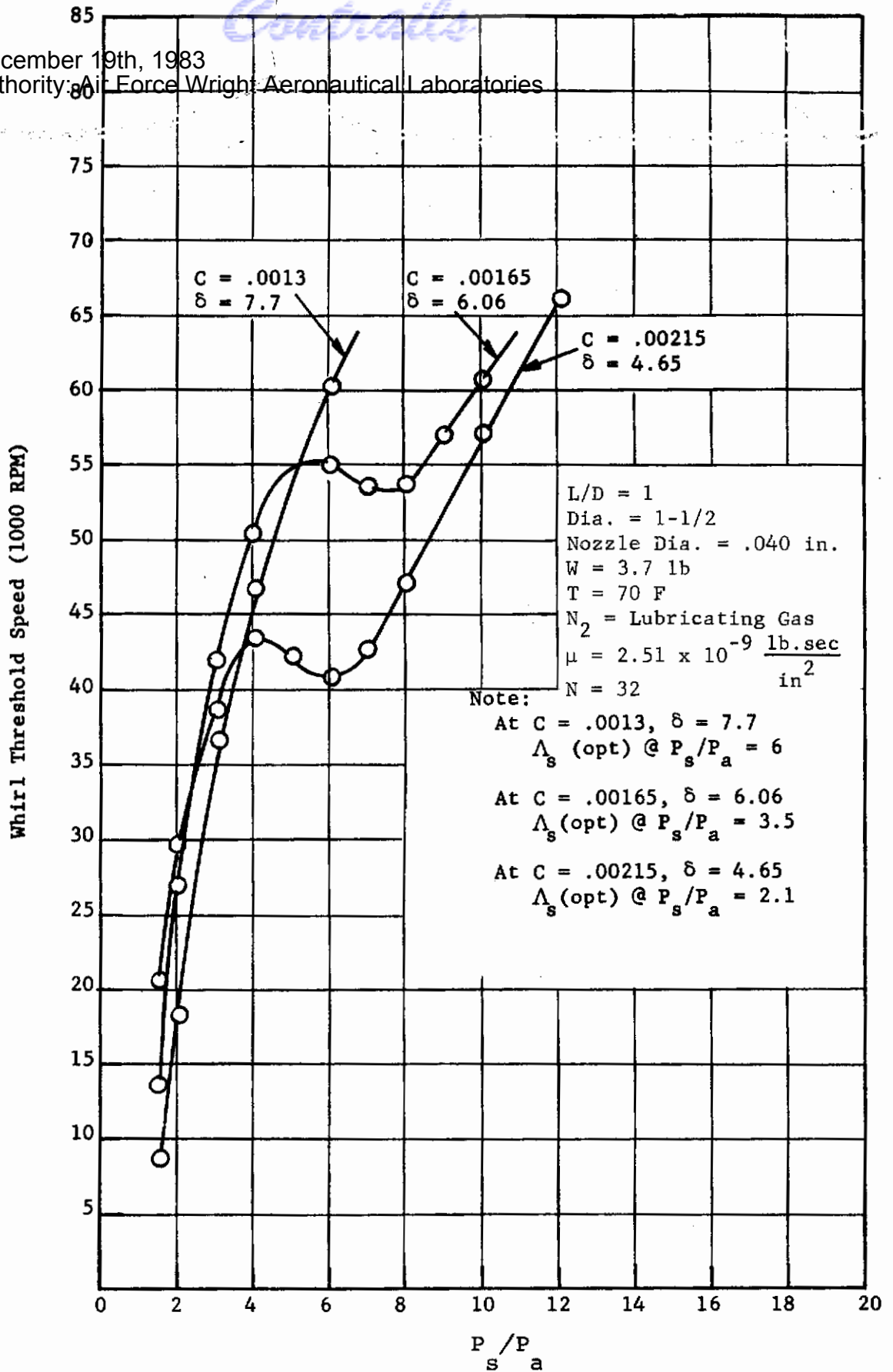


Fig. 13 Whirl Threshold Speed as a Function of Supply Pressure $2a = .040$

Cleared: December 19th, 1983

Clearing Authority: Air Force Wright Aeronautical Laboratories

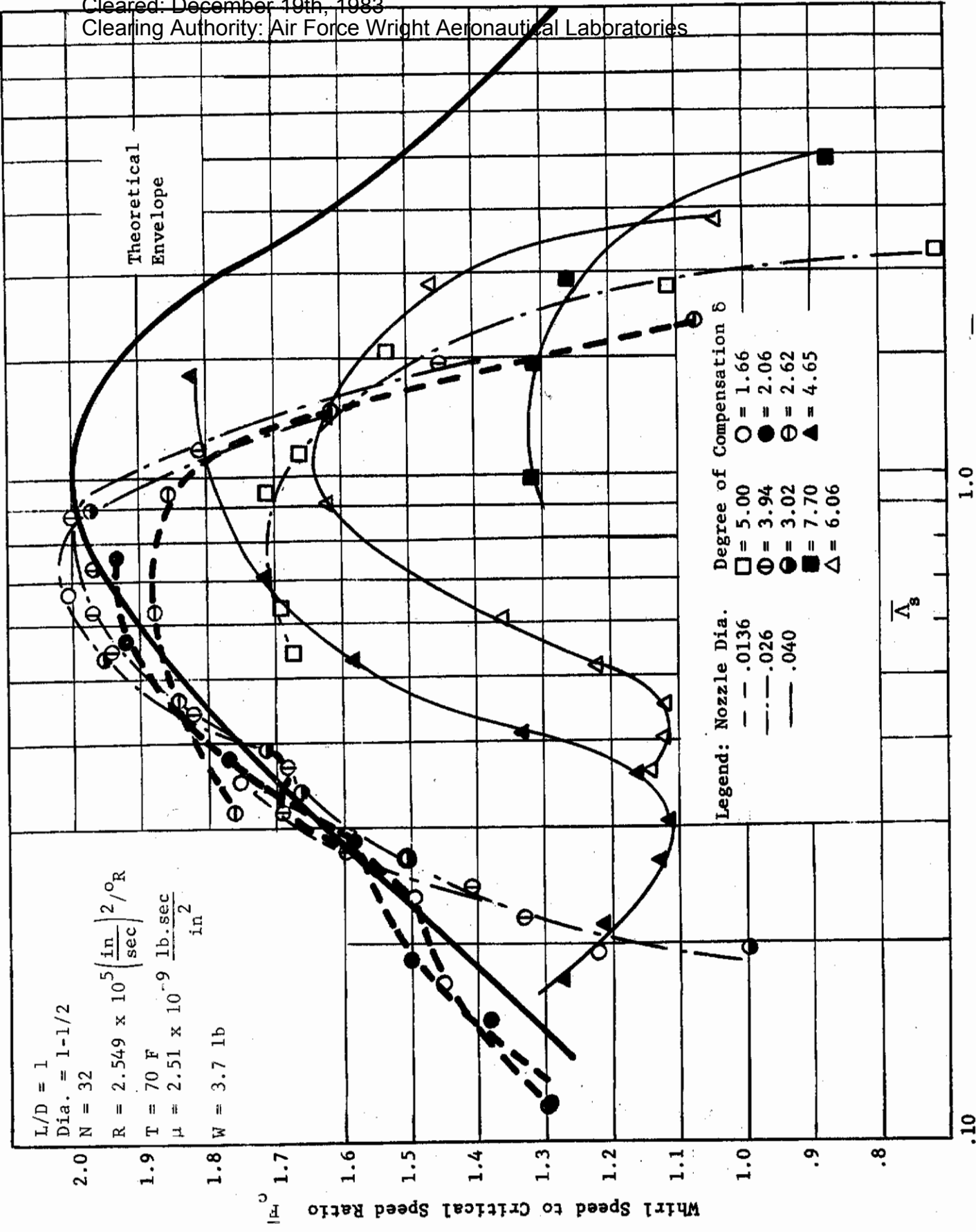


Fig. 14 Speed Ratio versus Feeding Parameter Ratio (Λ_s) - Inherently Compensated 360 Degree Hybrid Bearings

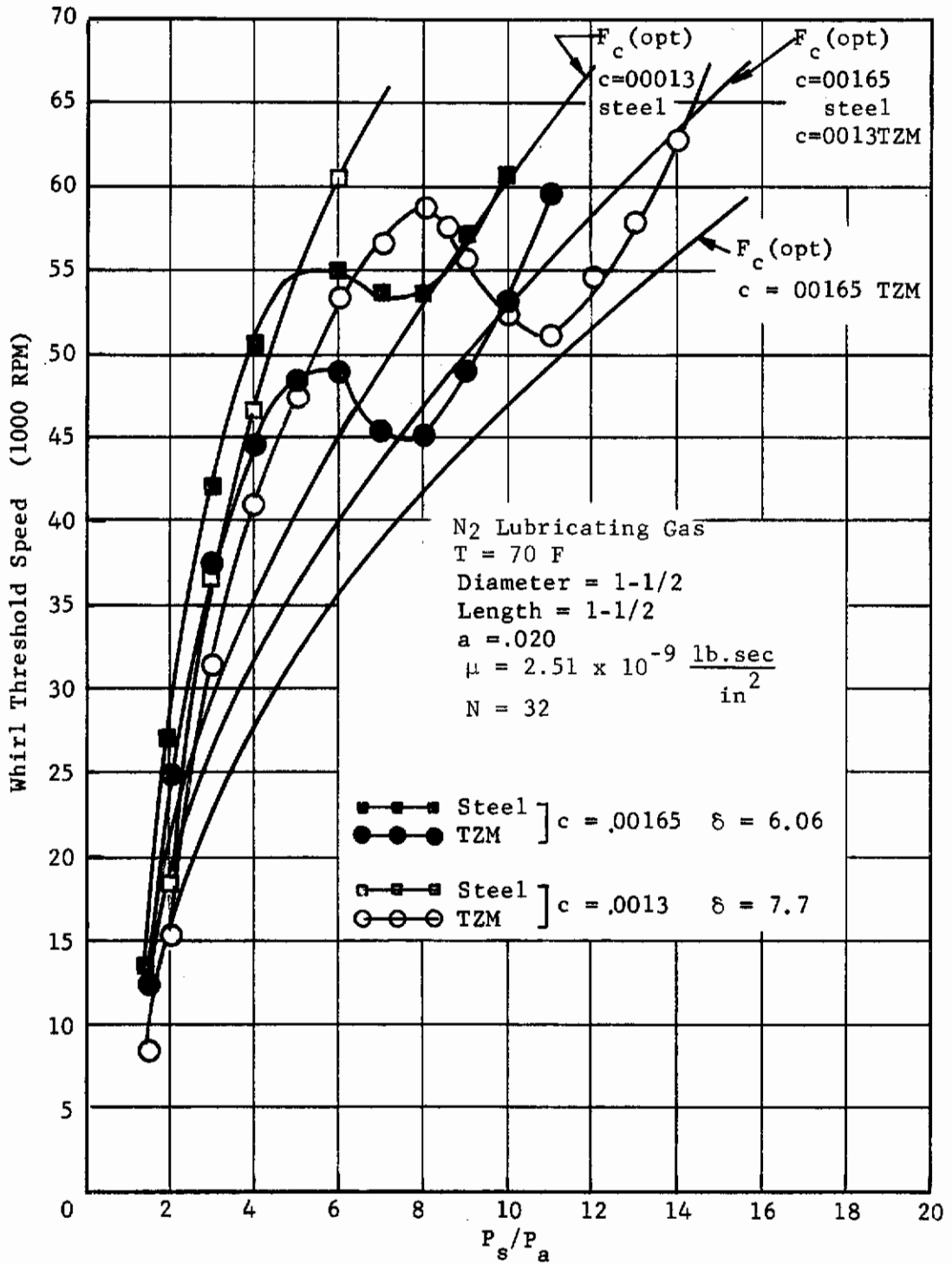


Fig. 15 Whirl Threshold Speed as a Function Supply Pressure for Two Rotor Masses

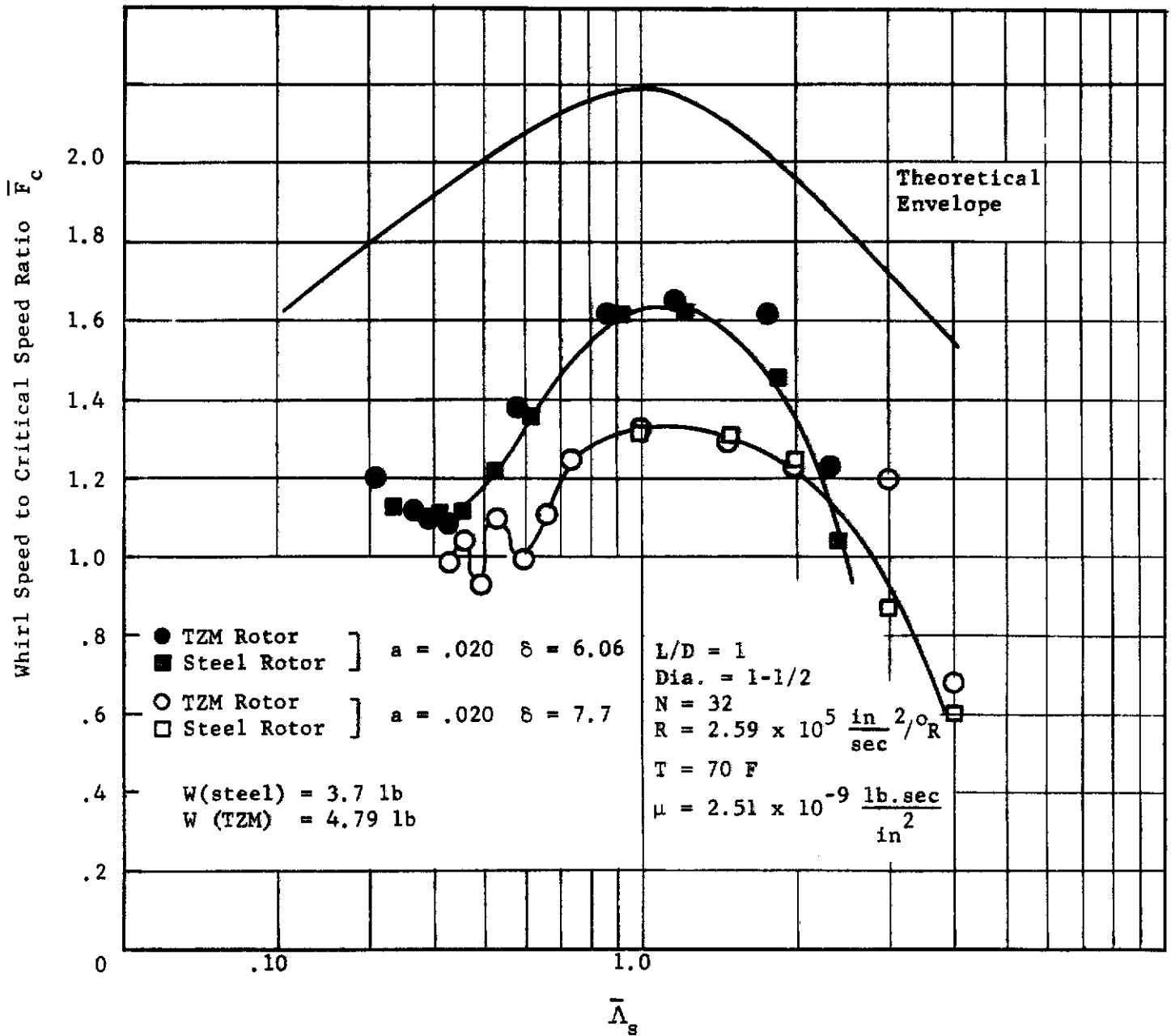


Fig. 16 Speed Ratio versus Feeding Parameter Ratio $\bar{\Lambda}_s$ - Comparison of Two Rotor Masses

Cleared: December 19th, 1983

Clearing Authority: Air Force Wright Aeronautical Laboratories

360 Degree Hybrid Bearing, Orifice Compensated

The term orifice compensation refers to the orifice as the major restriction in the feeding system. This is accomplished by providing a recess between the restrictor and the bearing wall. The bearing compensation number δ is now defined as

$$\delta = \frac{a^2}{dc}$$

where a = orifice radius inches
d = recess diameter inches
c = radial clearance inches

The smallest value of δ achieved during the inherent compensations tests was 1.66 which indicates that the cross section area of the orifice was greater than the annular area leading into the bearing clearance. With the orifice compensation tests the largest value of δ tested was 0.942 with a minimum value of 0.285. These small values of δ indicate that the annular restrictor at the entrance to the bearing film is no longer the major factor in controlling bearing flow but that control has now shifted to the orifice itself.

The orifice compensated bearing test series was performed in two parts; the first using clearances provided by three rotors of different diameters, an orifice diameter of 0.136 inches and a recess diameter of 0.040 inches; the second with the same rotors and orifice diameter but with a recess diameter of 0.080 inches. For each clearance, orifice size and recess diameter combination both the static and dynamic behavior of the rotor system was investigated over a wide range of supply pressures. The static properties investigated were bearing flow and stiffness (via load deflection data); critical speeds and instabilities were the dynamic behaviors studied.

Results of these investigations are presented in graphical form in Figure 17 through 25 and are divided into major groups as follows. Figures 17 and 18 give the flow data for all orifice compensated bearing tests. Figures 19 and 20 show bearing stiffness resulting from analysis of the load deflection data; Figures 21 through 25 show the observed critical speeds and instabilities. In Figure 26 are several photographs of CRO traces showing some of the typical forms the instabilities and critical speeds shown in Figures 21 and 22 take.

Cleared: December 19th, 1983

Clearing Authority: Air Force Wright Aeronautical Laboratories

Test Results for .040 Inch Recess

Test results for the first orifice compensation case tested (recesses diameter = .040) all were operated with $\delta > .5$ and all exhibited behavior similar to that of the inherent compensation cases.

Agreement between theory and experiment with required bearing flow fell within the approximate 20 percent range and caused no surprises (see Figure 17). For the most part, theoretical and experimental stiffness agreement was passable only for the low supply pressure cases. Except for an unexplained apparent loss of stiffness for $\delta = .94$ (see Figure 19) the experimental stiffness was substantially higher than the theoretical counterpart. This trend, however, is opposite to that experienced with the inherently compensated bearings.

The instability observations made during dynamic testing are shown in Figure 21. These instabilities were all fractional frequency translatory whirl. Again the effect of supply pressure and δ are identical to that found with inherent compensation. Threshold speeds rise with increasing supply pressure. However, at constant supply pressure, the whirl threshold is lower for small value of δ .

The dimensionless plot for the above bearing is shown in Figure 25. Although the shape of the plot appears to be consistent with previous data, the values are lower than would be expected from Figure 14.

Generally, for δ between .57 and .94, the absolute values of stiffness and threshold speed were not significantly different from the inherently compensated bearing. However, flow was generally higher. No real advantage was found for the orifice compensation in this range.

Cleared: December 19th, 1983

Clearing Authority: Air Force Wright Aeronautical Laboratories

Test Results for .080 Inch Recess

The second set of orifice compensation runs was made with a recess diameter increased to 0.080 inches. The static testing indicated again that good agreement between theoretically predicted and experimentally determined flow can be expected (Figure 18). An improvement in the prediction of stiffness can be noted in Figure 20 at very low δ values. This result is consistent with analysis since the theory assumes pure orifice compensation.

The largest deviation from previous test data trends occurred during the dynamic testing of this phase of the program. At no time when running the small δ orifice compensated bearings did pure fractional frequency whirl occur. This is not to imply that no instabilities occurred, as can be seen in Figures 22-24. The testing was plagued with instabilities. Since at no time was the ratio of the instability frequency to the running frequency equal or less than 1/2, fractional frequency whirl was not present. The conclusion to be drawn is that the instabilities were rotationally induced air hammer. In general, the observations followed this pattern:

1. At the lower pressure ratios, $P/P_a \leq 3$ distinct translatory rigid body critical speed is observed.
2. At the low supply pressures at speeds above the observed rigid body critical a threshold of instability is reached. This instability takes the form of very large orbit patterns on the scope screen. The angular velocity of the shaft center with respect to the bearing center corresponds to the rigid body critical frequency. This angular velocity remains unchanged with increases in rotor speed, however the amplitude increases. The maximum speed is limited by the bearing clearance. Similarly, the angular velocity of the instability is not changed by decreasing speed up to the point where the instability is no longer self-sustaining.
3. At higher pressure ratios, $P/P_a > 3$ the threshold of instability is below the first rigid body critical.
4. Under some operating conditions at a rotor speed exactly 1/2 the instability frequency an increase amplitude was observed on the CRO trace monitoring the journal. The vibration is translatory in nature and has an angular velocity identical to the instability frequency. Normally, the speed could be increased beyond this points.
5. At higher pressure ratios, the threshold speed was less than or equal to the instability frequency.

Figure 26 groups several photographs of some data points shown in Figure 22. Photograph 26a shows the results of a rotor operating above the rigid body critical with an instability frequency corresponding to the rigid body. Figure 26b shows the orbit for a rigid body critical. Figure 26c shows the onset of instability where the instability frequency is lower than the running speed.

Cleared: December 19th, 1983
 Clearing Authority: Air Force Wright Aeronautical Laboratories

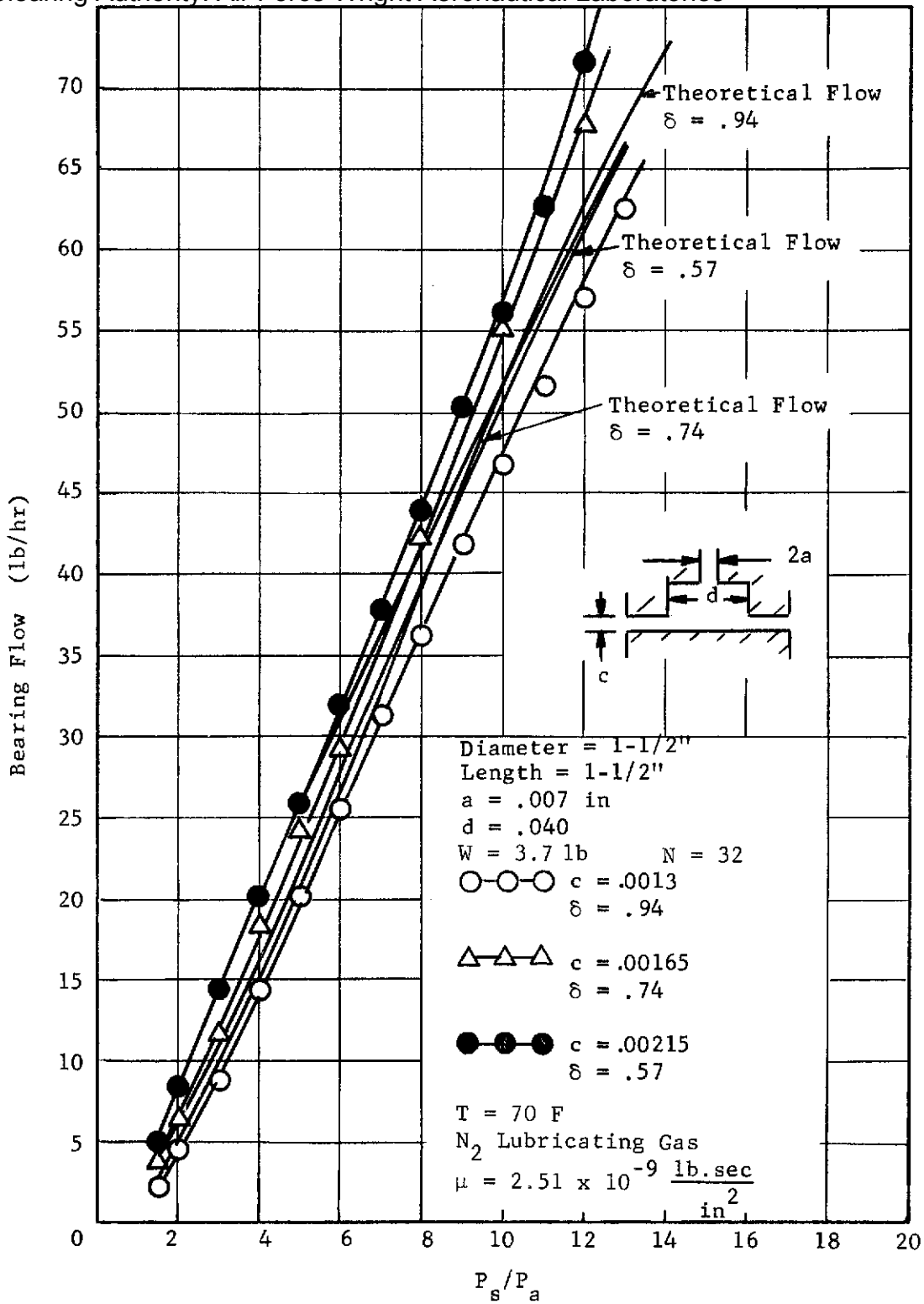


Fig. 17 Bearing Gas Flow as a Function of Supply Pressure
 $d = .040$ in

Cleared: December 19th, 1983

Clearing Authority: Air Force Wright Aeronautical Laboratories

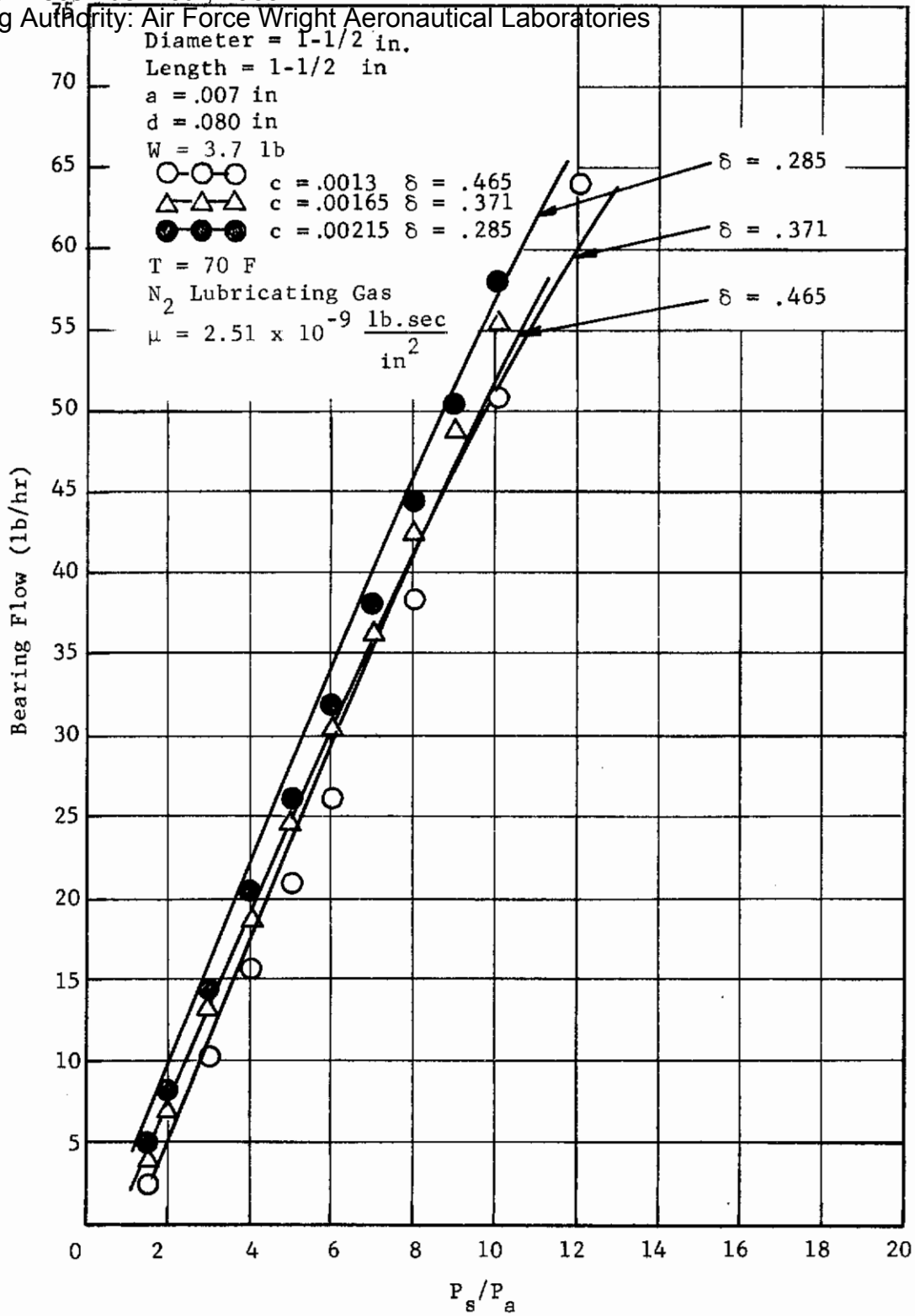


Fig. 18 Bearing Gas Flow as a Function of Supply Pressure
d = .080

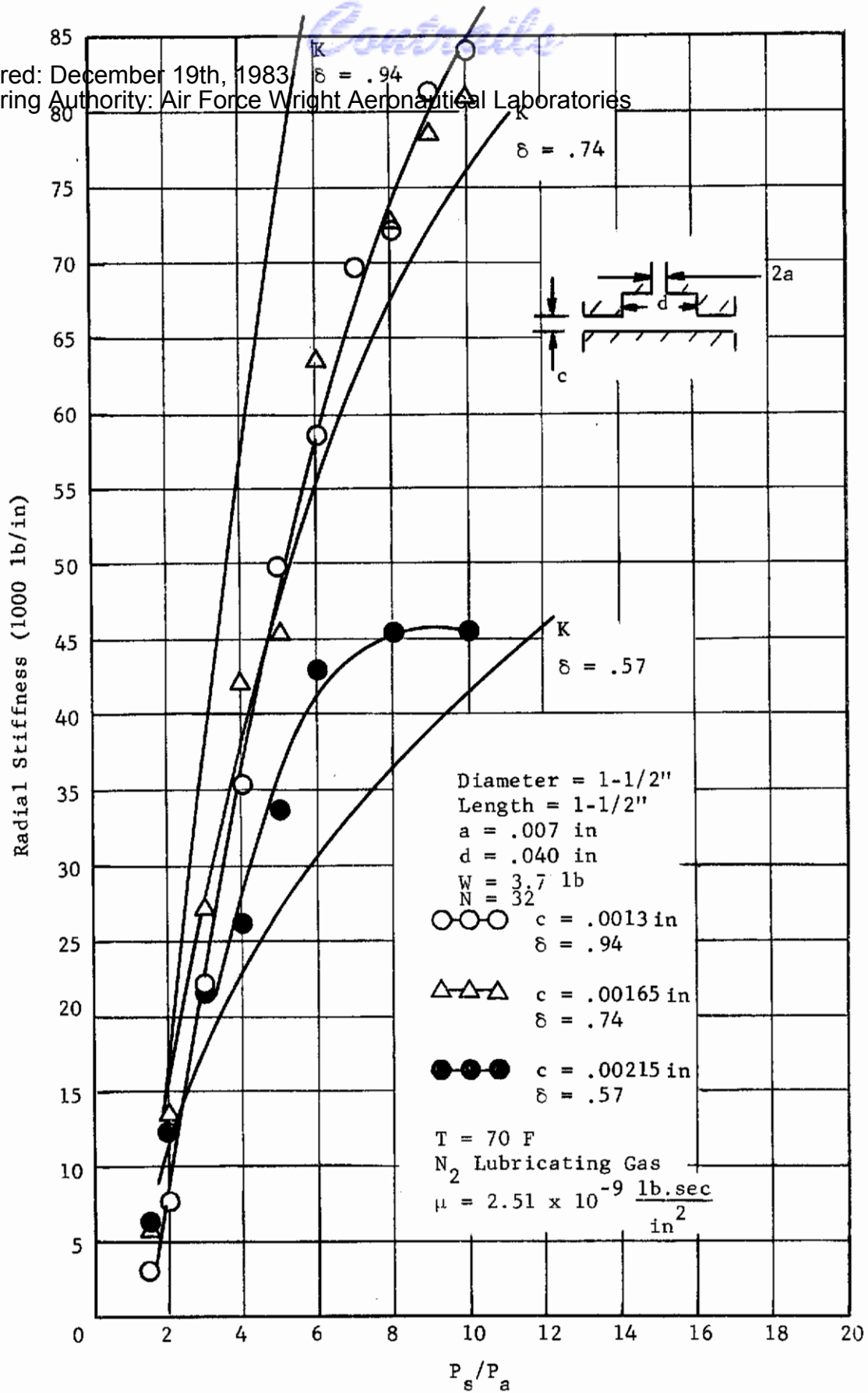


Fig. 19 Radial Stiffness as a Function of Supply Pressure
 $d = .040$

Cleared: December 19th, 1983
 Clearing Authority: Air Force Wright Aeronautical Laboratories

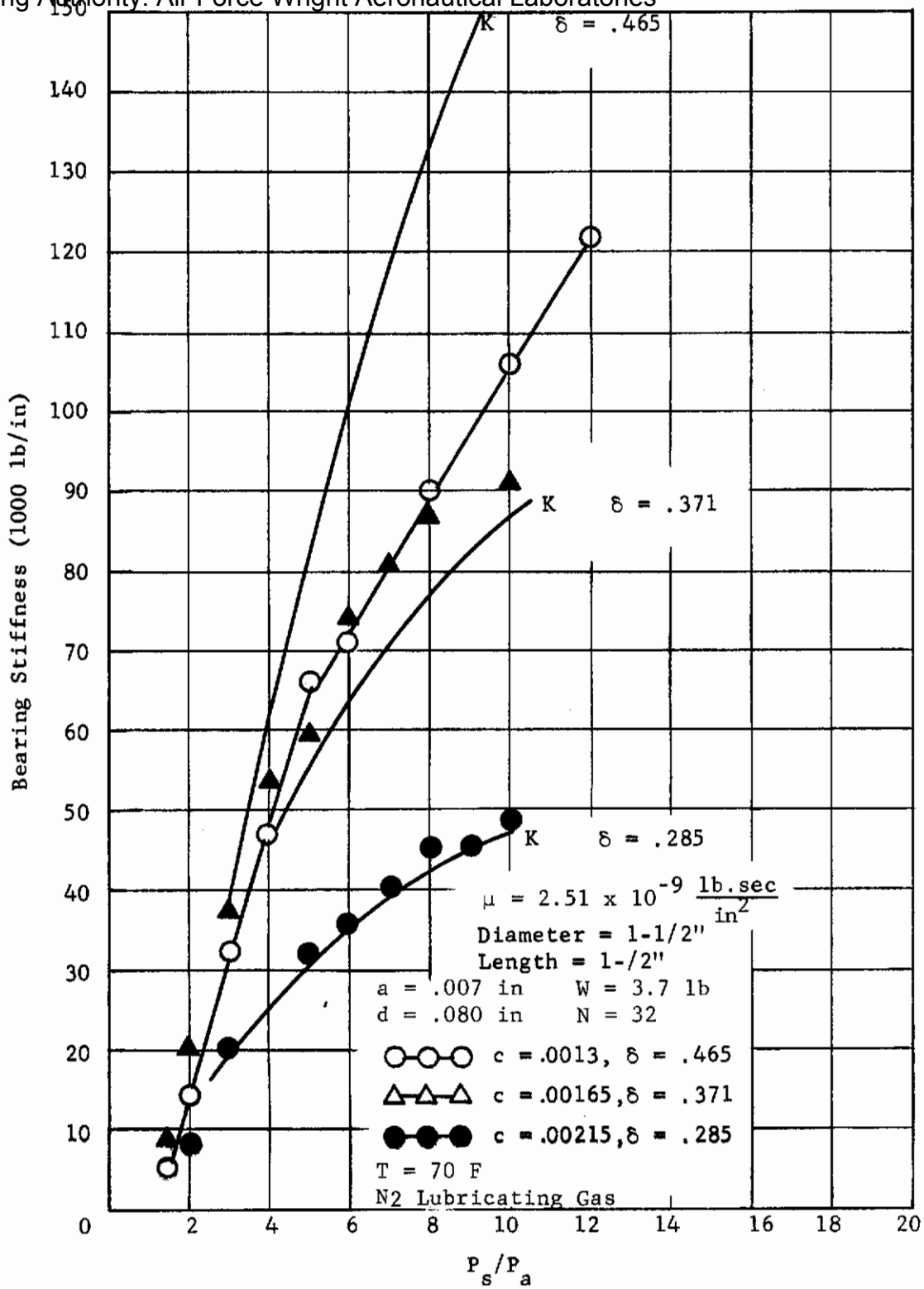


Fig. 20 Radial Stiffness as a Function of Supply Pressure $d = .080$

85
 Cleared: December 19th, 1983
 Clearing Authority: Air Force Wright Aeronautical Laboratories

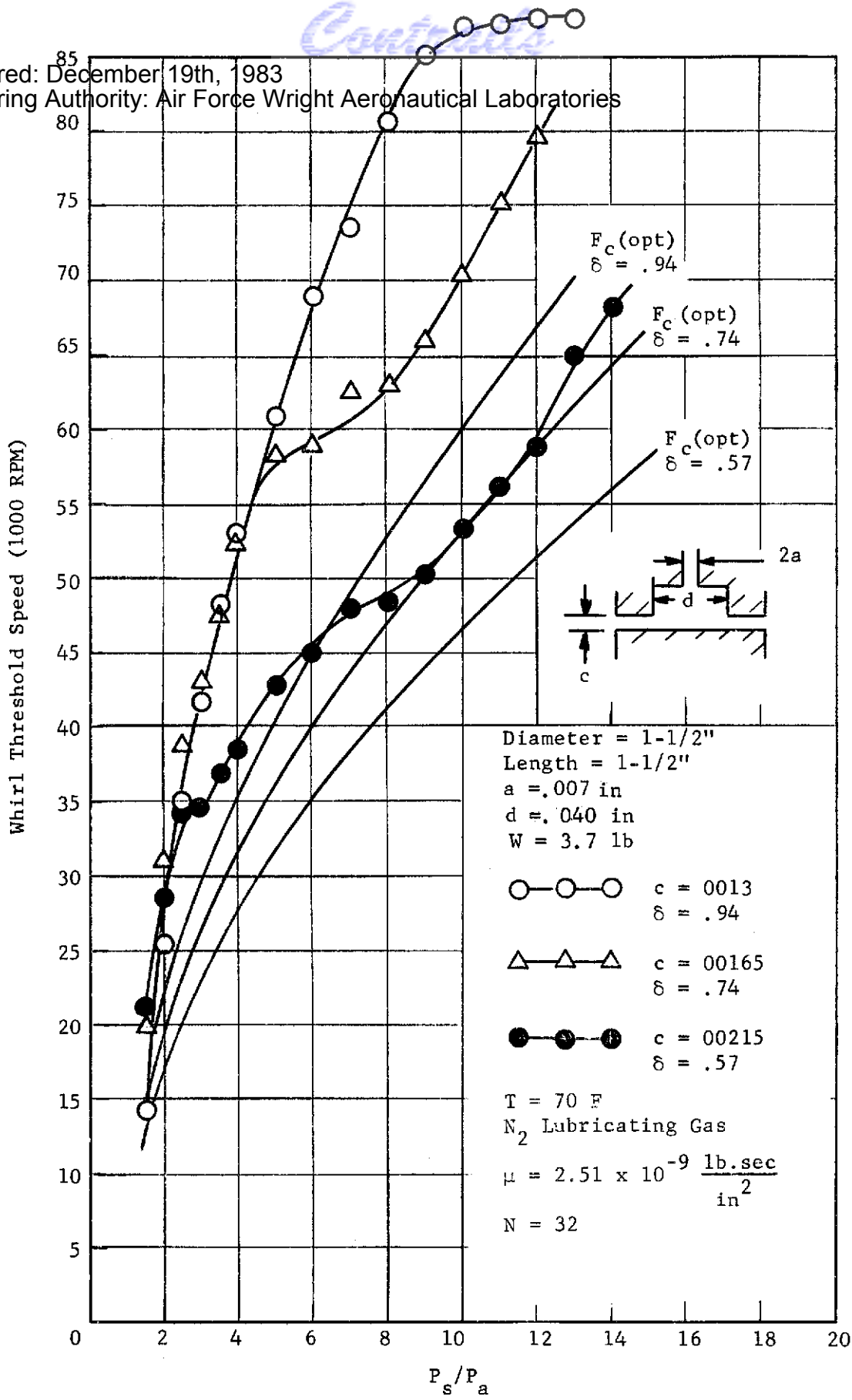


Fig. 21 Whirl Threshold Speed as a Function of Supply Pressure $d = .040$

Cleared: December 19th, 1983
 Clearing Authority: Air Force Wright Aeronautical Laboratories

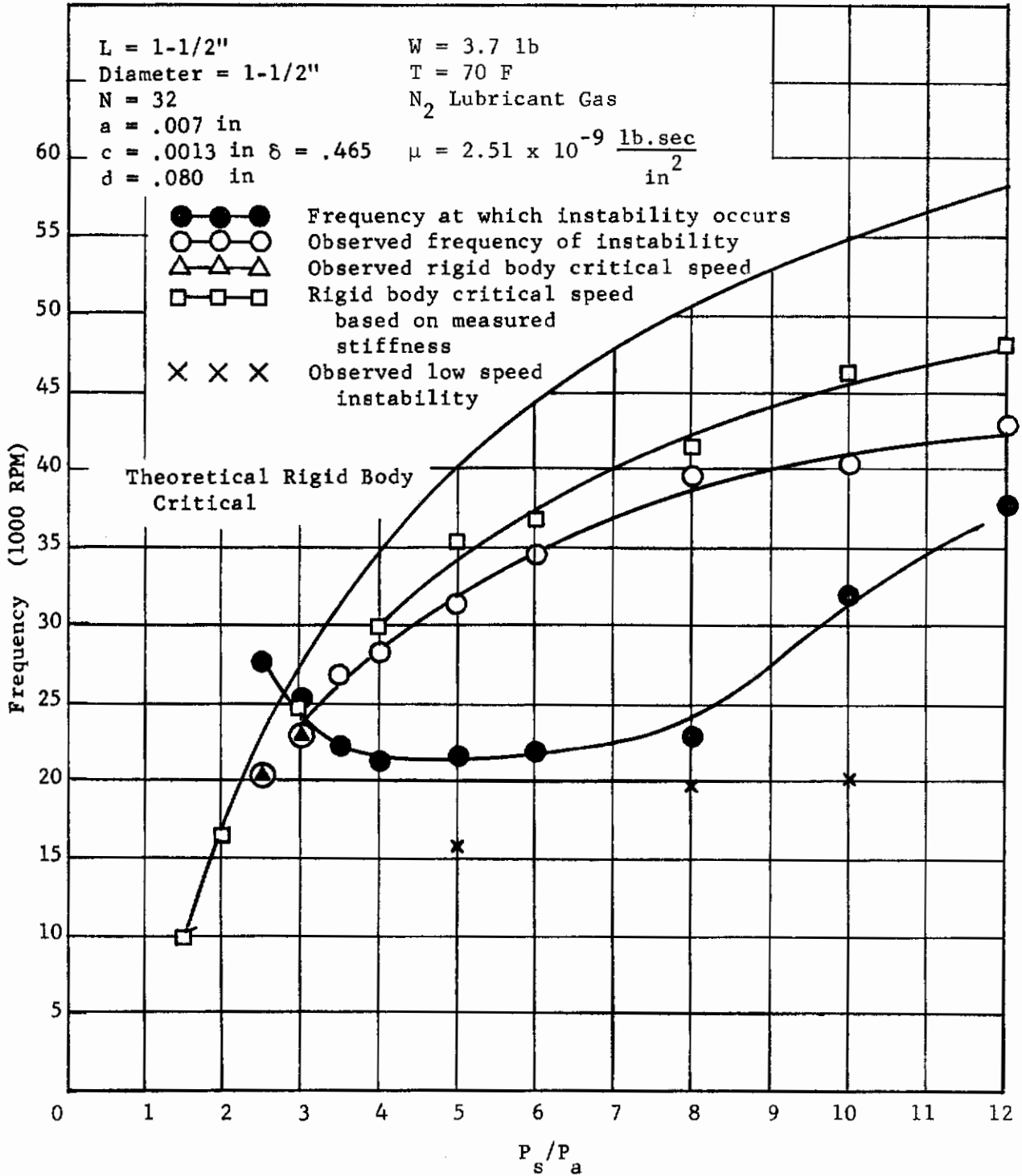


Fig. 22 Critical Speeds and Instabilities as a Function of Supply Pressure $\delta = .465$

Cleared: December 19th, 1983
 Clearing Authority: Air Force Wright Aeronautical Laboratories

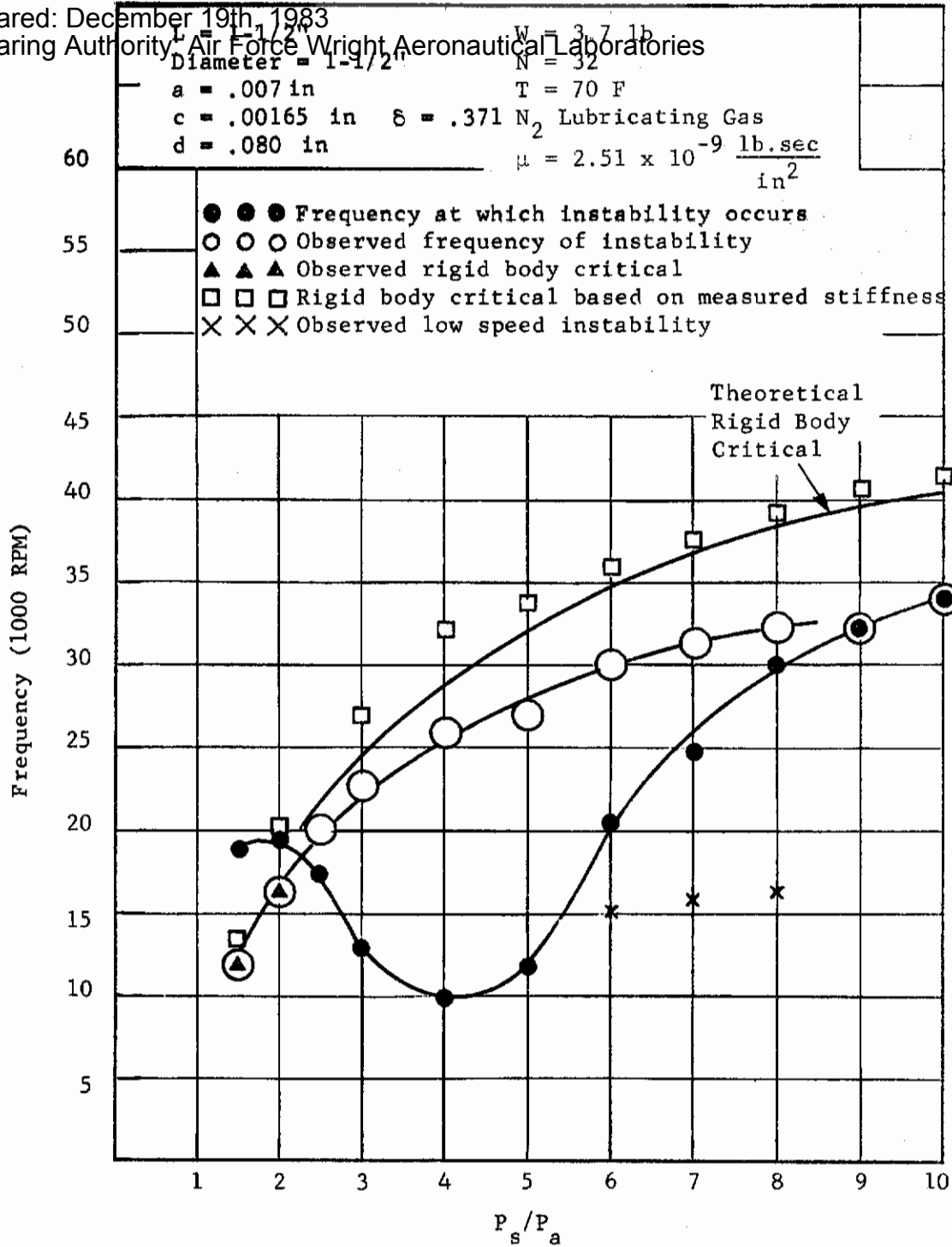


Fig. 23 Critical Speeds and Instabilities as a Function of Supply Pressure $\delta = .371$

Cleared: December 19th, 1983
 Clearing Authority: Air Force Wright Aeronautical Laboratories

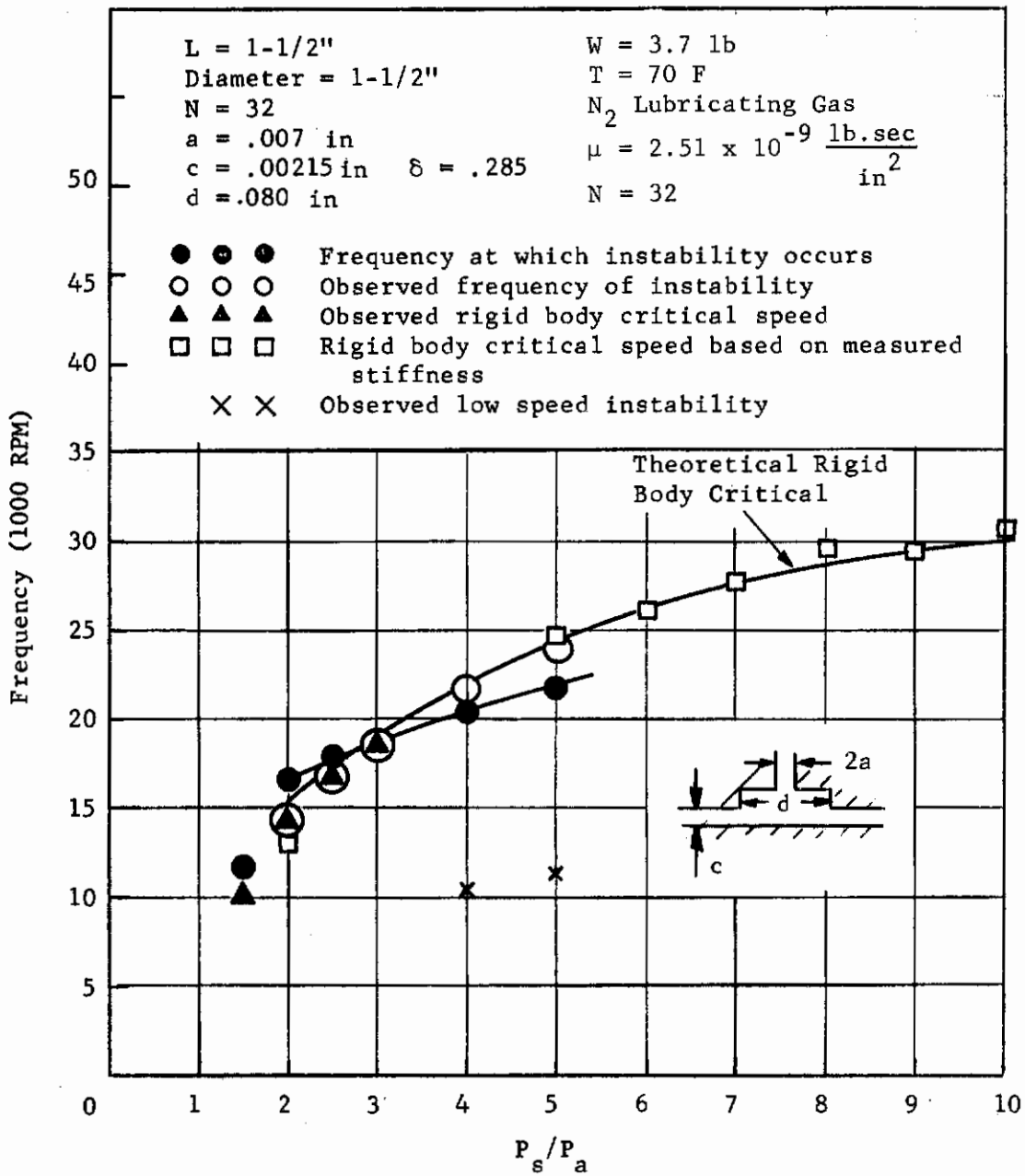


Fig. 24 Critical Speeds and Instabilities as a Function of Supply Pressure $\delta = .285$

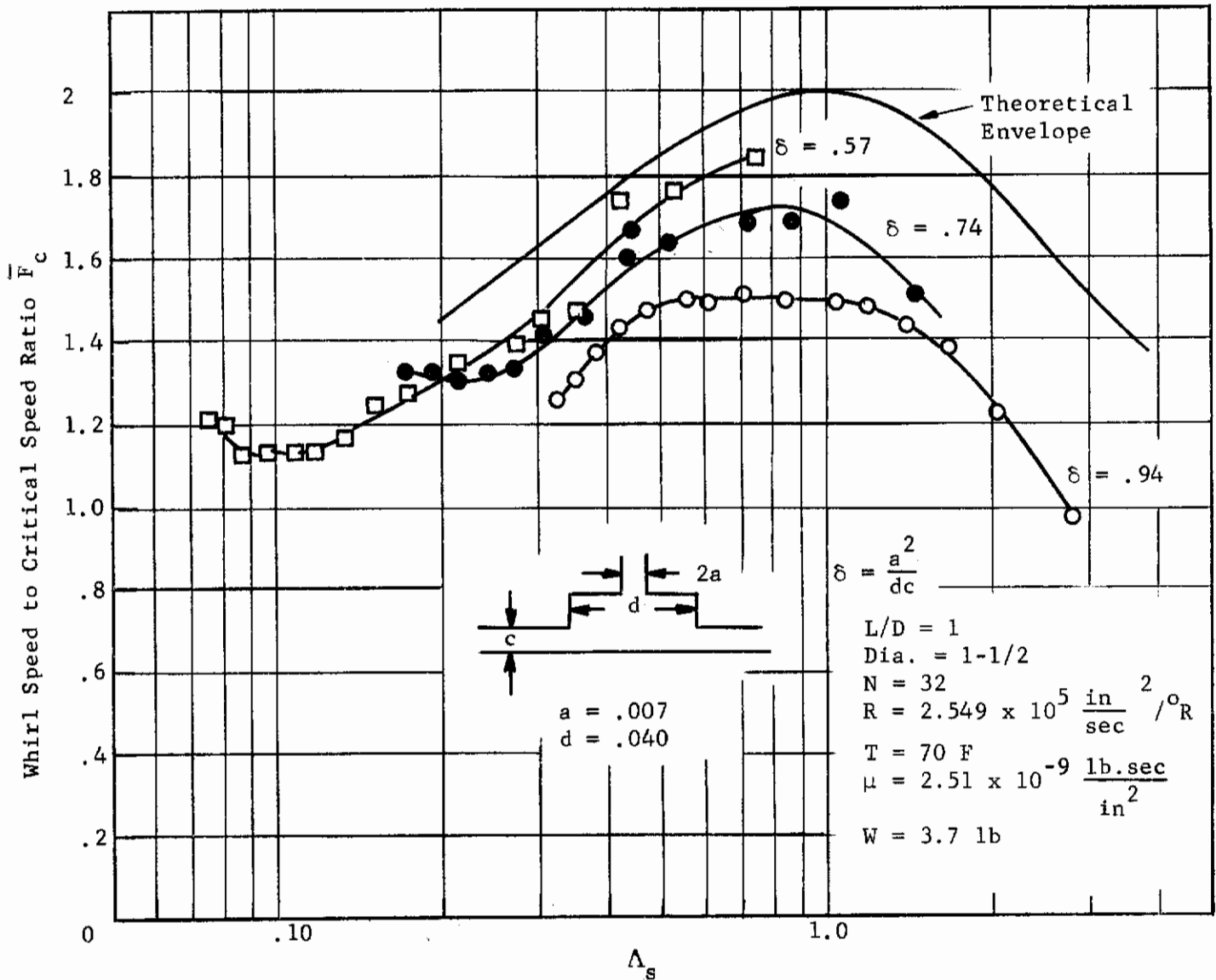
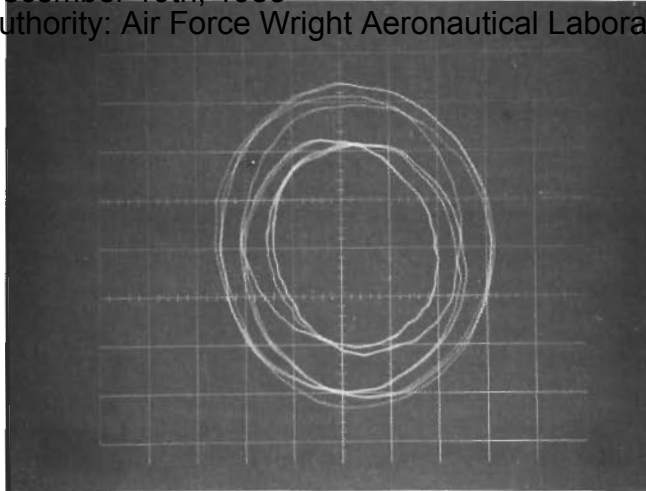
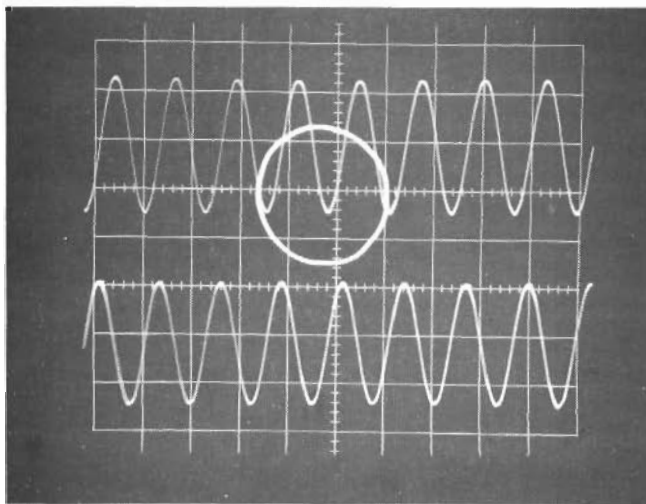


Fig. 25 Speed Ratio Versus Feeding Parameter Ratio $\bar{\Lambda}_s$ - Orifice Compensated 360 Degree Hybrid Bearing

Cleared: December 19th, 1983
Clearing Authority: Air Force Wright Aeronautical Laboratories

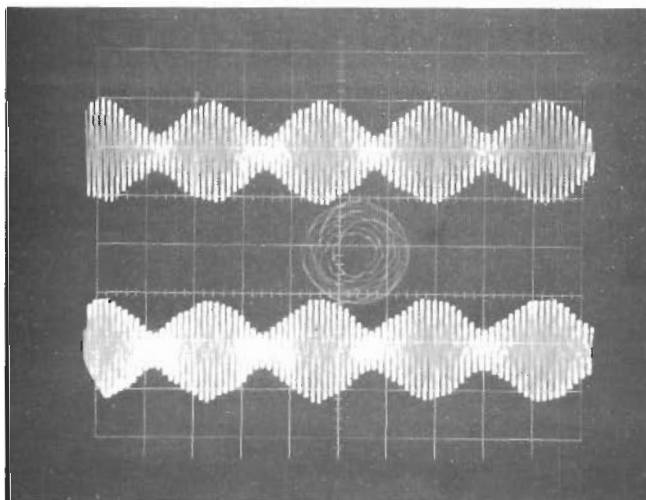


$P_s/P_a = 2-1/2$ $d = .080$
 $c = .0013$ $a = .007$
 $N = 27,600$
 $N_i = 20,400$



$P_s/P_a = 3$ $d = .080$
 $c = .0013$ $a = .007$
Sweep 20 msec/cm
Sensitivity 78.5 μ in/cm

$N = 22,800$
Rigid Body Critical



$P_s/P_a = 3$ $d = .080$
 $c = .0013$ $a = .007$
Sweep 2 msec/cm
Sensitivity 157 μ in/cm

$N = 25,400$
 $N_c = 22,800$

Fig. 26 Some Operational Photographs of Orifice Compensated 360 Degree Hybrid Bearing

Cleared: December 19th, 1983

Clearing Authority: Air Force Wright Aeronautical Laboratories

Experimental Program - Elevated Temperature Evaluations

The intent of the elevated temperature evaluations was to verify the predictions of the stability map previously established. The stability map established by room temperature testing was shown as Figure 3. The shaft and bearings for the test series were TZM. The two clearances resulted in δ values of 2.785 and 2.04. The nearest comparable values from Figure 3 are for δ of 2.62 and 2.04. Non-dimensional results for tests on the TZM system at temperatures of 70F, 300F and 500F are shown in Figure 27 with the corresponding predictions from Figure 3. The agreement is good indicating that the corrections for temperature and viscosity variation with temperature are sufficient using the dimensionless relationships.

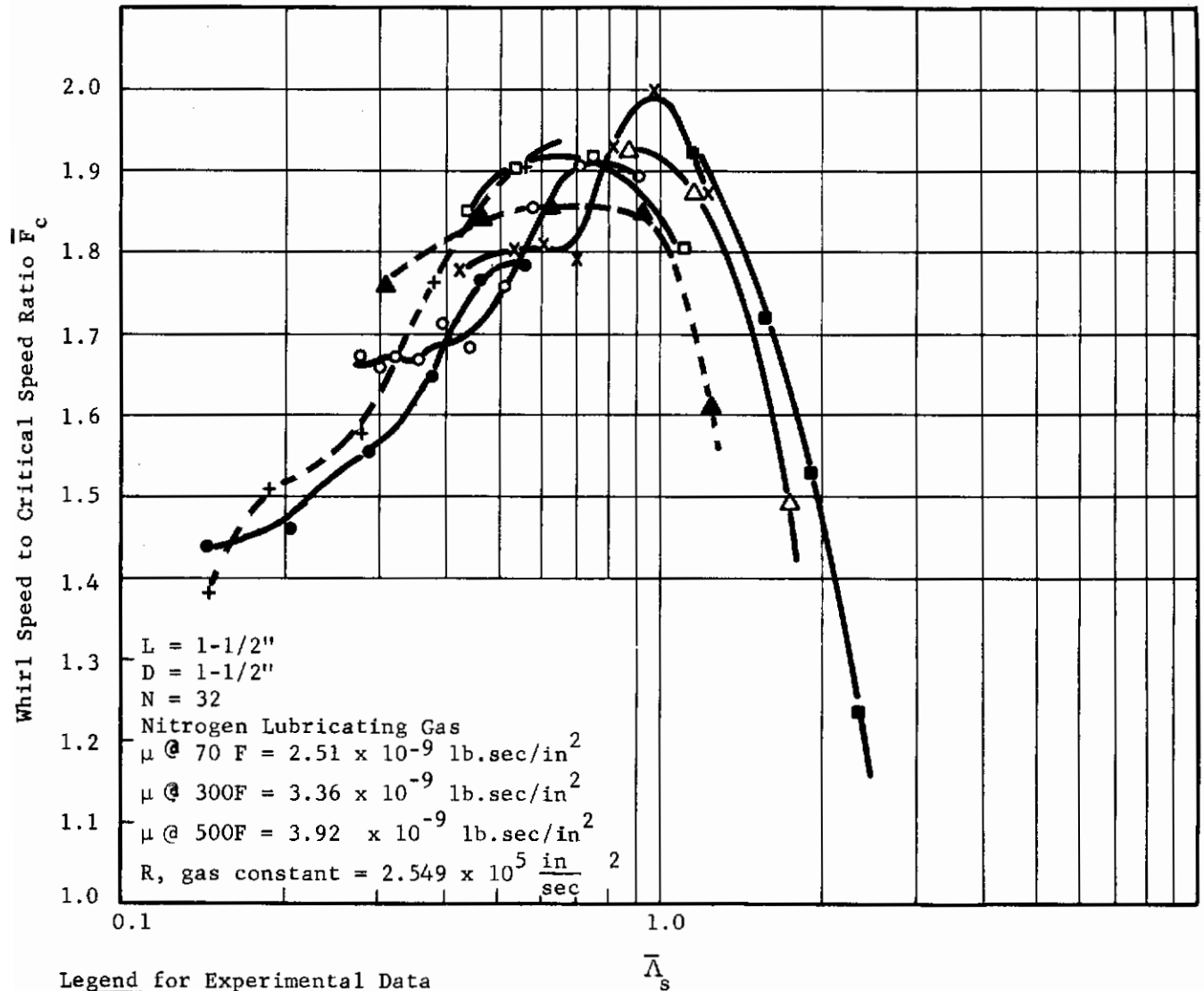
In previous tests, geometry and temperature were fixed and Λ_S was varied by changes in supply pressure. These changes in Λ_S were accompanied by variations in the dimensionless load as shown in Figure 1. In the current test series, the variations were accomplished by changing temperature.

Referring to Figure 1, it is noted that to the left of optimum, increasing temperature results in larger values of Λ_S and the dimensionless load. The converse is true on the right of the optimum point: increases in temperature and Λ_S result in a reduction in the dimensionless load. The dimensionless load is proportional to stiffness. Consequently, stiffness and threshold speed follow a similar trend with Λ_S and temperature. A set of charts showing journal bearing load versus deflection data obtained at the above temperatures are shown in Figures 28 through 33. Figures 34 and 35 show how the journal bearing stiffness varies with pressure ratio and temperature.

Figure 36 shows the theoretical dimensionless presentation for an orifice-fed thrust bearing. The effect of temperature is similar to that for the journal bearings.

The thrust bearing was tested for load-deflection characteristics at five supply pressures (50, 60, 70, 80 and 90 psig) and at three temperatures (70 F, 300 F, 500 F). Difficulty was encountered in obtaining an accurate zero reference and for this reason, the exact location with respect to zero clearance of the several deflection curves is not absolute. However, the slopes of these curves were used to give the relationship of stiffness to supply pressure, load and temperature. The data obtained are shown in Figures 37 through 39. The comparative results shown in Figure 40 showed very little stiffness variation with supply pressure, and the 500 F data indicated a decreasing stiffness. There is a difficulty in comparison since the different temperature runs were not at the same film thickness. This results from the fact that once the high temperature runs are in progress, the loading gas line cannot be cut off to establish the zero film thickness reference without the possibility of burning out the preheater line. However, the thrust bearing data will be checked further against the theoretical and rerun.

Cleared: December 19th, 1983
 Clearing Authority: Air Force Wright Aeronautical Laboratories



Legend for Experimental Data

- $T=70^\circ\text{F}$]
- $T=300^\circ\text{F}$] TSM Rotor & Bearings $C=.00165 \delta=2.04 a = .0065 W = 4.79 \text{ lb}$
- × $T=500^\circ\text{F}$]
- $T=70^\circ\text{F}$]
- △ $T=300^\circ\text{F}$] TSM Rotor & Bearings $C=.00121 \delta=2.785 a = .0065 W = 4.79 \text{ lb}$
- $T=500^\circ\text{F}$]
- ▲ $T=70^\circ\text{F}$ $C=.0013 \delta=2.04$] Steel Rotor $a = .0065 W = 3.7 \text{ lb}$
- + $T=70^\circ\text{F}$ $C=.00165 \delta=2.62$]

Fig. 27 Speed Ratio versus Feeding Parameter Ratio $\bar{\Lambda}_s$ - Elevated Temperature Operation - With Comparison to Previous Data

Cleared: December 19th, 1983
Clearing Authority: Air Force Wright Aeronautical Laboratories

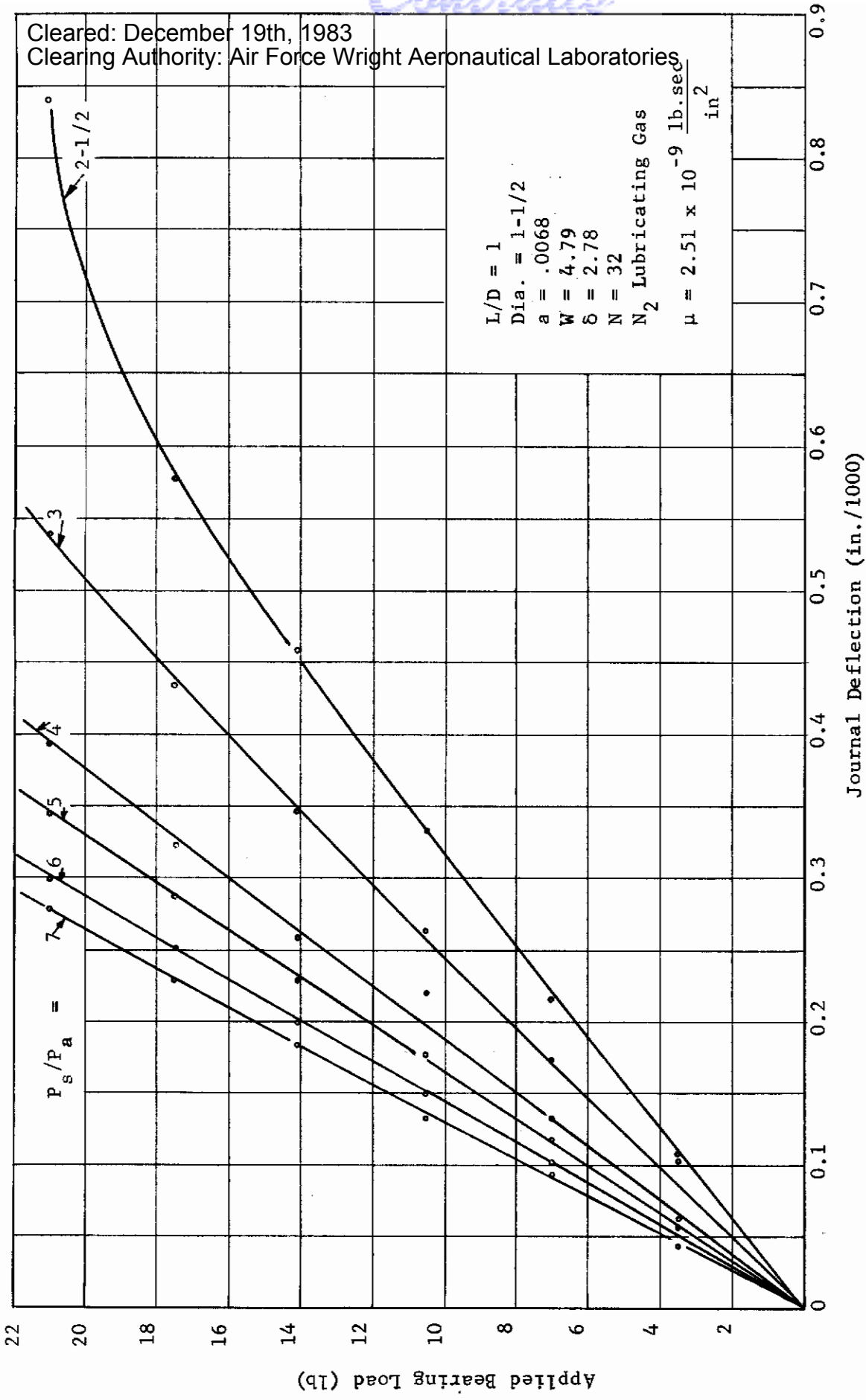


Fig. 28 Journal Bearing Load Deflection Characteristics $C = .00121$ $T = 70^\circ\text{F}$

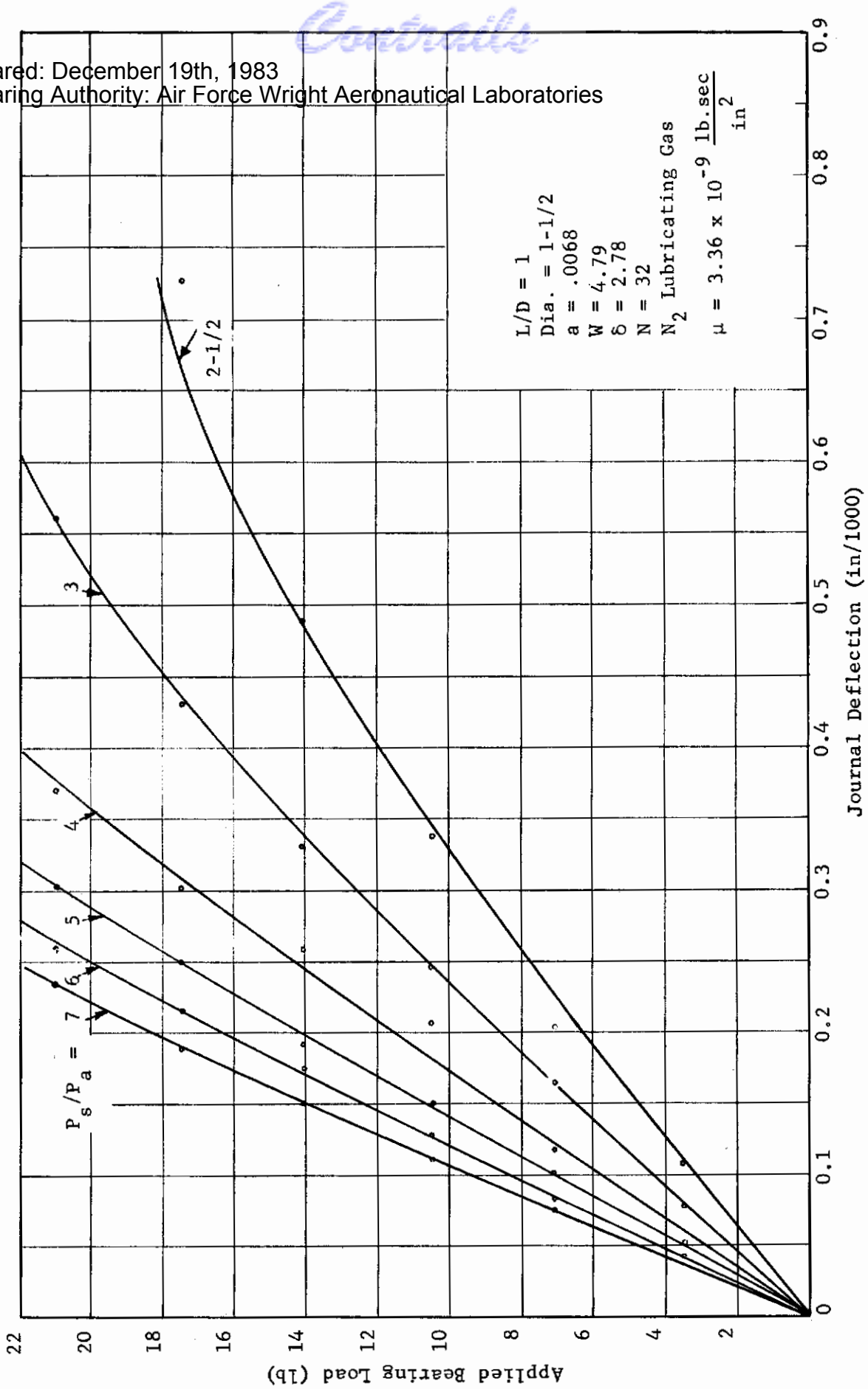


Fig. 29 Journal Bearing Load Deflection Characteristic $C = .00121$ $T = 300^\circ\text{F}$

Cleared: December 19th, 1983
 Clearing Authority: Air Force Wright Aeronautical Laboratories

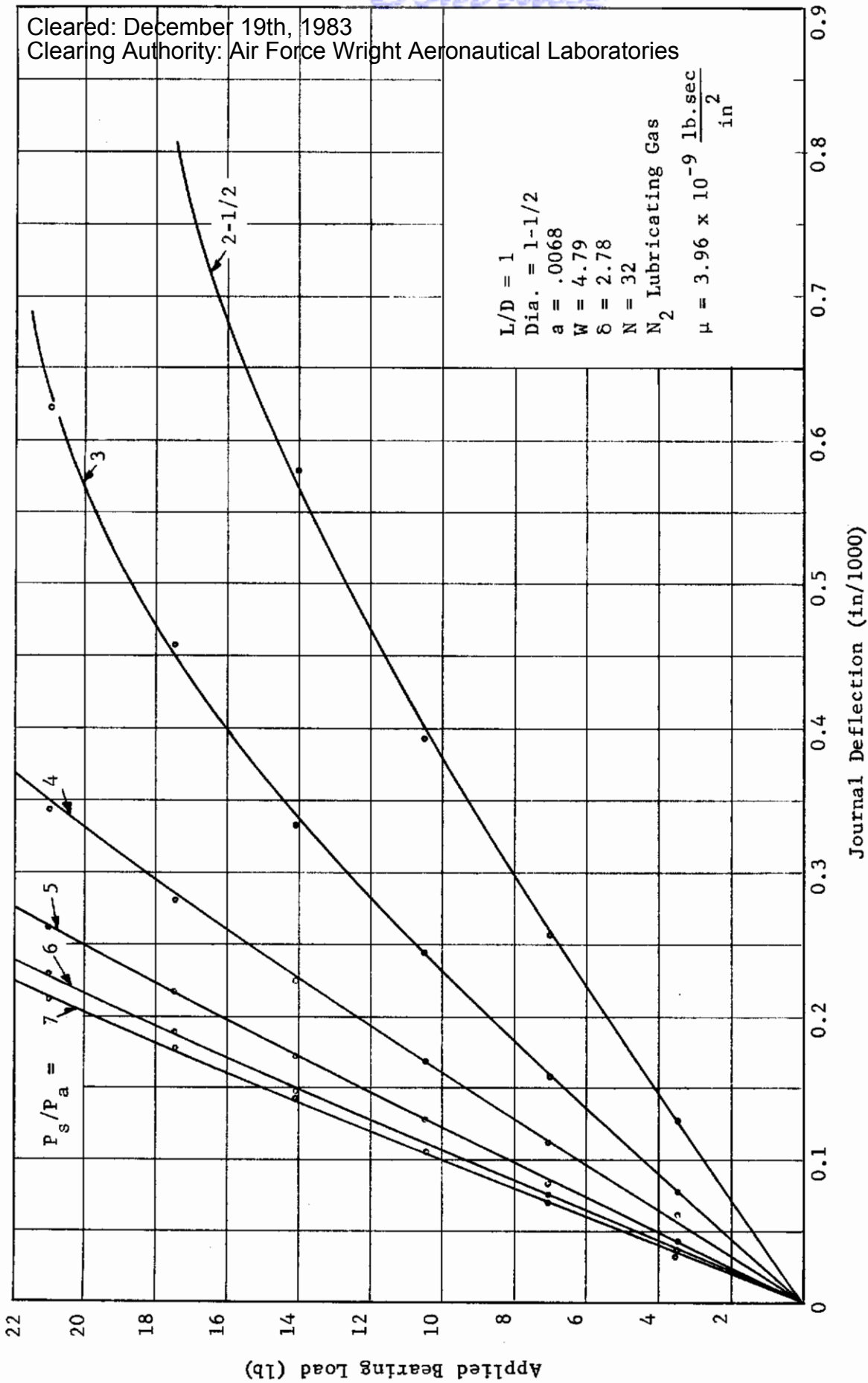


Fig. 30 Journal Bearing Load Deflection Characteristic $C = .00121$ $T = 500^\circ\text{F}$

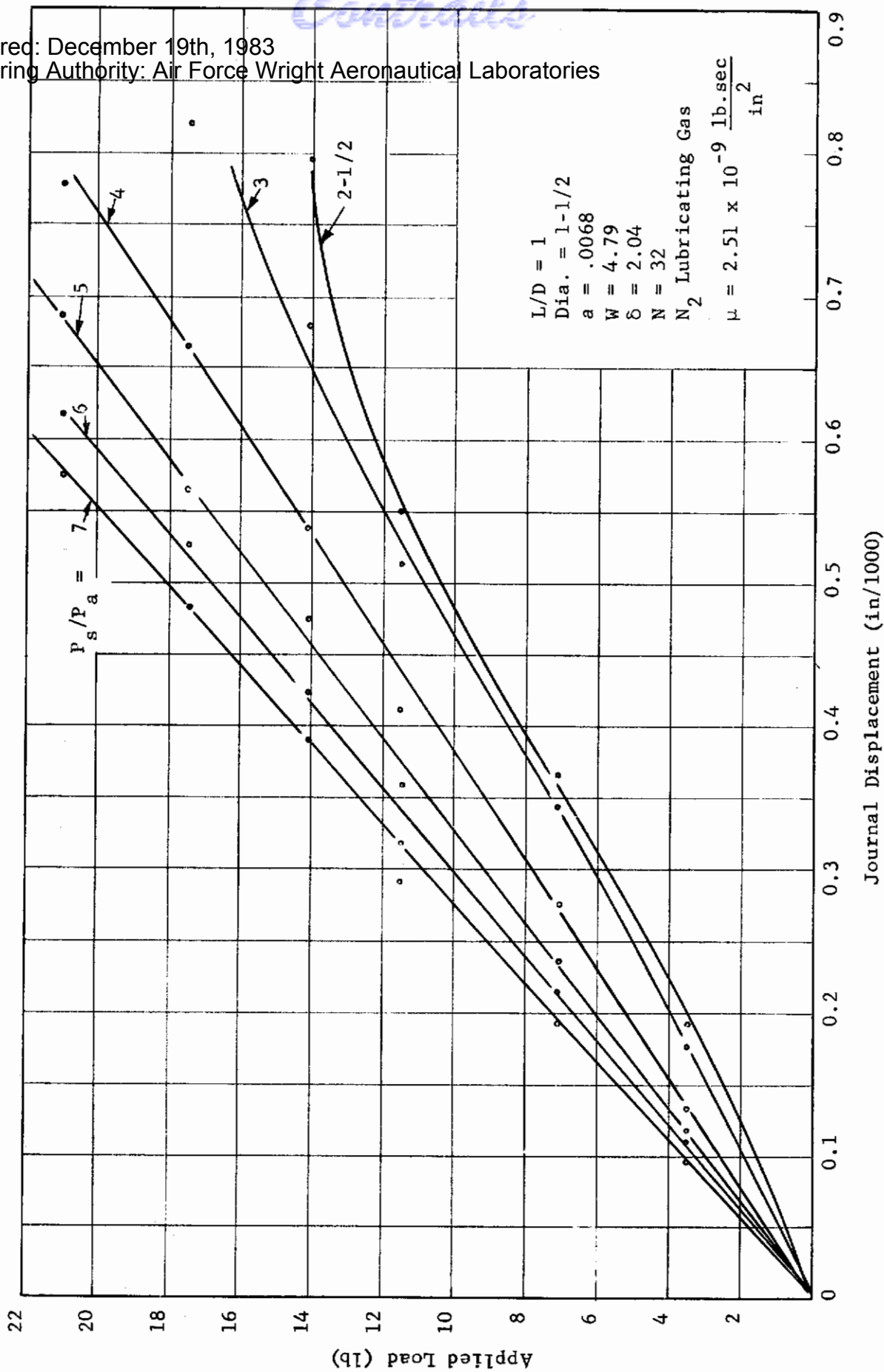


Fig.31 Journal Bearing Load Deflection Characteristic $C = .00165$ $T = 70^\circ\text{F}$

Contracts

Cleared: December 19th, 1983
Clearing Authority: Air Force Wright Aeronautical Laboratories

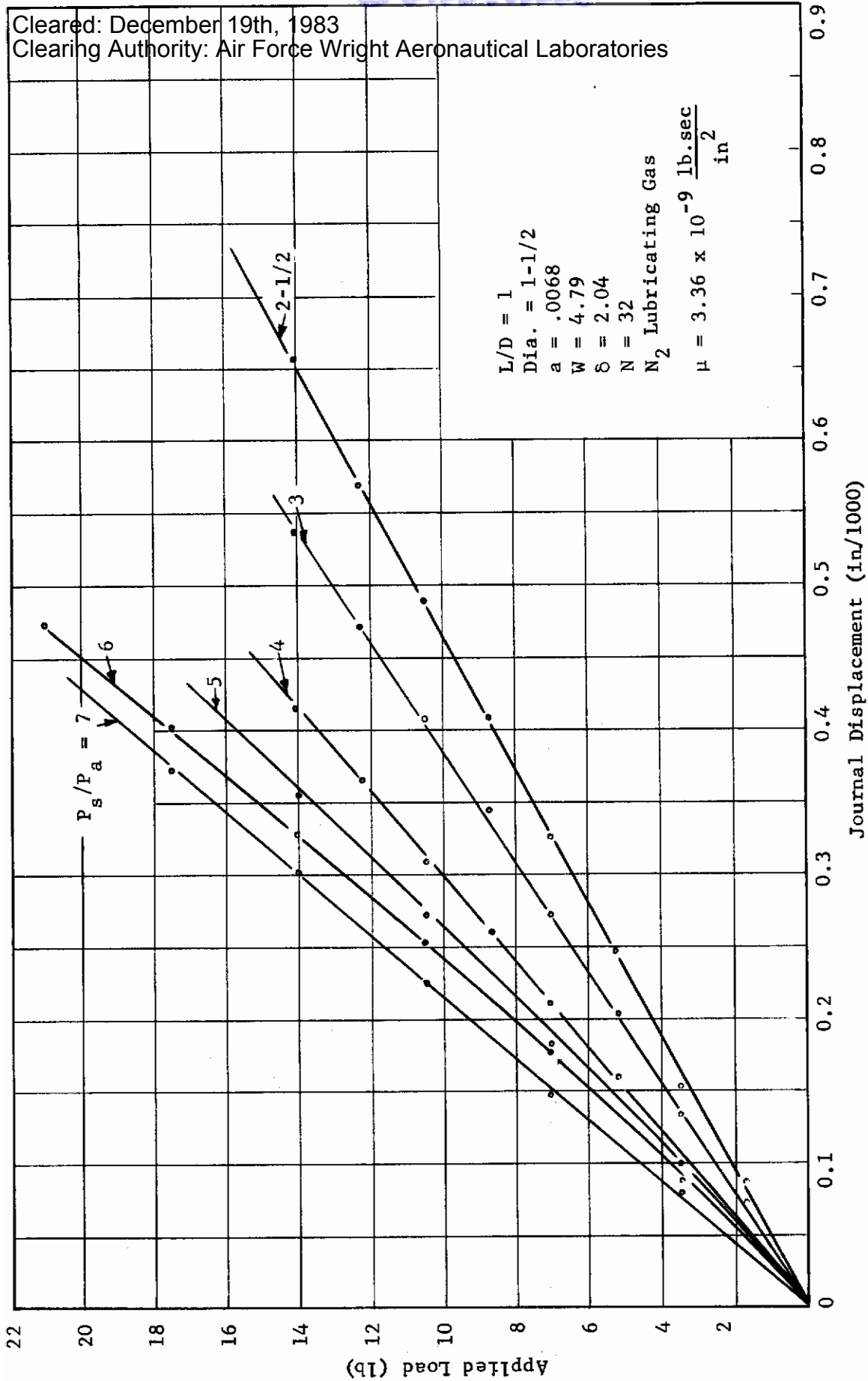


Fig.32 Journal Bearing Load Deflection Characteristic $C = .00165$ $T = 300^\circ\text{F}$

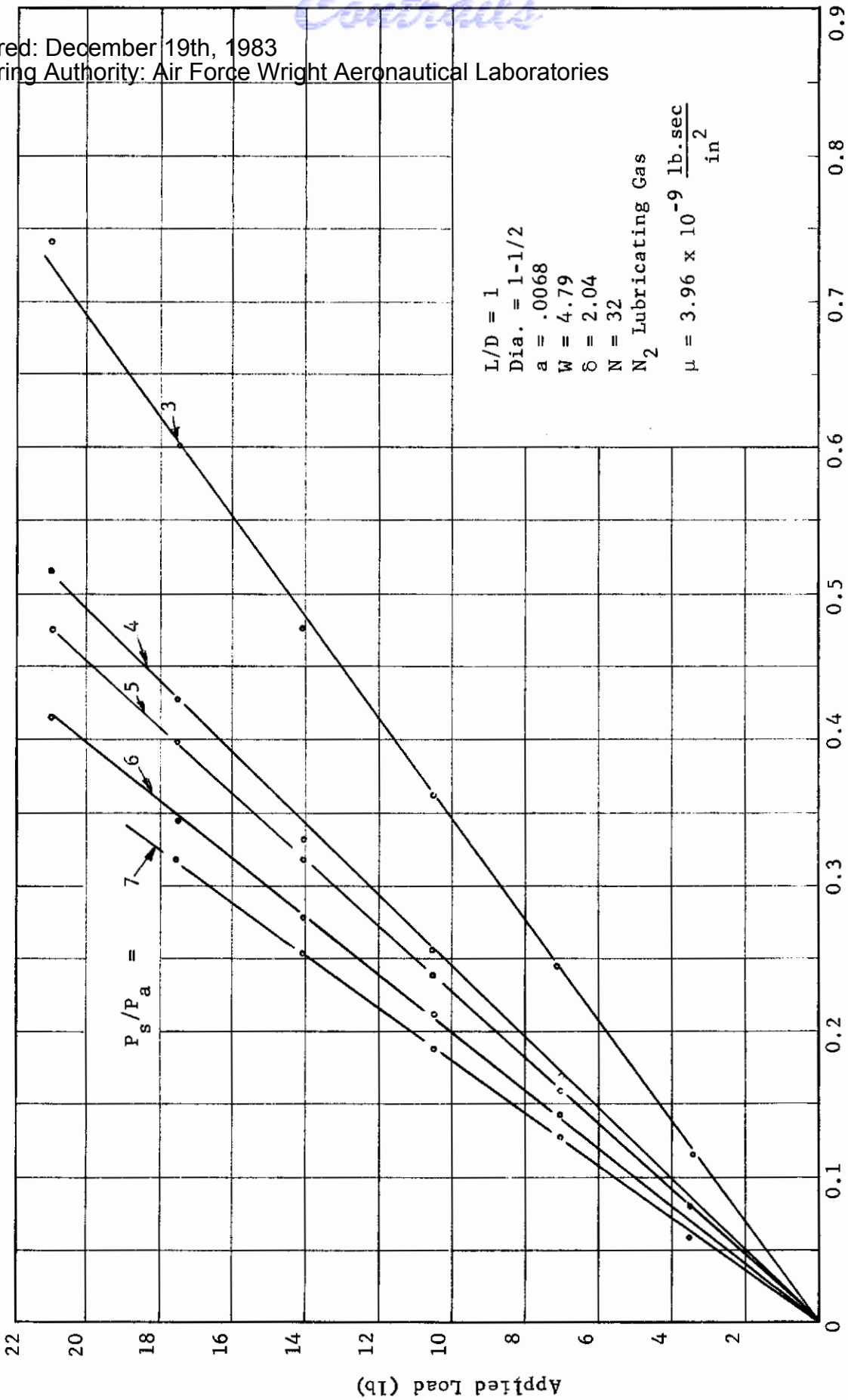


Fig. 33 Journal Bearing Load Deflection Characteristic $C = .00165$ $T = 500^\circ F$

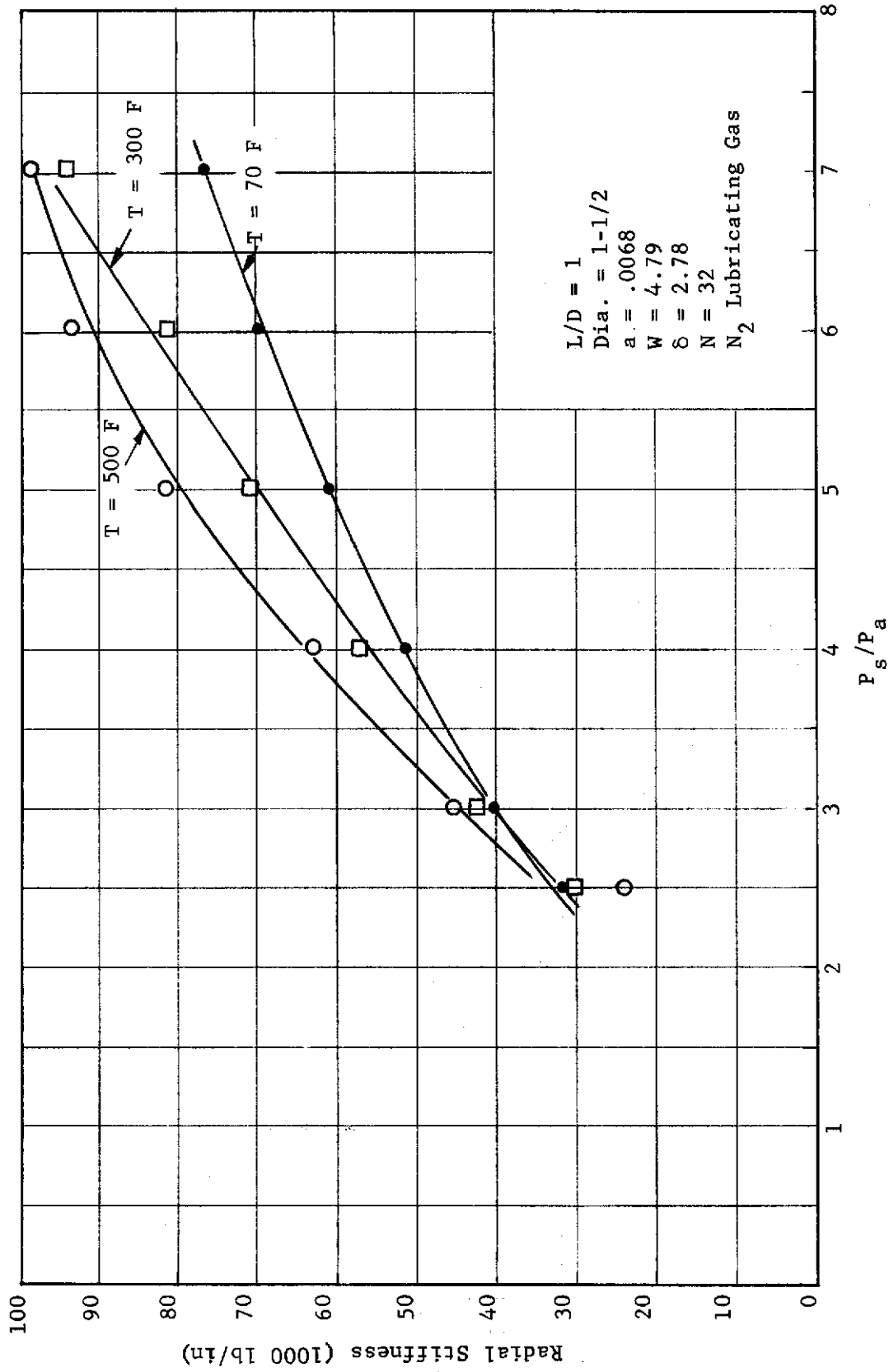


Fig.34 Temperature Effects on Journal Bearing Stiffness $C = .00121$

Cleared: December 19th, 1983
 Clearing Authority: Air Force Wright Aeronautical Laboratories

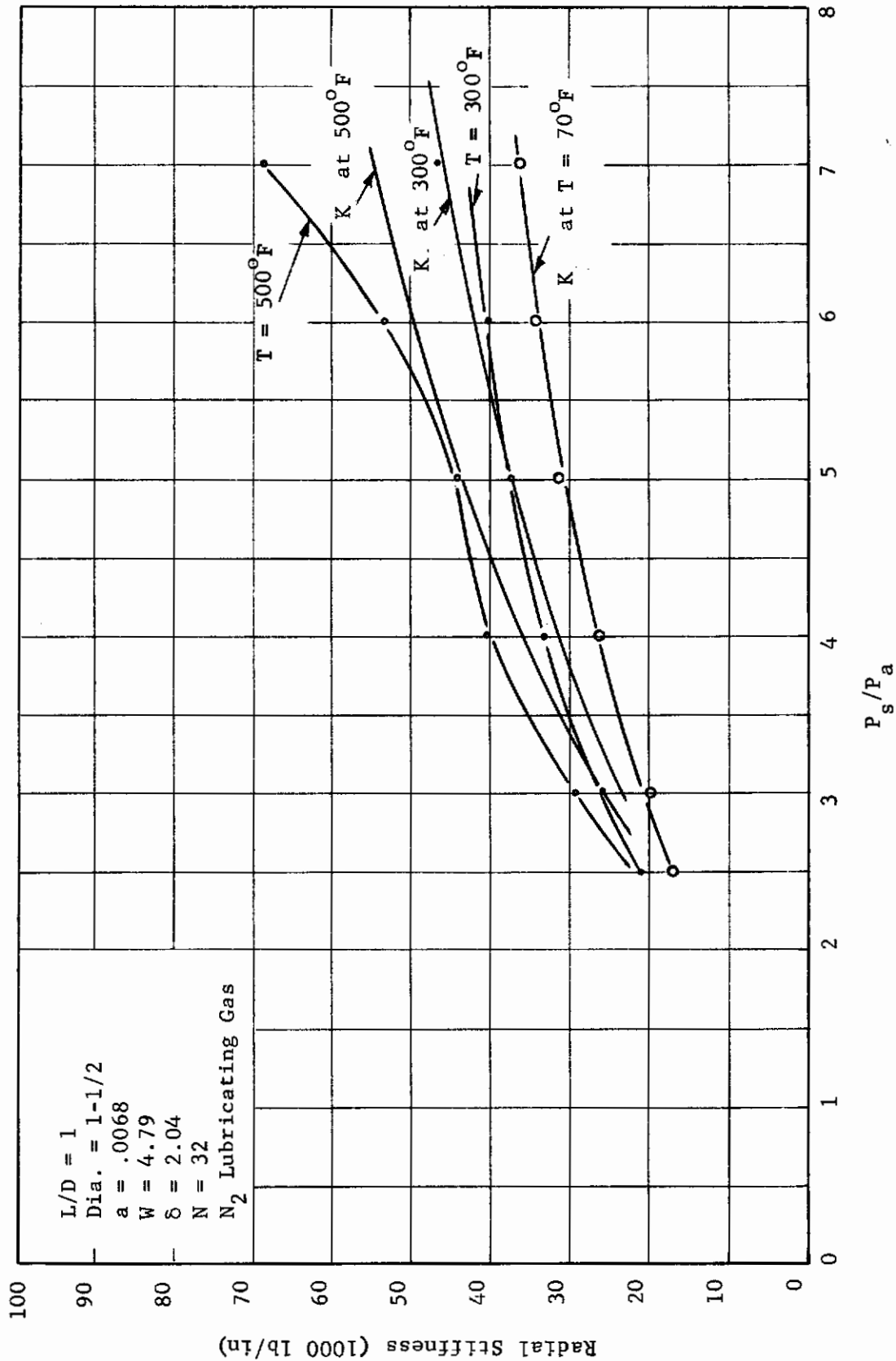
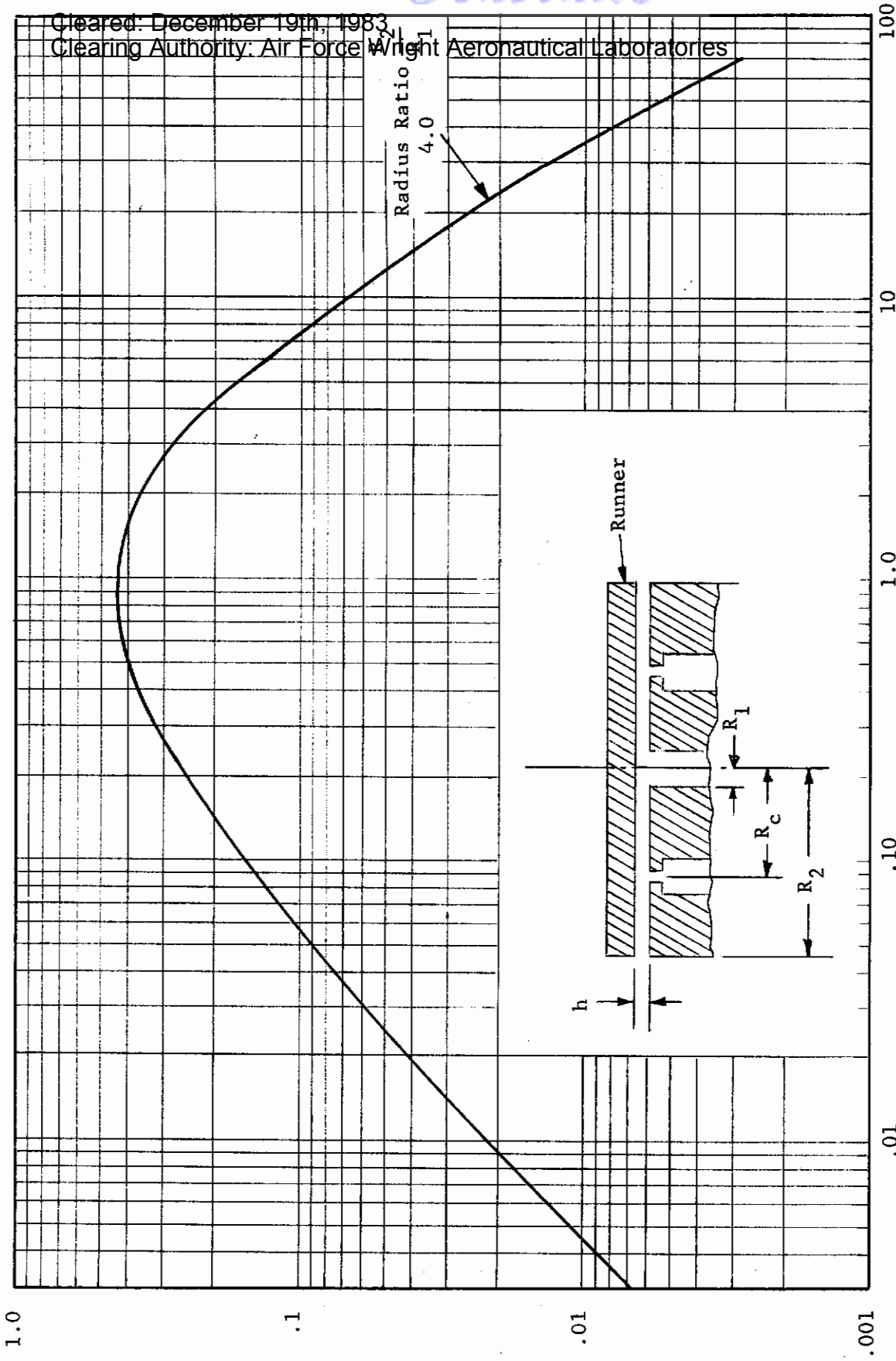


Fig. 35 Temperature Effects on Journal Bearing Stiffness $C = .00165$

Cleared: December 19th, 1983
 Clearing Authority: Air Force Wright Aeronautical Laboratories



$$\Lambda_s = \frac{6\mu N a^2 \sqrt{RT}}{P_3 h^3 \sqrt{1 + \delta^2 I}}$$

$$\frac{1 + \delta^2}{1 + \frac{3}{2} \delta^2} \frac{K}{(R_1^2 - R_2^2)(P^S - P^A)}$$

Fig. 36 Theoretical Thrust Bearing Stiffness versus Feeding Parameter

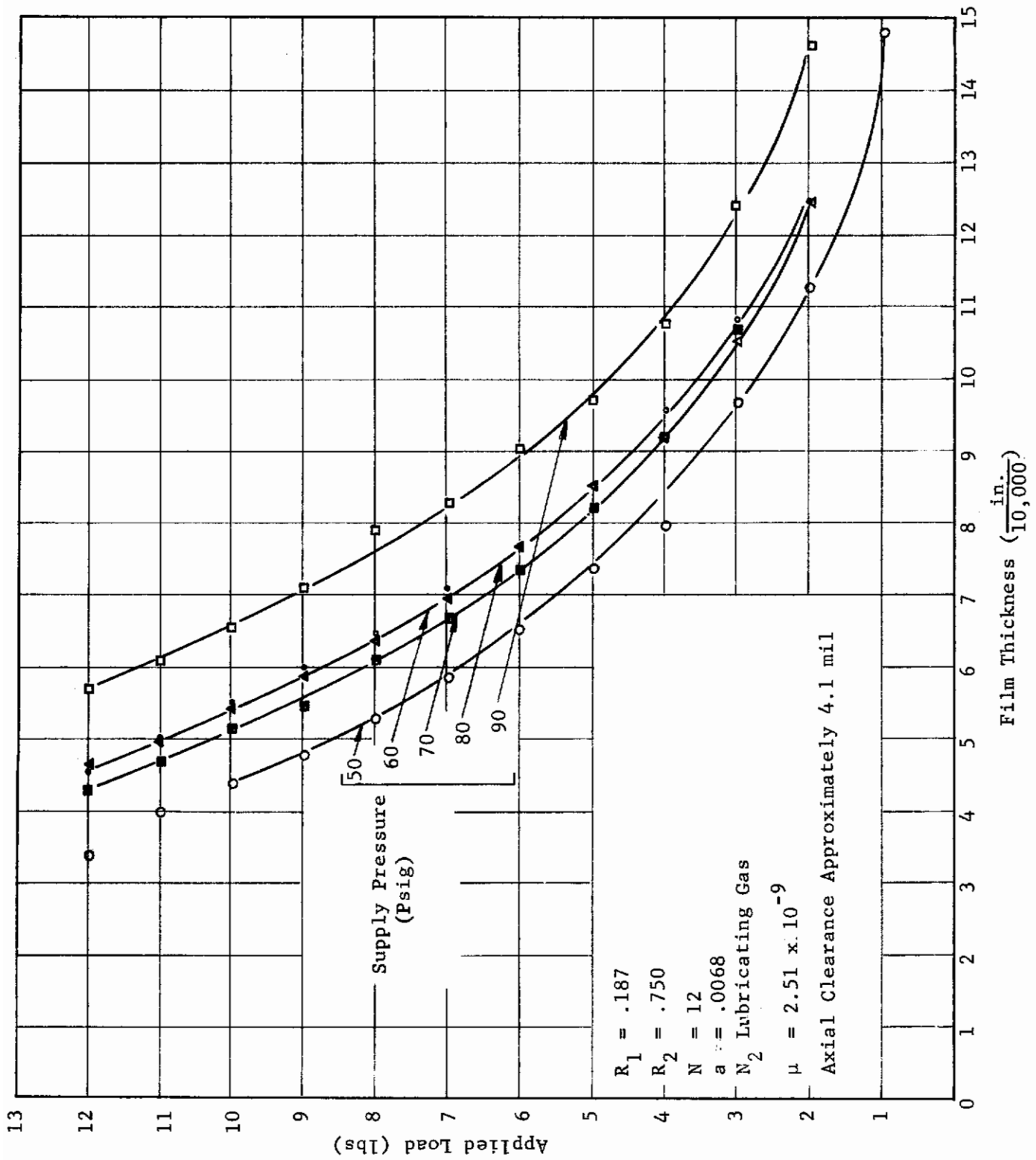


Fig. 37 Thrust Bearing Load Deflection Characteristics T = 70 F

Cleared: December 19th, 1983
Clearing Authority: Air Force Wright Aeronautical Laboratories

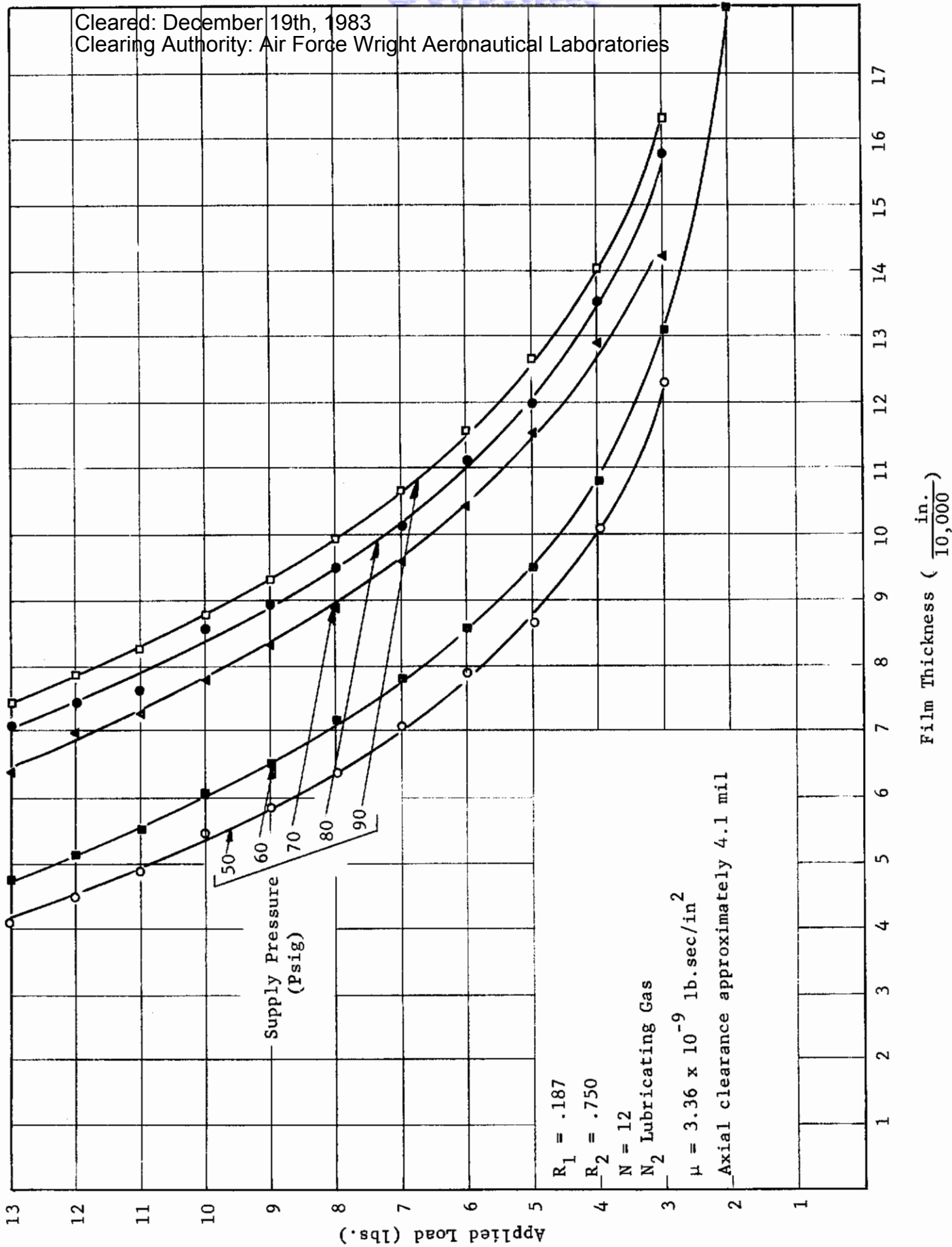


Fig. 38 Thrust Bearing Load Deflection Characteristics T = 300°F

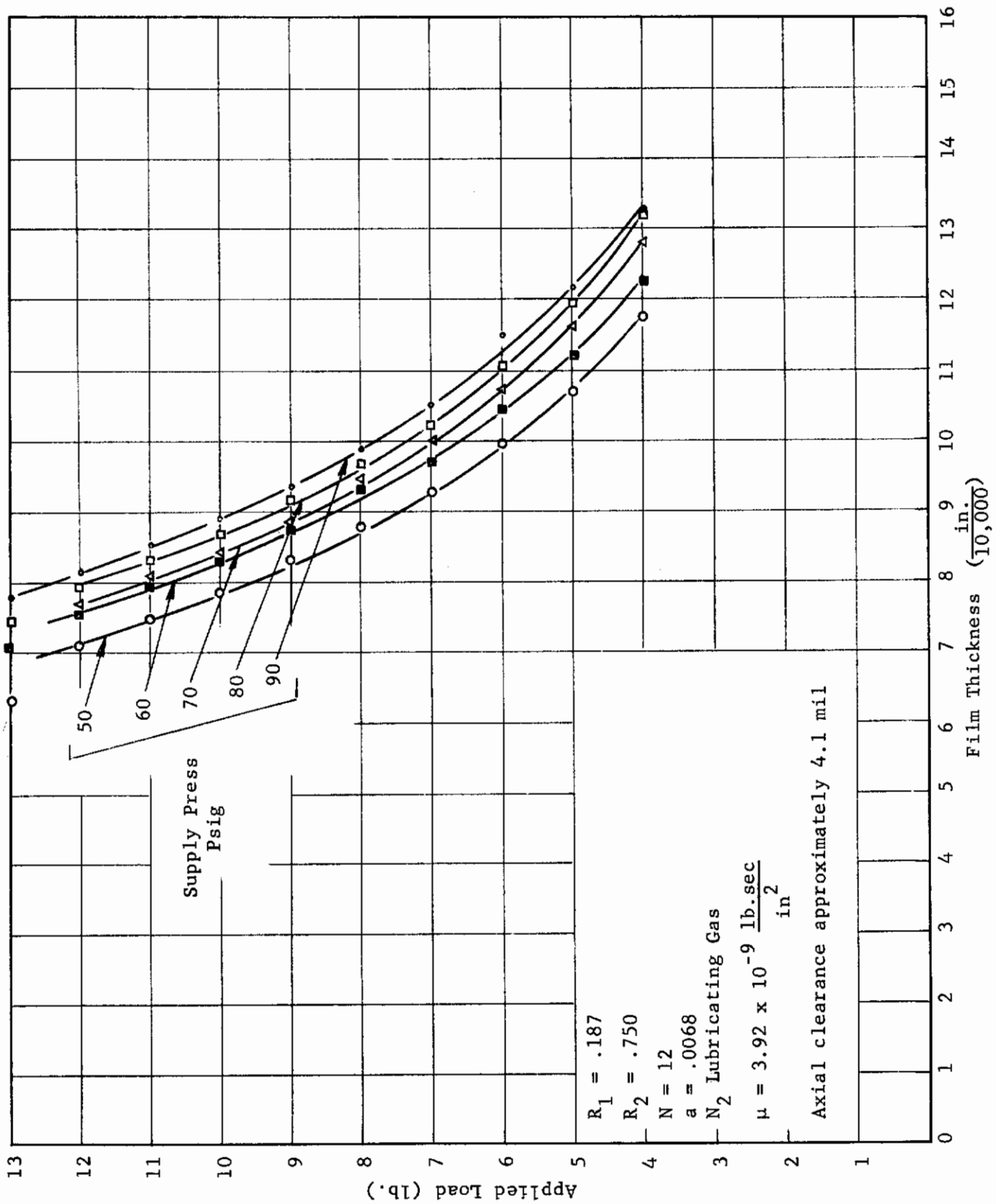


Fig. 39 Thrust Bearing Load Deflection Characteristics $T = 500^\circ\text{F}$

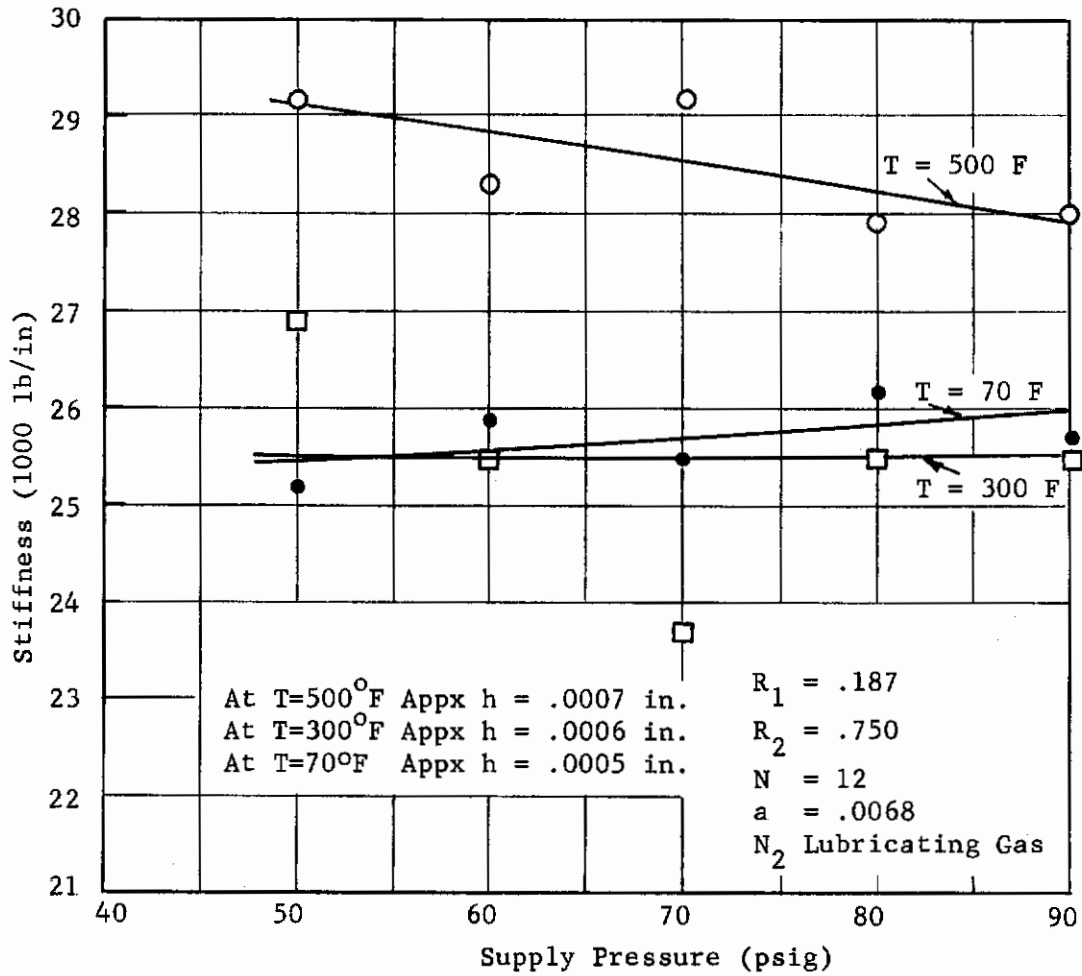


Fig. 40 Temperature Effects on Thrust Bearing Stiffness

Cleared: December 19th, 1983
Clearing Authority: Air Force Wright Aeronautical Laboratories

Modified 360 Degree Hybrid Bearing Design

As indicated in Table 1, improved alignment and tolerance to thermal gradients is possible with the 360 degree hybrid bearing if it is mounted flexibly.

One of the major problems with the rigidly mounted 360 degree bearing and most of the other bearing types is the inability to accommodate radial temperature gradients. It would be desirable if a design could be provided which could tolerate radial gradients while maintaining the bearing sleeve at the same temperature as the shaft. This can be accomplished if the bearing sleeve has low thermal mass and is thermally isolated since heat transfer is good across the gas film. If, in addition, growth of the bearing sleeve is independent of the mounting and housing, radial thermal gradients can be tolerated. A bearing sleeve supported by tangential spokes has these characteristics. The spokes also act as gas supply passages. Such a design is shown in Figure 41. It should be noted that the radial stiffness of the mounting can be made high, thereby eliminating a reduction in the stable operating range.

Table I
Ranking of Hybrid Bearing Types

Bearing Type	Stability	Alignment	Tolerance to Distortion		Flow	Manufacturing Difficulty	Design Complexity
			And Thermal Gradients	Stiffness			
A. Hybrid 360 Rigid	3*	4	4	1	1	1	1
B. Hybrid 360 Flex. Mt.	4	2	1	2	1	2	2
C. Hybrid Pad Pivoted-Normal Pivot	1	1	2	1	2	3	4
D. Hybrid Pad Hydrostatic Pivot	2**	1	2	2	3	4	4
E. Hybrid Pad Flex. Mt.	2	1	1	1	2	3	3
F. Hybrid 360 Hydrostatic 360	2**	2	2	2	3	2	4
G. Hybrid 360	2**	1	2	2	3	3	4

* Lowest number corresponds to the most desirable

** Considers also the pneumatic hammer type of instability

Cleared: December 19th, 1983
 Clearing Authority: Air Force Wright Aeronautical Laboratories

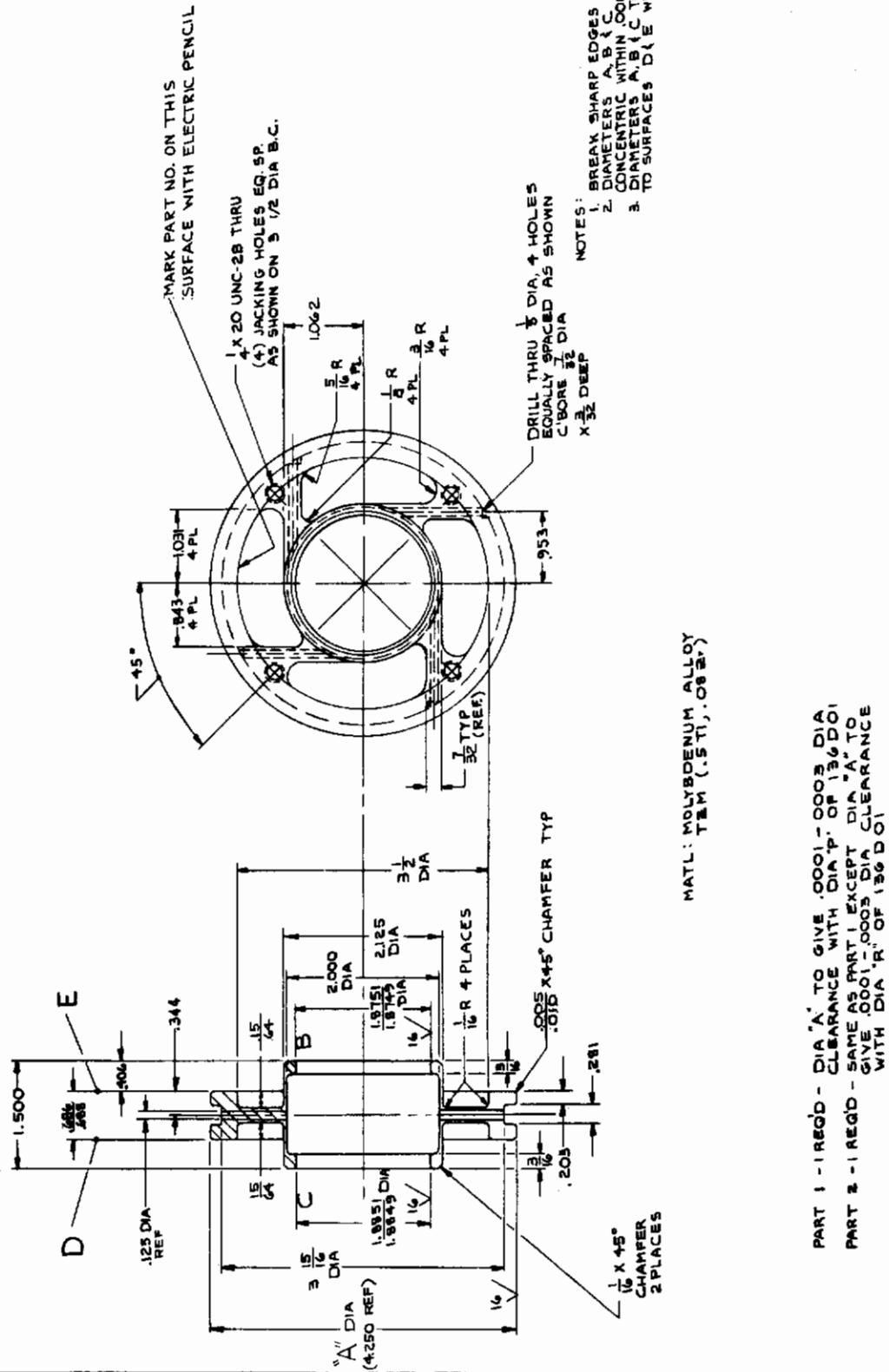


Fig. 41 Tangential Spoke 360 Degree Hybrid Bearing

Cleared: December 19th, 1983
~~Clearing Authority: Air Force Wright Aeronautical Laboratories~~

As was previously discussed, this bearing concept was selected to be considered as an advanced concept. The reasoning behind this selection is demonstrated by ranking the various bearing types in terms of the following factors:

1. Stability (Stable operating range)
2. Ability to Align
3. Tolerance to Distortion and Thermal Gradients
4. Stiffness
5. Flow
6. Manufacturing Difficulty
7. Design Complexity
8. Potential Materials Problems
9. Availability of the Design for Use with Respect to Time

The approach to this bearing type was to use a radial support to avoid radial support flexibility for the initial work. This removes the ability of the bearing to compensate for radial growth. However, the number of variables and possible interactions during evaluation are reduced.

The design procedure and prototype for this concept were discussed in Reference 1. The assembly drawing of the design shown in Figure 42 is the final result which was used for initial evaluations of this bearing type. The unit shown in Figure 42 has the mounting ring and flexure rods as an integral unit. An annular groove in the mounting ring acts as a gas manifold which supplies gas through the hollow flexure rods. The gas passage in the rod communicates with a countersink on the outside diameter of the pad, and then to two axial holes in the pad which supply the orifices. The one-piece assembly for mounting ring and flexure rod was necessary for accuracy and strength. Figures 43 and 44 show details of this design. Figure 43 shows the flexure detail and other manufacturing information, while Figure 44 shows the pad construction. This bearing can be installed in the test rig housing in the same manner as the 360 degree bearing. The test pieces ordered for initial room temperature evaluation consist of steel flexure supports and bronze pads. Configurations for high temperature use would have to be made of TZM.

The manufacture of this unit has been difficult. The initial concept was to "pot" the unit with a low melting alloy for support during machining. However, it was found that changes occurred when the potting was removed. This necessitated the construction of the lapping fixture shown in Figure 45. Indications were that the dimensions were held by the use of this fixture.

Contrails

Cleared: December 19th, 1983

Clearing Authority: Air Force Wright Aeronautical Laboratories

The first checks on the flex pad bearing were dimensional, followed by the determination of resonances. The accuracy after lapping was good, within 0.0001 inches. The resonance was checked by driving the pad with a magnetic drive coil. This indicated a bending resonance of 550 CPS for axial and radial bending. Attempts were made to get the torsional mode. These were very difficult to drive, but indications were that the frequency was similar.

The first tests were static tests to determine stiffness and flow. These data are shown in Figures 46 and 47. Figure 46 compares the stiffness of the flex pad bearing with an equivalent 360 degree bearing. This indicates no appreciable gain in stiffness for this design at pressure ratios below 6. The stiffness was practically the same as that for the 360 degree bearing. The flow comparison is shown in Figure 47 and indicates that some early concern that a penalty of the flexibly mounted hybrid pad bearing would be higher flow was well grounded.

Runs on the flex pad bearing showed clearly defined rigid body criticals at lower pressure ratios. Although fractional frequency whirl was detected in some runs, this was not consistent. Distinct shifts were noted which indicated erratic pad behavior. Examination indicated touching on the edge of the pad and pad shifting. Several probable causes for this behavior were:

1. Clamping forces on the mounting ring which changed initial dimensions.
2. Orifice plugging as a result of lapping.
3. Running at the low pressure ratios gives insufficient stiffness to insure tracking.
4. Shifting of parts.

The parts were checked and subjected to a new cleaning technique after which additional runs were made.

Since some movements had been noted in the pad location, residual stress was one of the areas to consider. Therefore, the first step was to subject the assemblies to a stress relief. In the stress relieved condition, the units were reassembled. The next step is to get an accurate measurement on the unit so as to determine subsequent machining or processing steps.

In order to obtain an accurate indication of the concentricity of the pad assemblies, a fixture was machined to accurately locate the bearing and provide a reference diameter. This is shown schematically in Figure 48. Measurements were made with and without the pads in place.

Measurements made on the assembled bearing when mounted in the fixture indicated warpage of the radial spokes to an extent which made the bearing unusable in its present state. It was concluded that a grinding operation would have to be performed on the pad mounting ring to provide true surfaces to mount the individual pads. In order to stiffen the spokes prior to this grinding operation, the spokes were case hardened to an approximate depth of .007 inches by a gas carburizing process. The machining is in progress.

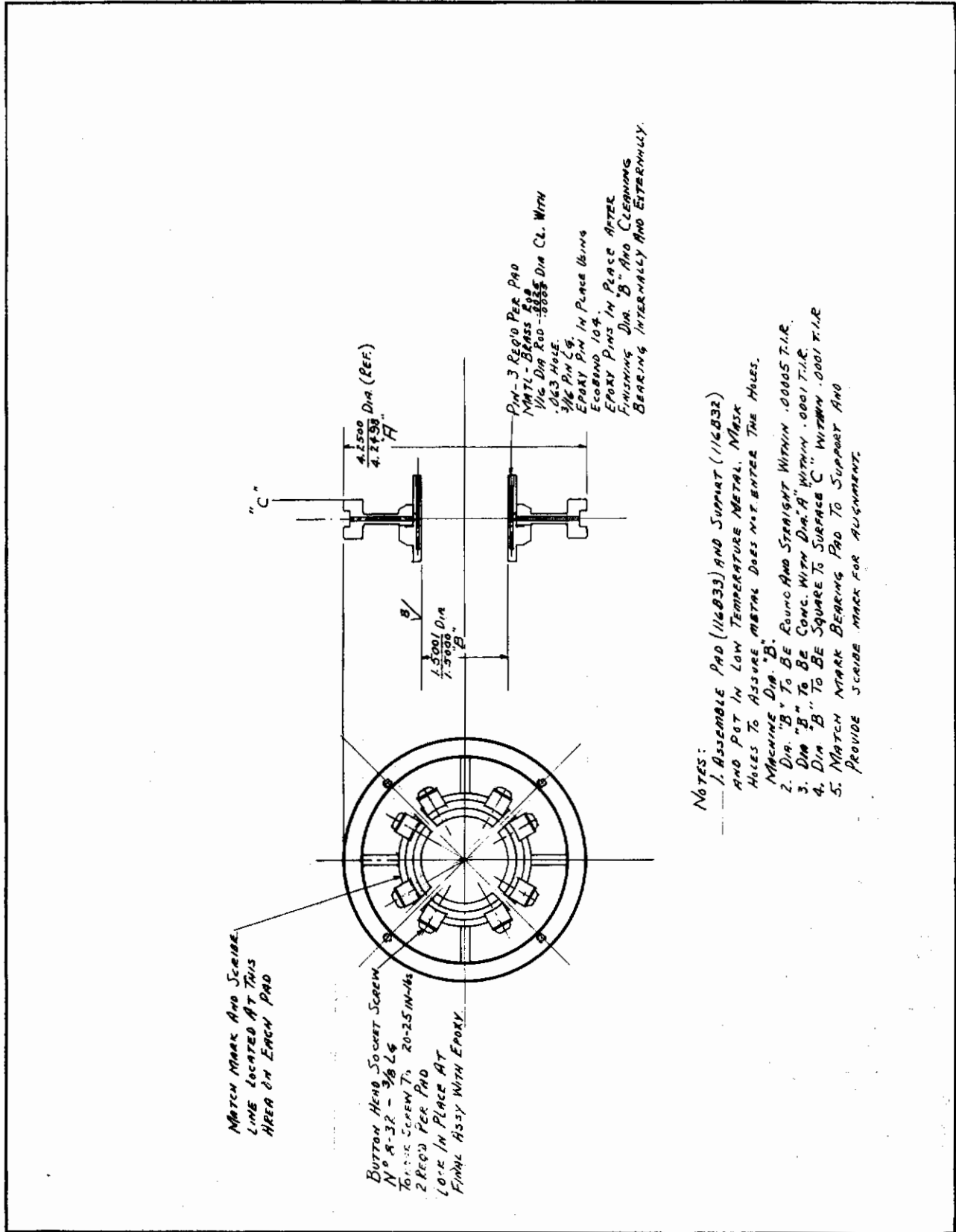
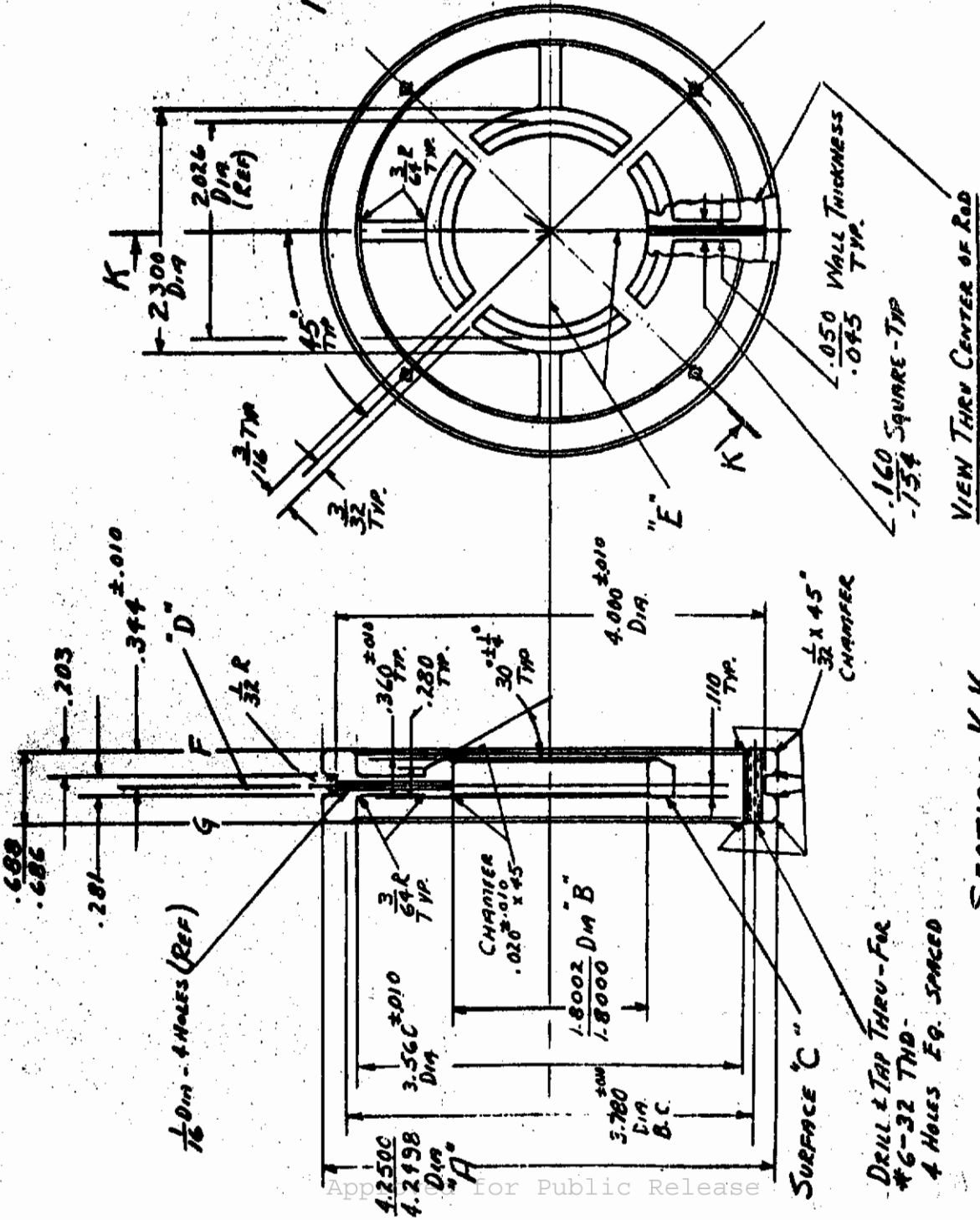


Fig. 42 Assembly of Flexure Mounted Hybrid Pad Bearings

NOTES:

1. **MATL.** - AISI 4340 - EN 220 - 250
 ANNEALED CONDITION
2. **FINISH** - ZINC PHOSPHATE COAT AND TREAT WITH CORROSION INHIBITING OIL ON ALL EXTERIOR SURFACES.
3. **E, D** OF FOUR RODS TO BE $\frac{1}{16}$ " TO DIA. B. WITHIN .001 T.I.R.
4. **E, E'** OF FOUR RODS TO BE ROUND AND PASS THRU CENTER OF DIA. B WITHIN .001 T.I.R. E, E' OF FOUR RODS TO BE EQUALLY SPACED AND LOCATED WITHIN .010 T.I.R.
5. **DIA. A** TO BE ROUND WITHIN .0002 T.I.R.
6. **DIA. B** TO BE CONC. TO DIA. A WITHIN .0002 T.I.R.
7. **SURFACE C** TO BE $\frac{1}{16}$ " TO DIA. B WITHIN .0002 T.I.R.
8. **SURFACE F** TO BE $\frac{1}{16}$ " TO DIA. A AND PARALLEL TO SURFACE G - WITHIN .0002 T.I.R.
9. UNSPECIFIED CONC, SQUARENESS, AND PARALLELISM TO BE WITHIN .005 T.I.R.
10. STRESS RELIEVE AS REQD. TO INSURE ASSEMBLY IS DIMENSIONALLY STABLE WITHIN THE TOLERANCES SPECIFIED.
11. BREAK SHARP CORNERS AND REMOVE BURRS.

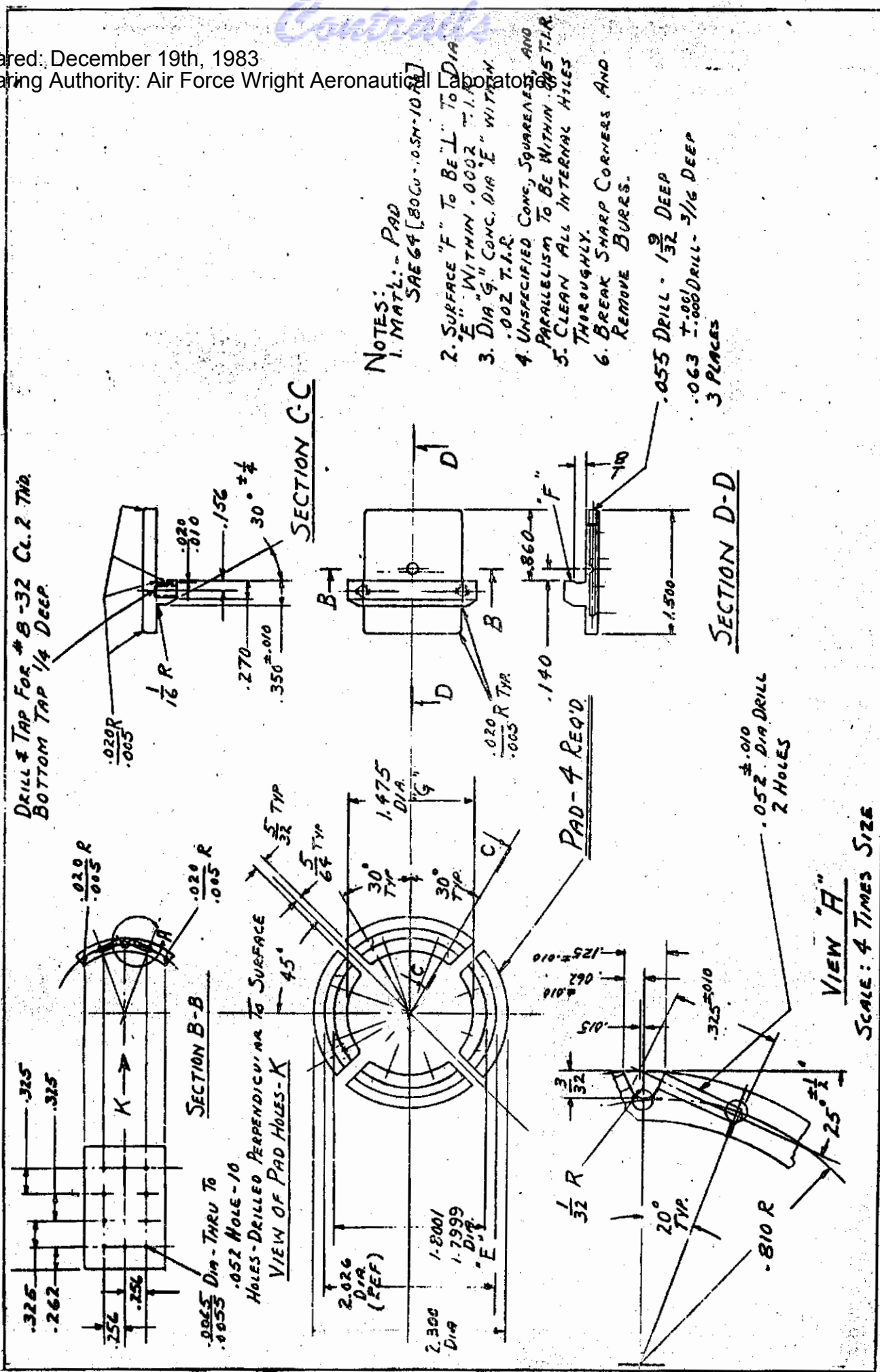


SECTION K-K

VIEW THRU CENTER OF ROD

Fig. 43 Detail of Flexure Assembly

Controls



- NOTES:
1. MATL: - PAD
 SAE 64 [80Cu-10Sn-10Al]
 2. SURFACE "F" TO BE "L" TO DIA
 "E" WITHIN .002 T.I.A.
 3. DIA "G" CONC. DIA "E" WITHIN
 .002 T.I.R.
 4. UNSPECIFIED CONC, SQUARENESS, AND
 PARALLELISM TO BE WITHIN .005 T.I.R.
 5. CLEAN ALL INTERNAL HOLES
 THOROUGHLY.
 6. BREAK SHARP CORNERS AND
 REMOVE BURRS.

Fig. 44 Hybrid Pad Design

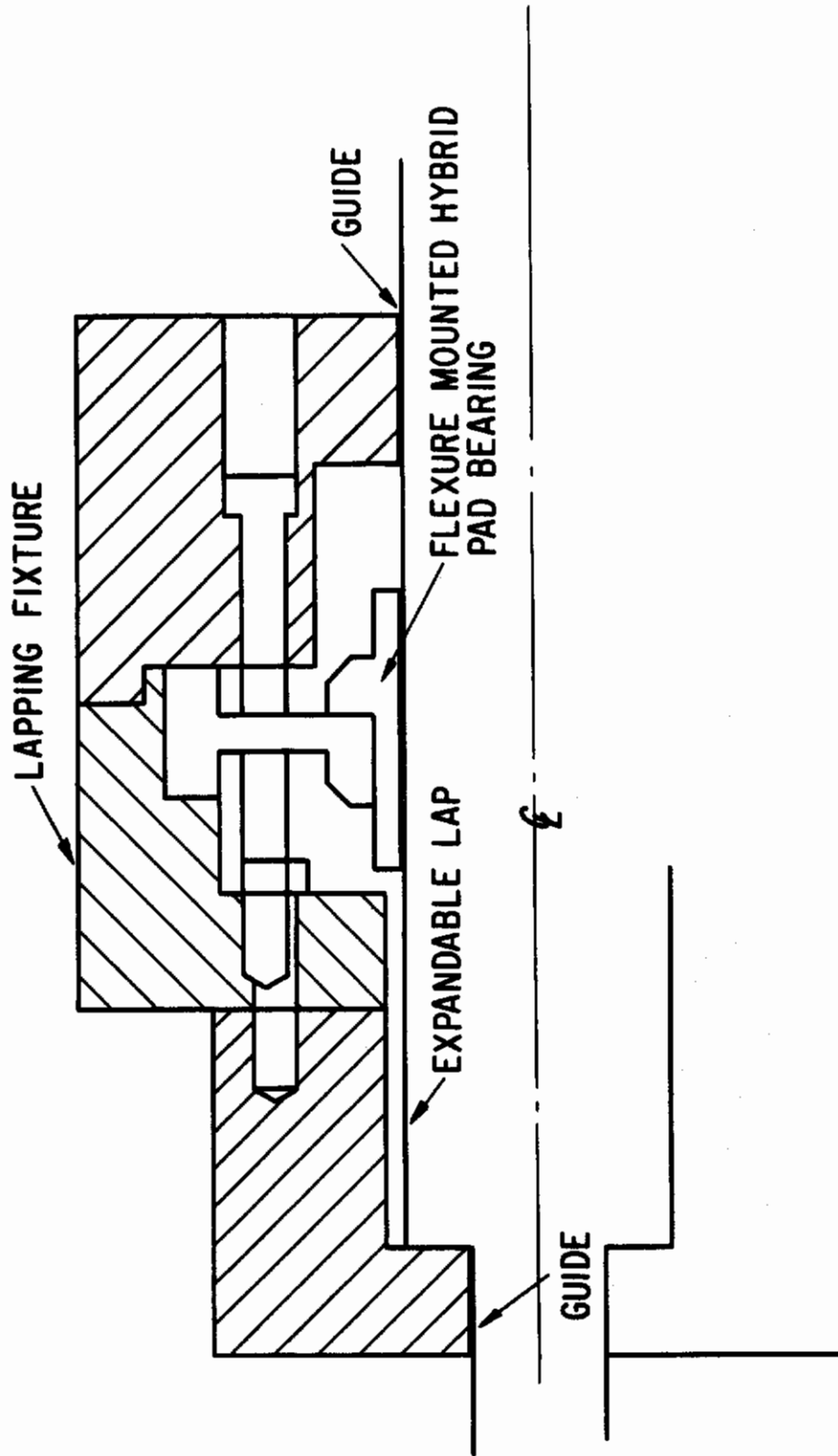


Fig. 45 Lapping Fixture for Flex Bearing

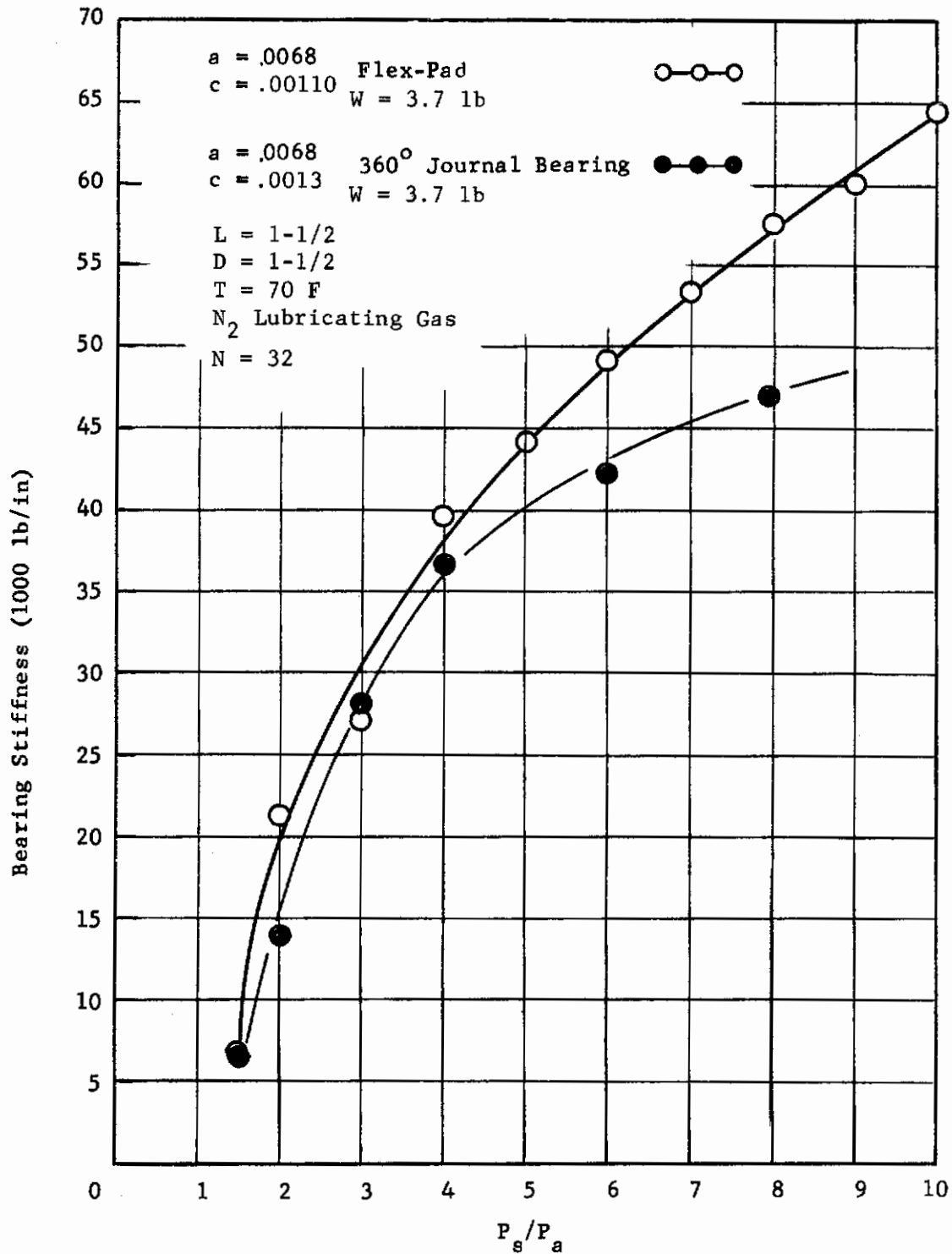


Fig. 46 Radial Stiffness as a Function of Supply Pressure:
 Load Vector on Pad

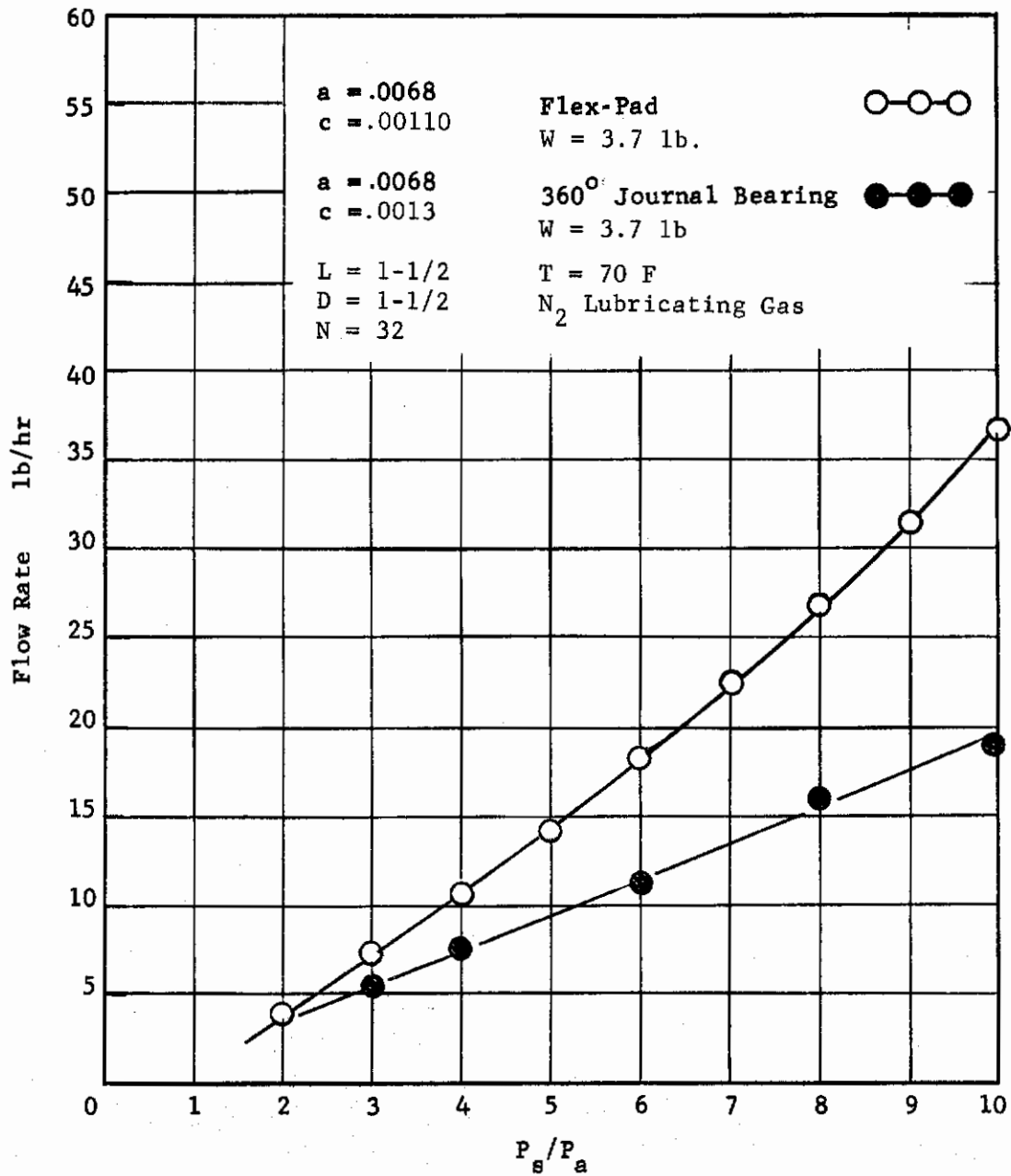


Fig. 47 Bearing Gas Flow as a Function of Supply Pressure; Load Vector on Pad

Cleared: December 19th, 1983
Clearing Authority: Air Force Wright Aeronautical Laboratories

TABLE 2

Experimental Results on Flexure Mounted Hybrid Pad Bearing

<u>Run</u>	<u>Pressure Ratio</u> P_s/P_a	<u>Whirl Speed or</u> <u>Speed at Failure</u>	<u>Reason For</u> <u>Terminating Test</u>
1	1-1/2	6,000 RPM	Whirl
2	2	13,250 RPM	Rubbed Shoe
3	3	30,000 RPM	Rubbed Shoe
4	1-1/2	55,800 RPM	Thrust Bearing
5	1-1/2	16,200 RPM	Whirl
6	2	23,730 RPM	Whirl
7	3	32,370 RPM	Rubbed Shoe
8	2	17,220 RPM	Whirl
9	3	30,120 RPM	Rubbed Shoe
10	4	42,840 RPM	Whirl
11	5	48,300 RPM	Whirl
12	5	51,900 RPM	Rubbed Shoe
13	6	54,110 RPM	Rubbed Shoe
14	6		No Lift
15	11	30,750 RPM	Rubbed Shoe

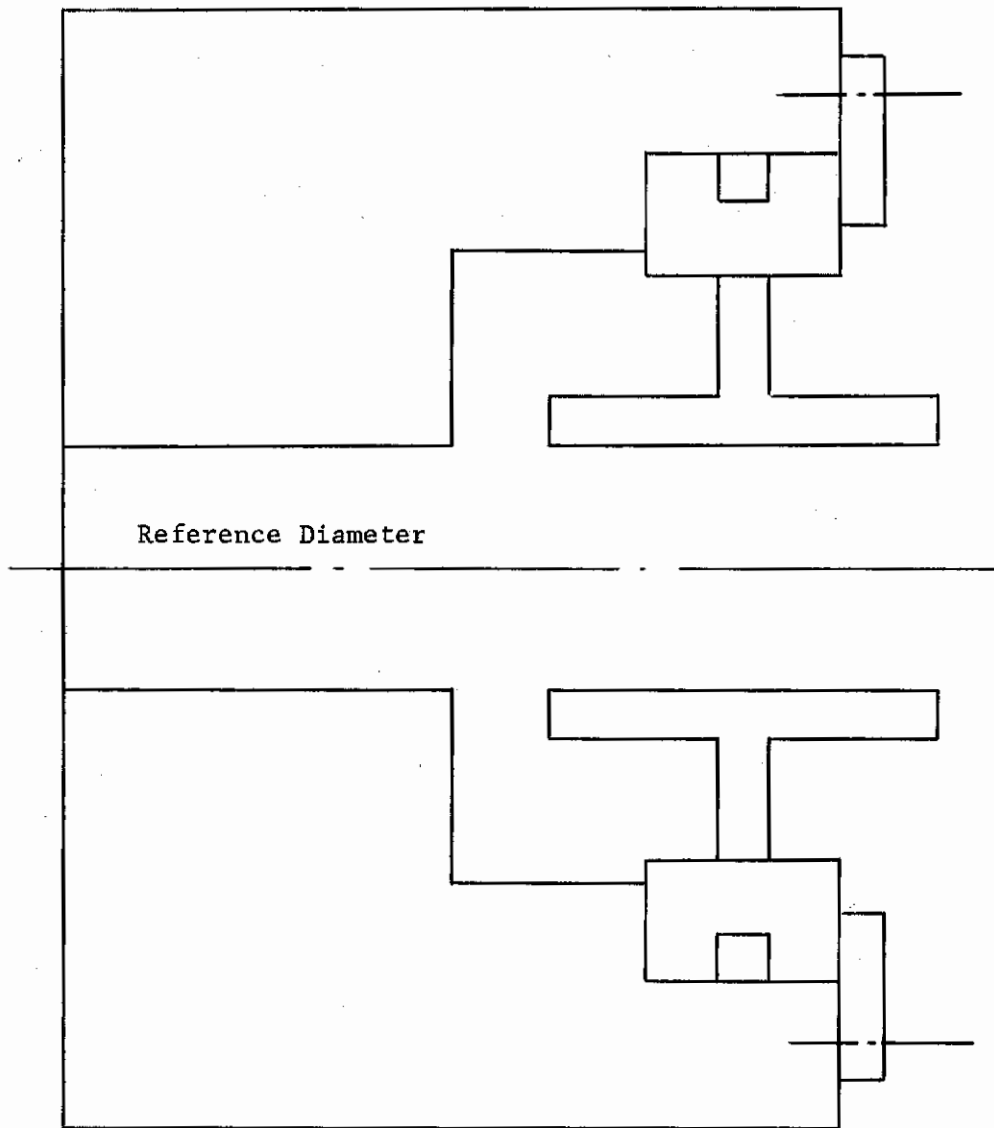


Fig. 48 Flex Pad Measurement Fixture

Cleared: December 19th, 1983
Clearing Authority: Air Force Wright Aeronautical Laboratories

TEST FACILITY

Several modifications have been made to the Test Facility to improve control and operation. These are summarized in this section.

Test Rig

The unit consists of a solid shaft supported on two journal bearings with a loading bearing sector at the mid-span of the two journal bearings. A thrust bearing and thrust load act on opposite ends of the shaft. The unit is turbine driven with turbine blades machined on one end of the shaft. The journal bearings are removable. The housing is a cylindrical block. All instrumentation is brought to the housing block.

Figure 49 is the assembly drawing for the test rig, showing the relationship between the major components. The thrust bearing on the left side and the thrust loader and turbine nozzle block on the right side are simply clamped against the housing ends by through-bolts. This assembly method is feasible, since the concentricity requirements of these separate plates are not critical. The journal bearing loader is machined as an integral part of the housing. The journal bearings are installed in close tolerance recesses in the housing, machined concentric to the journal loader. The bearings are clamped in place with spacer rings which support the axial force of the through bolts holding the thrust plates in place. Detailed descriptions of the test rig components are given in Reference 1.

Oven and Enclosure

Some modification to the oven was necessitated by the decision to use an inert atmosphere blanket to prevent oxidation of the test rig. Consideration was given to the design of a sheet metal "can" fitted over the test rig enclosing a minimum volume. However, the multitude of connections for gas supply lines and instrumentation (which would have to pass through the wall of such a can at various points) made this approach impractical for the early testing. Installing a pressure-tight jacket around the outside of the oven would allow the use of low temperature materials, but would enclose within the inert area all of the air in the oven insulation. It was therefore decided to modify the liner inside the oven chamber to create a relatively, gas-tight chamber inside the oven insulation, but enclosing the oven heater elements as well as the test rig.

Inconel sheet metal end covers for the liner were fabricated with simple baffle-type joints. Minimum clearance holes are provided for the bundle of gas supply tubes and the bundle of instrumentation leads. The resulting enclosure is not completely gas-tight, but the inert blanket will be ensured by injecting sufficient nitrogen into the enclosure to maintain a slight positive pressure.

The oven has been used several times for high temperature probe calibration and has operated satisfactorily. It has been used for all testing to 500 F.

Because of the concern that this system could not be positively inert gas blanketed, a pressure-tight enclosure is to be used for evaluations above 600 F.

Cleared: December 19th, 1983

Clearing Authority: Air Force Wright Aeronautical Laboratories

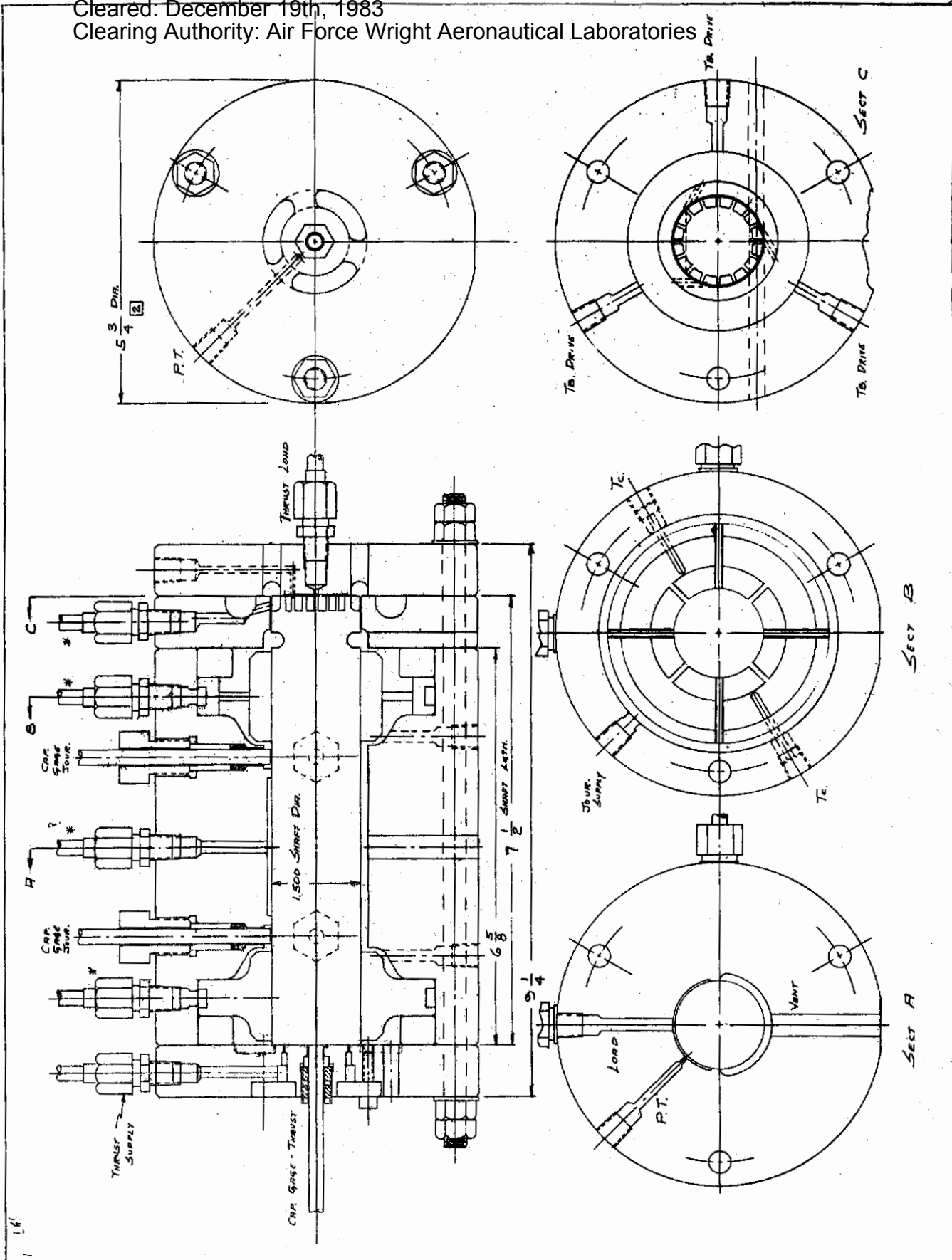


Fig. 49 Assembly Drawing of Test Rig

Cleared: December 19th, 1983

Clearing Authority: Air Force Wright Aeronautical Laboratories

The enclosure is a pressure vessel with a mounting flange on one end. The vessel is supported in the horizontal position with the test equipment cantilevered from the flange cover. All feedthroughs are brought through the cover. The present configuration is shown in Figure 50. Figure 51 shows the equipment in the process of assembly to the cover of the enclosure. Thermal insulation encased in stainless steel foil line the enclosure to keep the enclosure below 500 F when the unit is operating at 1900 F. A radiation baffle is between the insulation and rig. A heater coil around the test housing will be used to control housing temperature. The pressure vessel, insulation, and radiation baffle are shown in Figure 52.

Preheater

The gas preheater design places the heating elements outside the gas flow path. It is described in detail in Reference 1. Difficulty was encountered in the gas preheater because of overheating of the preheater tube coils. This was due in large measure to low gas velocity through the tubes and the resulting poor heat transfer between the tubes and the gas. To remove this problem, a bypass or bleed was incorporated into all six of the gas supply circuits. The bleed is located at the exit from the gas preheater and is used to increase the flow velocities through the preheater. The performance at gas and bearing temperatures of 300 F and 500 F have indicated no difficulties in control or excessive tube temperatures.

Controls

The basic gas preheater controls are described in detail in the first annual report (Reference 1). However, the decision to incorporate the test rig into a pressure vessel during high temperature testing has required some modification of the control system.

To prevent damage to the test rig when used in the enclosure for tests above 600 F due to possible mishaps such as loss of electrical power and low pressure in any of the six gas supply lines, a fail-safe control system has been designed and installed. This system, shown in Figures 53 through 55 will automatically shut down the turbine supply, turn off the effected gas-preheater circuit, and turn on an auxiliary nitrogen gas supply when a low pressure condition is detected in any of the six feed lines. This would reflect a possible leak or opening of a gas line. In case of a power failure, the control circuit will automatically shut off the turbine supply, turn on the auxiliary supplies and shut off the entire gas preheater. Figures 56 and 57 show the fail safe components. Figure 56 shows the relay panel and Figure 57 shows the pneumatic controls.

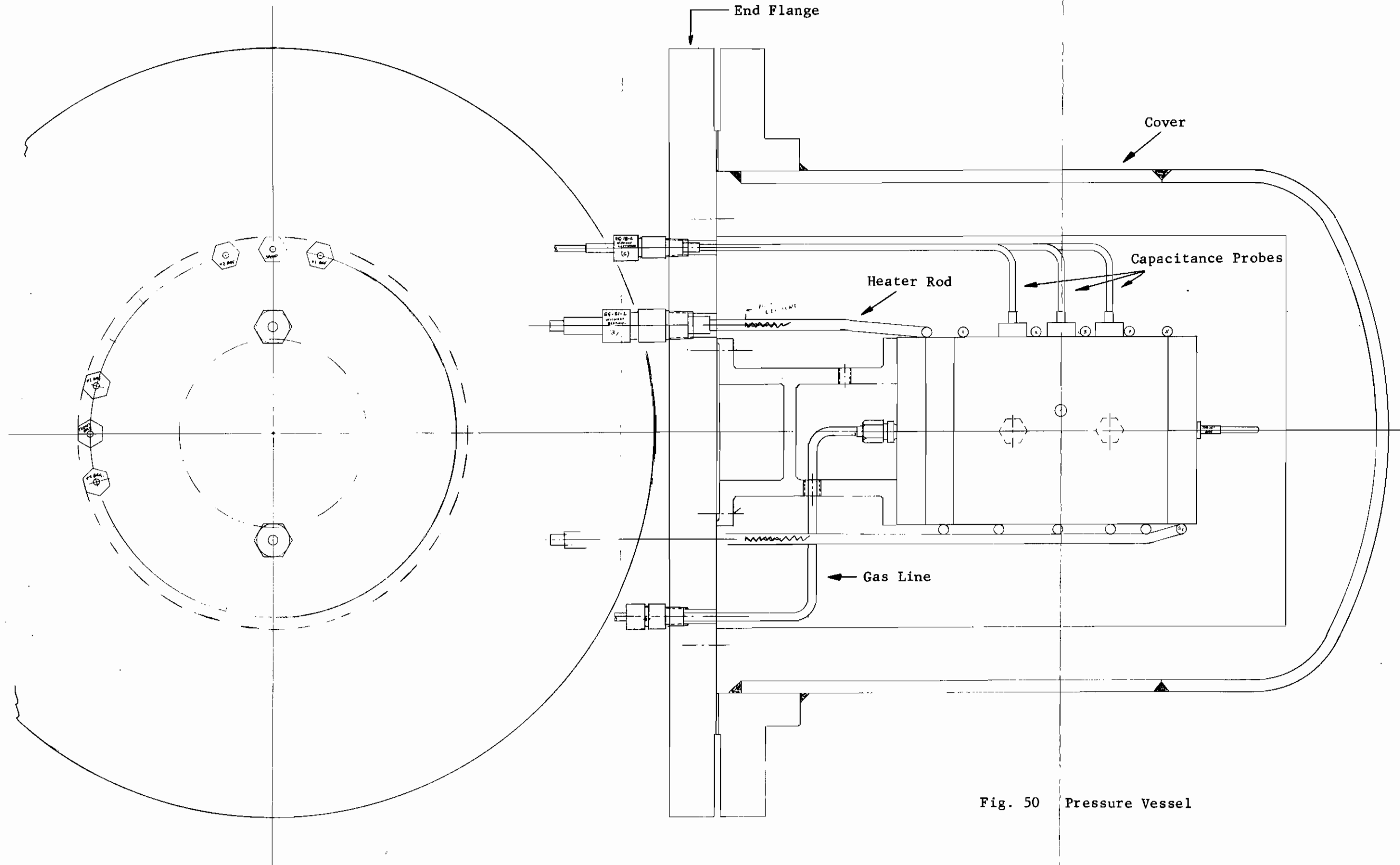


Fig. 50 Pressure Vessel

Cleared: December 19th, 1983

Clearing Authority: Air Force Wright Aeronautical Laboratories

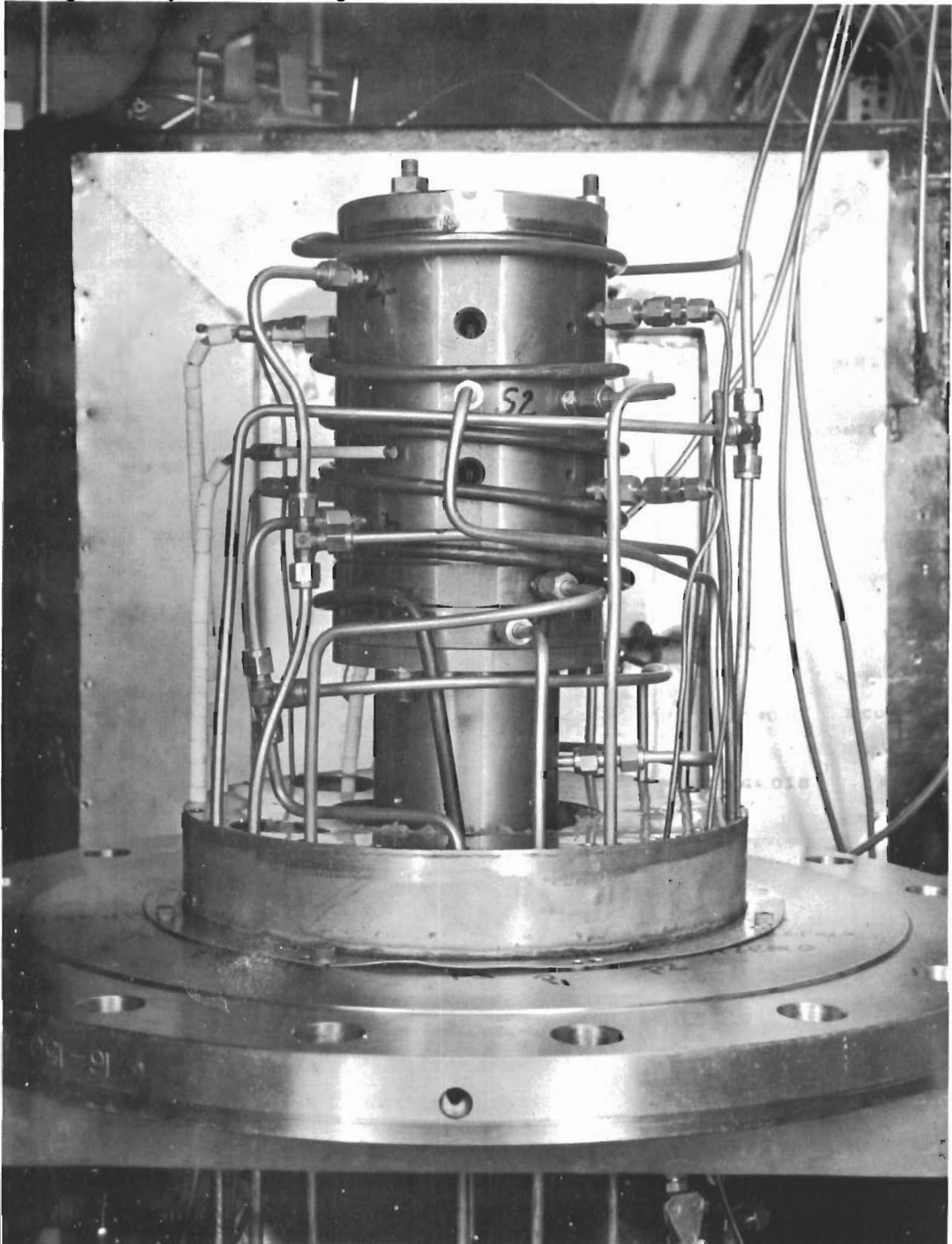
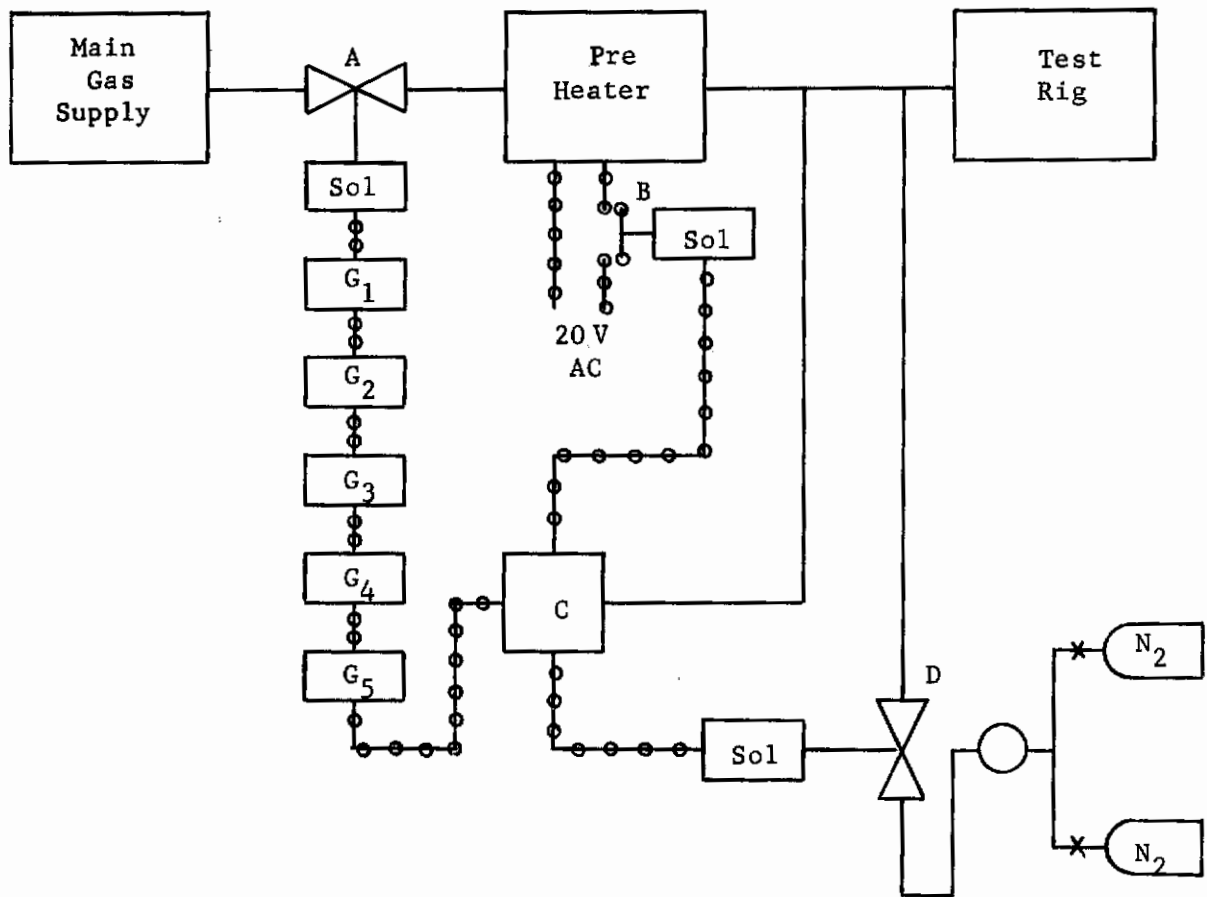


Fig. 51 Early Stages of Assembly of Rig to Pressure Vessel Flange

Cleared: December 19th, 1983
Clearing Authority: Air Force Wright Aeronautical Laboratories



Fig. 52 Pressure Hull, Insulation and Radiation Shield for High Temperature Testing

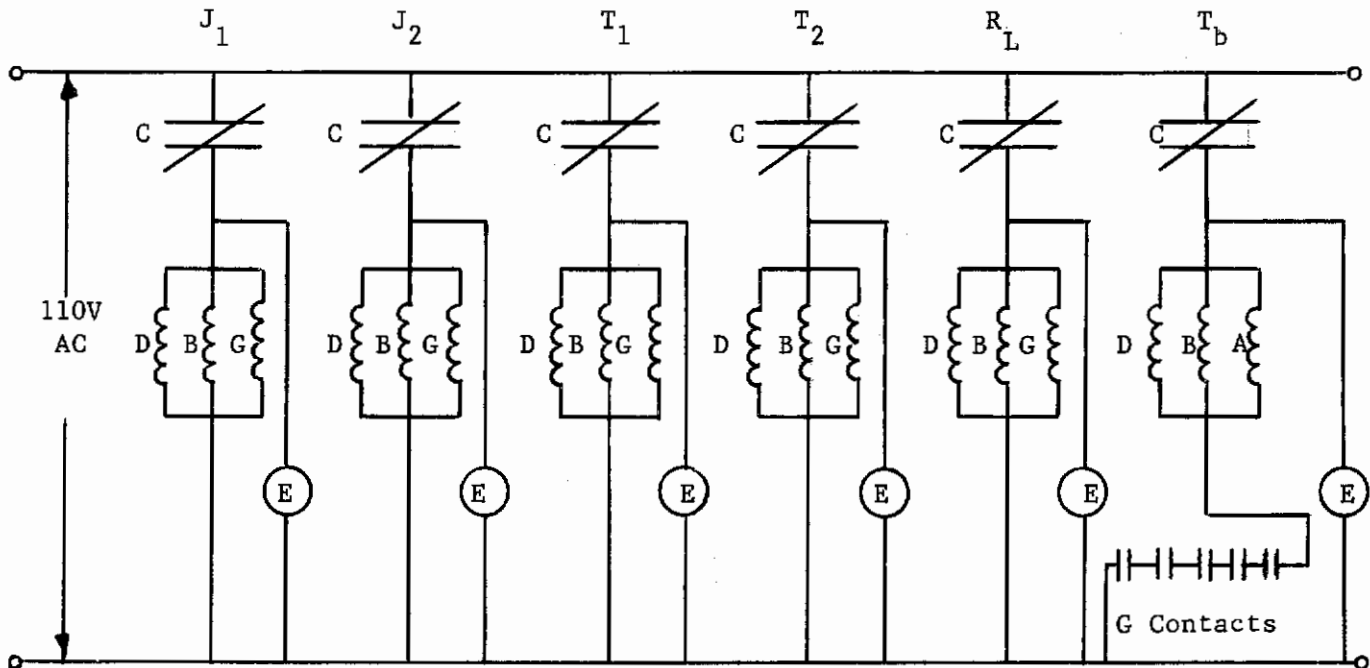


Turbine Supply*

* For Other Supplies Eliminate Valve A and Relays G₁ Through G₅

Fig. 53 Fail Safe Schematic Diagram

Cleared: December 19th, 1983
 Clearing Authority: Air Force Wright Aeronautical Laboratories



J₁ Journal Bearing #1

J₂ Journal Bearing #2

T₁ Thrust Bearing

T₂ Axial Loader

R_L Radial Loader

T_b Turbine

C = Pressure Switch

A Holding Coil Valve A

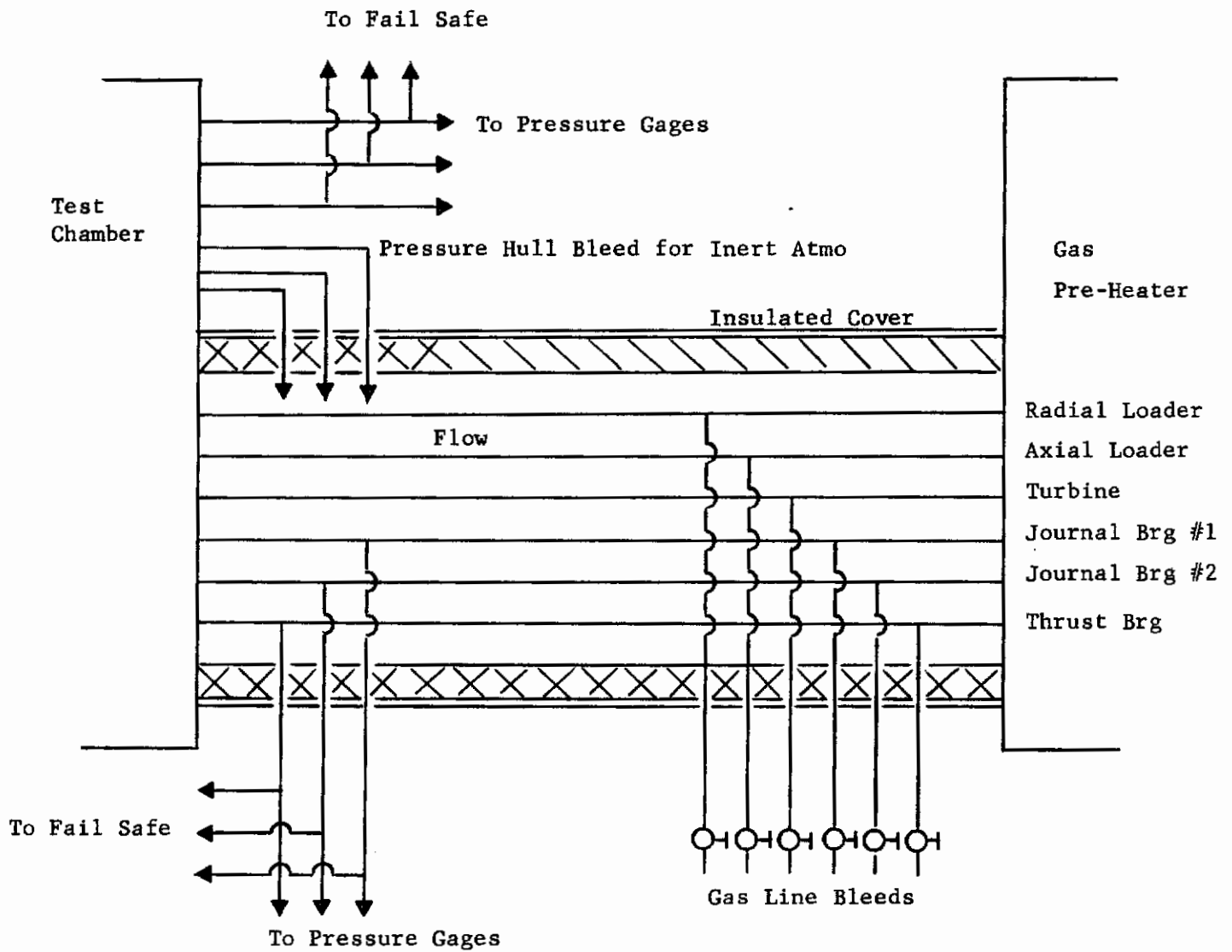
B Holding Coil Relay B

D Holding Coil Valve D

G Holding Coil Relay G

E Neon Indicating Light

Fig. 54 Fail Safe Wiring Diagram



<u>Item</u>	<u>No. Req'd.</u>
Thermocouples	5
Capacitance Probes	5
Gas Feeds	6
Pressure Taps	3
Return Bleeds	6

Fig. 55 Fail Safe Tubing Diagram

Cleared: December 19th, 1983

Clearing Authority: Air Force Wright Aeronautical Laboratories

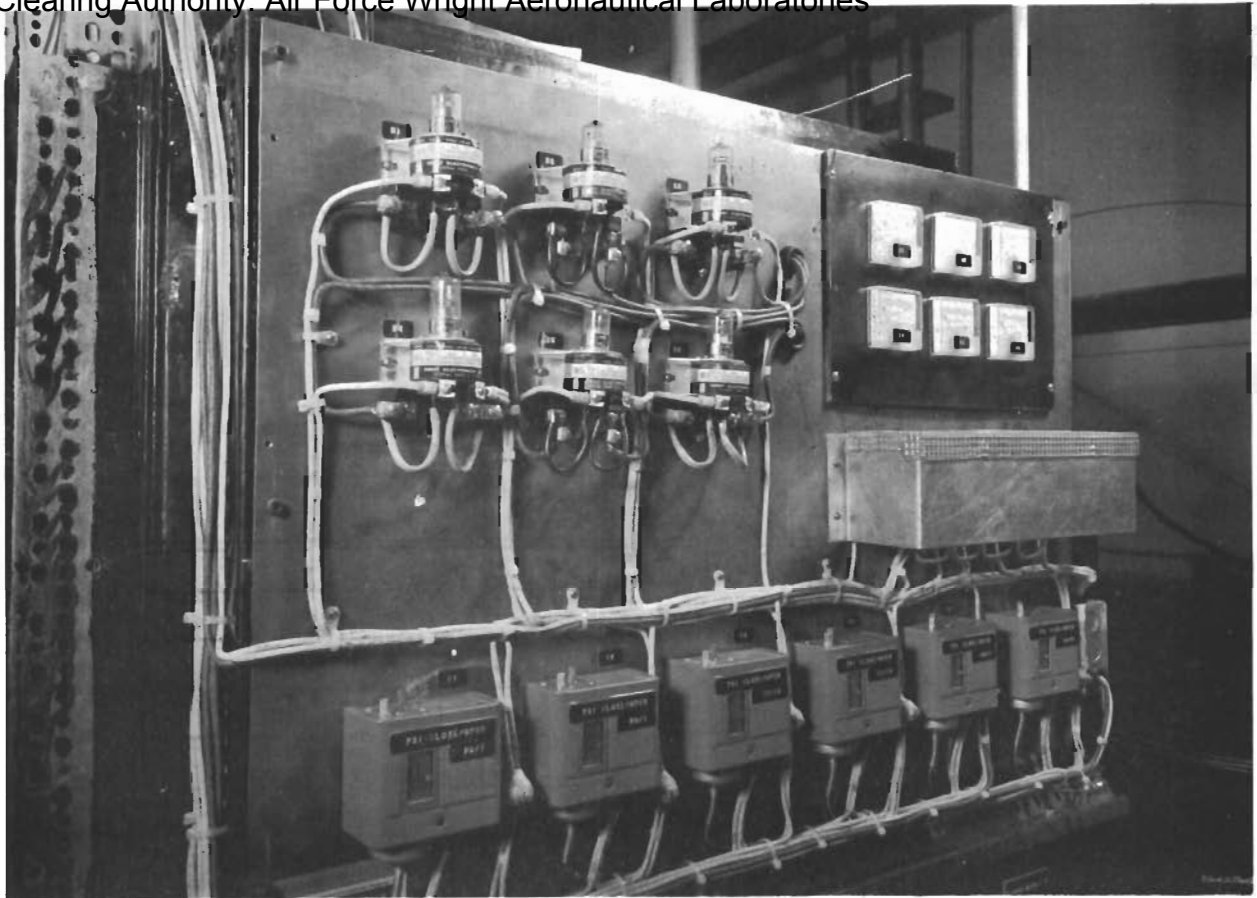


Fig. 56 Relay Panel of Fail Safe

Cleared: December 19th, 1983
Clearing Authority: Air Force Wright Aeronautical Laboratories

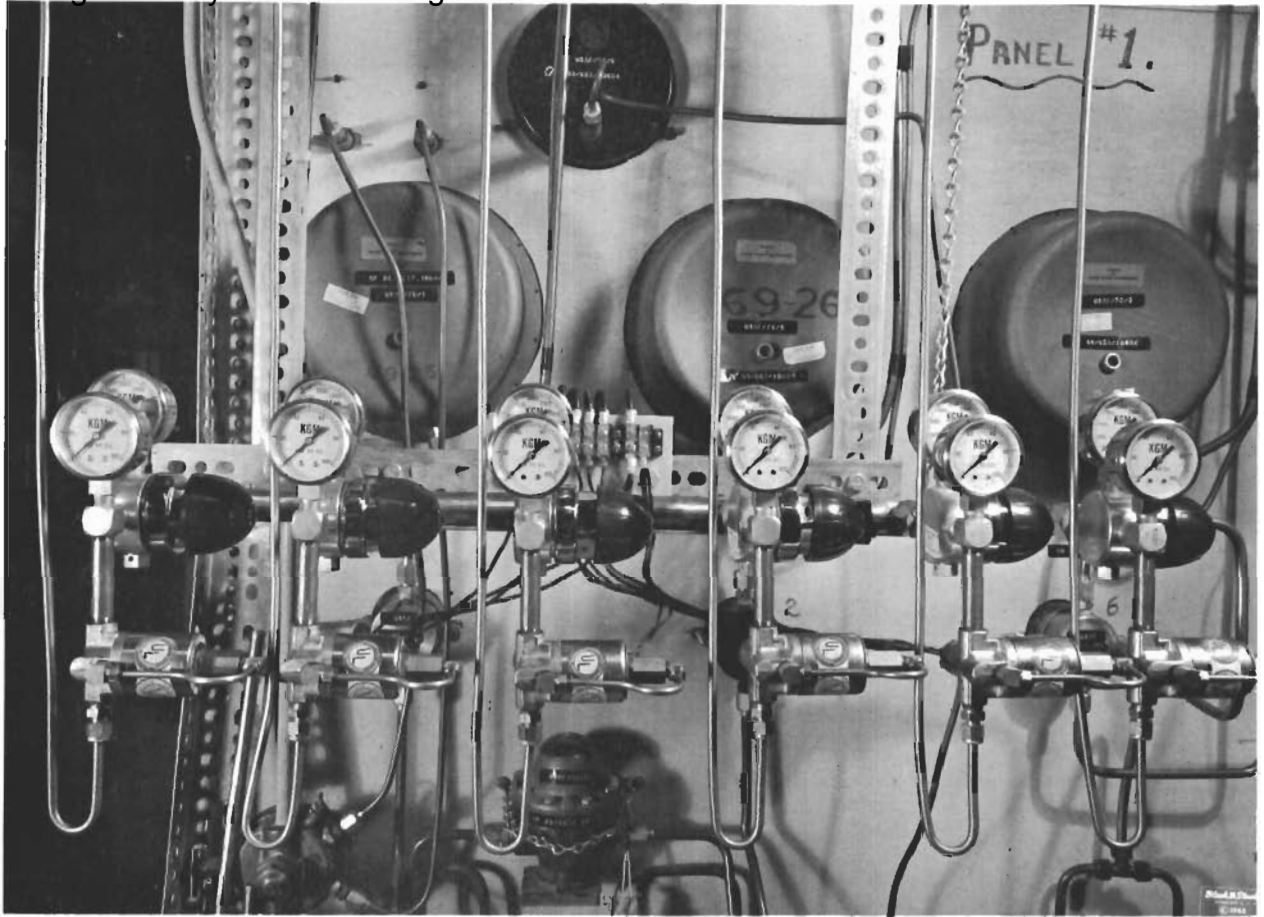


Fig. 57 Pneumatic Controls of Fail Safe

Cleared: December 19th, 1983

Clearing Authority: Air Force Wright Aeronautical Laboratories

REFERENCES

1. First Annual Report, "Research on Gas Lubrication at High Temperatures and Low Flow Rates", Technical Documentary Report No. APL TDR 64-56, March, 1964, prepared for the AF Aero Propulsion Laboratory, Research and Technology Division, Air Force Systems Command, Wright-Patterson Air Force Base, Ohio, by P. Lewis and J. Meacher, Mechanical Technology Inc. under contract AF33(657)-10694.
2. J. W. Lund, "The Hydrostatic Gas Journal Bearing with Journal Rotation and Vibration", JOURNAL OF BASIC ENGINEERING, TRANS. ASME, Series D, Vol. 86, 1964, pp. 328-336.
3. G. Heinrich, "The Theory of the Externally-Pressurized Bearing with Compressible Lubricant", Proceedings of the First International Symposium on Gas Lubricated Bearings, ONR/ACR-49, October, 1959, pp. 251-265.
4. H. H. Richardson, "Static and Dynamic Characteristics of Compensated Gas Bearings", TRANS. ASME, Vol. 80, 1958, pp. 1503-1509.
5. W. A. Gross, "Investigation of Whirl in Externally-Pressurized Air-Lubricated Journal Bearings", JOURNAL OF BASIC ENGINEERING, TRANS. ASME, Series D, Vol. 84, 1962, pp. 132-138.
6. L. W. Winn and B. Sternlicht, "The Load Carrying Capacity and Stability of Hybrid Gas Bearings". Report for ONR, November 3, 1962.
7. R. H. Larson and H. H. Richardson, "A Preliminary Study of Whirl Instability for Pressurized Gas Bearings", JOURNAL OF BASIC ENGINEERING, TRANS. ASME, Series D, Vol. 84, 1962, pp. 511-520.
8. "Hybrid Gas Journal Bearing Instability", J. W. Lund, MTI 63TR60, (accompanied Third Quarterly Progress Report), December 27, 1963.

Contracts

Security Classification
Cleared: December 10th, 1983

Clearing Authority: Air Force Wright Aeronautical Laboratories

DOCUMENT CONTROL DATA - R&D

(Security classification of title, body of abstract and indexing annotation must be entered when the overall report is classified)

1. ORIGINATING ACTIVITY (Corporate author) Mechanical Technology Incorporated 968 Albany-Shaker Road Latham, New York		2a. REPORT SECURITY CLASSIFICATION UNCLASSIFIED	
		2b. GROUP	
3. REPORT TITLE Research on Gas Lubrication at High Temperatures and Low Flow Rates			
4. DESCRIPTIVE NOTES (Type of report and inclusive dates) Technical Documentary Report			
5. AUTHOR(S) (Last name, first name, initial) Lewis, P. and Eusepi, M.			
6. REPORT DATE March 1965		7a. TOTAL NO. OF PAGES 80	7b. NO. OF REFS 8
8a. CONTRACT OR GRANT NO. AF 33(657)-10694		9a. ORIGINATOR'S REPORT NUMBER(S) APL-TDR-64-56 Part II	
b. PROJECT NO.		9b. OTHER REPORT NO(S) (Any other numbers that may be assigned this report)	
c. Project No. 3044			
d. Task No. 304402			
10. AVAILABILITY/LIMITATION NOTICES Foreign Announcement and dissemination of this report by DDC is not authorized.			
11. SUPPLEMENTARY NOTES		12. SPONSORING MILITARY ACTIVITY Research and Technology Division AF Aero Propulsion Laboratory Wright-Patterson Air Force Base, Ohio 45433	
13. ABSTRACT This report describes the second year's effort on a program that has as its objective the development of nitrogen gas lubricated bearings that have the best potential for stable operation at temperatures up to 1900°F and speeds to 60,000 RPM with low flow rates. The program concentrated on attaining quantitative performance data on dynamic rotor bearing behavior. The report summarizes the equipment, instrumentation and experimental work. Quantitative performance data and a dimensionless map which summarizes the stable speed capability of the 360 degree hybrid bearing are provided.			

DD FORM 1473
1 JAN 64

Security Classification

14. Clearing Authority: Air Force Wright Aeronautical Laboratories Key Words	LINK A		LINK B		LINK C	
	ROLE	WT	ROLE	WT	ROLE	WT
Gas Lubrication Gas Bearings Hybrid Bearings Hydrodynamic Lubrication Rotor bearing Stability High Temperature Lubrication						

INSTRUCTIONS

1. **ORIGINATING ACTIVITY:** Enter the name and address of the contractor, subcontractor, grantee, Department of Defense activity or other organization (*corporate author*) issuing the report.

2a. **REPORT SECURITY CLASSIFICATION:** Enter the overall security classification of the report. Indicate whether "Restricted Data" is included. Marking is to be in accordance with appropriate security regulations.

2b. **GROUP:** Automatic downgrading is specified in DoD Directive 5200.10 and Armed Forces Industrial Manual. Enter the group number. Also, when applicable, show that optional markings have been used for Group 3 and Group 4 as authorized.

3. **REPORT TITLE:** Enter the complete report title in all capital letters. Titles in all cases should be unclassified. If a meaningful title cannot be selected without classification, show title classification in all capitals in parenthesis immediately following the title.

4. **DESCRIPTIVE NOTES:** If appropriate, enter the type of report, e.g., interim, progress, summary, annual, or final. Give the inclusive dates when a specific reporting period is covered.

5. **AUTHOR(S):** Enter the name(s) of author(s) as shown on or in the report. Enter last name, first name, middle initial. If military, show rank and branch of service. The name of the principal author is an absolute minimum requirement.

6. **REPORT DATE:** Enter the date of the report as day, month, year, or month, year. If more than one date appears on the report, use date of publication.

7a. **TOTAL NUMBER OF PAGES:** The total page count should follow normal pagination procedures, i.e., enter the number of pages containing information.

7b. **NUMBER OF REFERENCES:** Enter the total number of references cited in the report.

8a. **CONTRACT OR GRANT NUMBER:** If appropriate, enter the applicable number of the contract or grant under which the report was written.

8b, 8c, & 8d. **PROJECT NUMBER:** Enter the appropriate military department identification, such as project number, subproject number, system numbers, task number, etc.

9a. **ORIGINATOR'S REPORT NUMBER(S):** Enter the official report number by which the document will be identified and controlled by the originating activity. This number must be unique to this report.

9b. **OTHER REPORT NUMBER(S):** If the report has been assigned any other report numbers (*either by the originator or by the sponsor*), also enter this number(s).

10. **AVAILABILITY/LIMITATION NOTICES:** Enter any limitations on further dissemination of the report, other than those

imposed by security classification, using standard statements such as:

- (1) "Qualified requesters may obtain copies of this report from DDC."
- (2) "Foreign announcement and dissemination of this report by DDC is not authorized."
- (3) "U. S. Government agencies may obtain copies of this report directly from DDC. Other qualified DDC users shall request through _____."
- (4) "U. S. military agencies may obtain copies of this report directly from DDC. Other qualified users shall request through _____."
- (5) "All distribution of this report is controlled. Qualified DDC users shall request through _____."

If the report has been furnished to the Office of Technical Services, Department of Commerce, for sale to the public, indicate this fact and enter the price, if known.

11. **SUPPLEMENTARY NOTES:** Use for additional explanatory notes.

12. **SPONSORING MILITARY ACTIVITY:** Enter the name of the departmental project office or laboratory sponsoring (*paying for*) the research and development. Include address.

13. **ABSTRACT:** Enter an abstract giving a brief and factual summary of the document indicative of the report, even though it may also appear elsewhere in the body of the technical report. If additional space is required, a continuation sheet shall be attached.

It is highly desirable that the abstract of classified reports be unclassified. Each paragraph of the abstract shall end with an indication of the military security classification of the information in the paragraph, represented as (TS), (S), (C), or (U).

There is no limitation on the length of the abstract. However, the suggested length is from 150 to 225 words.

14. **KEY WORDS:** Key words are technically meaningful terms or short phrases that characterize a report and may be used as index entries for cataloging the report. Key words must be selected so that no security classification is required. Identifiers, such as equipment model designation, trade name, military project code name, geographic location, may be used as key words but will be followed by an indication of technical context. The assignment of links, rules, and weights is optional.